THE MODELLING OF QUASI-RESONANT AND MULTI-RESONANT BOOST CONVERTERS

ADRIAN SZABO

A thesis submitted in partial fulfilment of the requirements of The Nottingham Trent University for the degree of Doctor of Philosophy

July 1998

Abstract

This thesis presents a method for the modelling of quasi-resonant and multi-resonant boost converters using the averaging technique.

The concept of characteristic functions is introduced, which allows the derivation of a unified model of all classes of boost converters - multi-resonant, quasi-resonant and pulse-width-modulated. The characteristic functions describe the average behaviour of switching devices in a dc-dc converter. Quasi-resonant converters have one characteristic function, which can be seen as the equivalent duty ratio of the converter, and its analytic expression is determined. Multi-resonant converters have two characteristic functions and a numerical method is developed to evaluate them.

The dc (steady-state) model of quasi-resonant and multi-resonant boost converters is related to the conventional pulse-width-modulated boost converter. The expression of the voltage conversion ratio of resonant boost converters is obtained from the pulse-width-modulated converter by replacing the duty ratio with the characteristic function. The dc models are verified by simulations using PSPICE and hardware implementation.

The small-signal model of resonant boost converters is obtained in circuit form. In this model, the switching devices are represented by controlled voltage and current sources, whose coefficients depend on the characteristic functions of the converters. The small-signal control-to-output and line-to-output transfer functions of the quasi-resonant and multi-resonant boost converters are derived. Their expressions are compared to the ones of the pulse-width-modulated converter. It is shown that the resonant elements do not increase the order of the small-signal model, therefore, the well-known methods for the design of the feedback loop of pulse-width-modulated converters can be applied to resonant converters.

This approach is extended to the buck and buck-boost converters and a general unified method for the modelling of quasi-resonant and multi-resonant dc-dc converters is presented.

Acknowledgements

I would like to express my gratitude to my supervisors, Dr. E S Ward and Mr. M Kansara, for their guidance, help and support during my doctoral studies and research. I would like to thank them for all their time and effort.

I acknowledge The Nottingham Trent University for offering me the research bursary and funding of my research project.

It was a pleasure to study and work in the Department of Electrical and Electronic Engineering of The Nottingham Trent University. I thank all my colleagues, researchers, academic staff and technicians, for making my stay in Nottingham meaningful and enjoyable.

I dedicate this thesis to my parents, Maria Rodica and Willibald Levente, for their love, encouragement and support.

Table of Contents

List of Symbols and Abbreviations

C - output capacitor

C_D - resonant capacitor (for ZVS-MRCs)

C_N - normalised ratio of resonant capacitances (for ZVS-MRCs)

C_r - resonant capacitor (for QRCs)

C_S - resonant capacitor (for ZVS-MRCs)

d - duty ratio of PWM converter

$\tilde{d}$ - small-signal variation of duty ratio

D - rectifying diode (passive switch)

f_n - normalised switching frequency

f_r - resonant frequency

f_S - switching frequency

$\tilde{f}_S$ - small-signal variation of switching frequency

G - characteristic function

G_i - characteristic function

G_v - characteristic function

i_D - current through diode D

$\bar{i}_D$ - average value of the current through diode D

i_D^* - normalised current through diode D

I_{in} - input current

$\tilde{i}_{in}$ - small-signal variation of input current

i_{Lr} - current through resonant inductor

i_{Lr}^* - normalised current through resonant inductor

I_{on} - peak current through the switch for PWM converter

I_{out} - output current

i_S - current through switch S

$\tilde{i}_S$ - small-signal variation of the current through the switch S

$\bar{i}_S$ - average value of the current through the switch S

i_S^* - normalised current through switch S

k_C - gain of control-to-output transfer function

k_L - gain of line-to-output transfer function

k_{vi}, k_{vv}, k_{vf}, k_{ii}, k_{iv}, k_{if} - transfer function k-parameters

k_{VCO} - gain of voltage-controlled-oscillator

L - input inductor

L_D - resonant inductor (for ZCS-MRCs)

L_r - resonant inductor (for QRCs)

L_S - resonant inductor (for ZCS-MRCs)

MRC - multi-resonant converter

PWM - pulse-width-modulation

QRC - quasi-resonant converter

r - normalised load resistance

R_{DS} - drain-to-source on-resistance of the power MOSFET

R_0 - load resistance

RHP - right half-plane

S - main power switch (active switch)

T_{off} - off-time of switch

T_{on} - on-time of switch

T_S - switching period

T_{01} - duration of the first operating stage

T_{12} - duration of the second operating stage

T_{23} - duration of the third operating stage

T_{34} - duration of the fourth operating stage

v_{Cr} - voltage across resonant capacitor

v_D - reverse voltage across diode D

$\tilde{v}_D$ - small-signal variation of the reverse voltage across the diode D

$\bar{v}_D$ - average value of voltage across the diode D

v_D^* - normalised voltage across diode D

V_{in} - input voltage

$\tilde{v}_{in}$ - small-signal variation of input voltage

V_{off} - peak voltage across the switch for PWM converter

V_{out} - output voltage

$\tilde{v}_{out}$ - small-signal variation of output voltage

v_S - voltage across switch S

$\overline{v}_S$ - average value of voltage across switch S

v_S^* - normalised voltage across switch S

VCO - voltage-controlled-oscillator

x - voltage conversion ratio

x_P - voltage conversion ratio of PWM converter

Z_r - characteristic impedance of the resonant tank

ZCS - zero-current-switching

ZVS - zero-voltage-switching

α - normalised inductor current

ω_D - resonant angular frequency (for MRCs)

ω_0 - undamped natural frequency of transfer function

ω_r - resonant angular frequency (for QRCs)

ω_S - resonant angular frequency (for MRCs)

ω_{SD} - resonant angular frequency (for MRCs)

ω_{ZC} - angular frequency of the zero of the control-to-output transfer function

ω_{ZL} - angular frequency of the zero of the line-to-output transfer function

1. Introduction

1.1. Overview of the Subject Area

The trend in today's electrical and electronics industry is one of miniaturisation. With the advancement of Very Large Scale Integration (VLSI), the size of control and information-processing electronics is shrinking tremendously. But the power supplies used in computers, telecommunications and instrumentation applications are still bulky, making them incompatible with microelectronics chips. Therefore, the designers of power converters focus their research and development efforts increasingly on producing small-size and light-weight converters of high efficiency [1-8].

There are three major directions which are currently being explored in the pursuit of higher power conversion densities. These are:

(i) higher switching frequencies;
(ii) higher levels of circuit integration;
(iii) improved thermal performance.

The relative portions of space [9] consumed in a square-wave switching dc-dc converter are:

-heatsink	42%
-energy storage components	17%
-PC board	10%
-power semiconductors	5.5%
-control circuits	5.5%
-drive circuits	1%
-unusable volume	19%

(i) The primary motivation for progressing to higher switching frequencies [10] is to reduce the size of the energy storage capacitors and inductors and of the transformers. Significant reductions in the size of these components are achieved when the switching

frequency is increased from tens of kHz to hundreds of kHz. The shift from hundreds of kHz to the megahertz range yields less significant size reductions, but other advantages become evident. In the megahertz range, the component values required for capacitances and inductances are comparable to parasitic elements such as leakage inductances of transformers, inductances of pcb tracks and intrinsic capacitances of switching devices. If these parasitic elements can be adequately controlled during the manufacturing process, they can be used in the design of a circuit, thereby replacing discrete components.

Current research in this area is focused on resonant, quasi-resonant and multi-resonant circuits, which convert power at frequencies up to several MHz or even more.

The belief that as frequency goes up, size goes down is approximately true up to frequencies of about 500 kHz [10]. However, beyond this frequency, phenomena not previously important become so, and size may well begin to increase. For instance, while the required value of capacitors goes down with increasing frequency, the ability of these smaller capacitors to handle currents also goes down, often resulting in a net increase in physical size. Also, capacitor types having a low equivalent series resistance and inductance are required for the operation at high switching frequencies. At some frequency the loss density in magnetic materials increases faster than inductance decreases, requiring larger cores to reduce flux density and loss. Skin and proximity effects are no longer negligible. By using new materials and processes, size reduction can be anticipated. Furthermore, these new materials and processes can result in manufacturing techniques that are reliable, efficient and mass production oriented.

(ii) The power semiconductors, control circuits and drive circuits account for only 12% of the total volume. This is a relatively small portion of the total converter volume because of the application of integration techniques. A second, more recent step, is the use of hybrid integrated circuits. These hybrid ICs incorporate the power semiconductor devices, control circuit and protection circuit. High voltage and high current capabilities are combined with low power electronics into a single monolithic silicon integrated circuit. One of the difficulties which have been encountered in integrating different

semiconductor technologies into a single silicon chip is that the power dissipated in the high voltage/high current section of the chip raises the temperature and thus lowers the reliability of the low power circuitry. However, significant progress is being made in this new technology [11,12].

(iii) The largest area is occupied by the heatsink. There are two factors in the design of the converter which can make a significant difference to the size of the heatsink required. The first is efficiency and the second is the thermal impedance between the power dissipating devices and their heatsinks. The power losses in the switches can be split into two components: the switching losses and the conduction losses. As switching frequency increases, switching losses also increase because the fixed amount of power dissipated during each cycle is repeated more frequently. Switching losses can be virtually eliminated when using quasi-resonant or multi-resonant converters. The conduction losses can be made smaller by reducing the on-state resistance of the power MOSFETs, which are frequently used as the power switch in high-frequency applications.

When using resonant converters a higher power density is achieved by increasing the switching frequency and improving the thermal dissipation by eliminating the switching losses. Further reduction in size and weight is achieved when incorporating the power semiconductors, control and protection circuit on the same chip.

A vast amount of circuit technology for resonant converters has been generated in the past decade and reported in numerous technical journals, conference proceedings and trade magazines. The large class of resonant power converters [13] falls within the following classification scheme:

- *Conventional resonant converters* are often referred to as series resonant converters or parallel resonant converters and their derivations [14]. They are controlled using the frequency modulation technique and can be operated either below or above the resonant frequency.

- *Quasi-resonant converters (QRCs)* [15-38] can be considered as a hybrid of pulse-width-modulated (PWM) converters and resonant converters. While the underlying power conversion principle of QRCs is the same as for PWM converters, a resonant network is employed to shape the current or voltage waveforms of the switch so that it is either operating under zero-current-switching (ZCS) or zero-voltage-switching (ZVS) conditions. The QRCs are suitable for operating at high switching frequencies due to the reduced switching losses. The ZCS quasi-resonant converters were first reported in 1984 and the ZVS quasi-resonant converters in 1986.

- *Multi-resonant converters (MRCs)* [39-62] can offer a wider load range and have a lower peak voltage across or peak current through the switching devices compared to quasi-resonant converters. MRCs are considered most desirable for high-frequency power conversion. Employing the ZVS multi-resonant technique, all semiconductor components in a converter can be operated under ZVS conditions. The multi-resonant converters were first reported in 1988.

1.2. Objectives and Motivations for the Present Work

The objective of this thesis is to present the modelling of quasi-resonant and multi-resonant converters. It is split into two major parts:
- steady-state (dc) modelling;
- small-signal (ac) modelling.
The investigation is carried out using the boost converter and is extended to the buck and buck-boost converters.

The steady-state modelling is based on the research into quasi-resonant and multi-resonant converters by a research group at Virginia Power Electronics Centre, USA, led by Professor Fred C. Lee. The dc model and steady-state characteristics are necessary for the design of the power stage of the converter. The most striking feature of the resonant converters is the wide variety of topologies available. However, there is no general approach that is applicable to the modelling of all classes of converters.

To design the control system and feedback loop, the small-signal model and ac characteristics are necessary. The feedback loop is critical. Feedback can speed up the transient response of a system, improve the recovery from unanticipated disturbances and make performance less sensitive to system variations. However, a system that is stable and insensitive to perturbations in open loop could become sensitive, slow to recover or even completely unstable in closed loop, if the controller reacts inappropiately to the feedback signals. The controller's actions could aggravate deviations from nominal operation instead of rapidly restoring nominal operation. In other words, to obtain the advantages of feedback control, the feedback loop has to be designed and implemented carefully. The first step in closing the loop is to determine the small-signal control-to-output transfer function.

The small-signal modelling is based on the research work carried out by Steve Freeland, R.D. Middlebrook and Slobodan Cuk from California Institute of Technology, USA. They present a method where the averaged model of a dc-dc converter is used to derive its small-signal model in circuit form. However, the expressions for the transfer functions of quasi-resonant converters are not derived. To the knowledge of the author, the derivation of the small-signal transfer functions of the buck, boost or buck-boost multi-resonant converters has not been reported so far. Moreover, there is no general unified method presented for the small-signal modelling of all dc-dc converters (the method is general if it can be applied to buck, boost and buck-boost converters; the method is unified if it can be applied to PWM, quasi-resonant and multi-resonant converters).

1.3. Major Results

The following points are believed to be original contributions to the advancement of knowledge in this field of study.

(i) The concept of characteristic functions is introduced, which describe the average behaviour of the switching devices in a converter. The use of characteristic functions allows the derivation of a general unified model of dc-dc converters.

(ii) A numerical method is described for the steady-state analysis and for the derivation of the characteristic functions of boost zero-voltage-switching multi-resonant converters. The algorithm is implemented in the C programming language.

(iii) A unified dc model describing all classes of boost converters is presented. The mathematical model is verified by simulations using PSPICE and experimental measurements.

(iv) A unified method for the small-signal modelling of boost quasi-resonant and multi-resonant converters is developed. The control-to-output and line-to-output transfer functions are derived. It is shown that the resonant elements do not increase the order of the small-signal model. Therefore, the large amount of knowledge for PWM converters can be applied to quasi-resonant and multi-resonant converters.

(v) The steady-state and small-signal modelling techniques are extended from the boost converter to the buck and buck-boost converters. Therefore, the mathematical models of all classes (ZCS-QRC, ZVS-QRC, ZVS-MRC) of buck, boost and buck-boost converters can be obtained by using the method proposed in this thesis.

1.4. Outline of the Thesis

This thesis consists of seven chapters, a list of references and seven appendices.

Chapter 1 presents a short overview of the subject area, the objectives and motivations for the present work and the major results obtained.

In chapter 2 the fundamentals of the pulse-width-modulated, quasi-resonant and multi-resonant power converters are described.

Chapter 3 presents the steady-state operation, the dc modelling and the derivation of the characteristic functions of boost converters. Analytical results are obtained for quasi-

resonant converters. A numeric method is also described for the analysis of boost multi-resonant converters.

Chapter 4 describes a method for the small-signal modelling of the boost converters, which is based on the averaging technique. The small-signal models in circuit form are obtained and the control-to-output and line-to-output transfer functions are derived.

In chapter 5 the simulation techniques are described, as well as the hardware implementation. The theoretical models are verified by simulation and experimental measurements.

Chapter 6 extends the modelling method to the buck and buck-boost converters and presents a generalised method for the modelling of dc-dc converters.

In chapter 7 the overall conclusions are stated and suggestions for further work are given.

Appendix 1 presents the difference between the half-wave mode and full-wave mode of operation of resonant boost converters. Appendices 2 and 3 show the derivation of the voltage-conversion ratio and characteristic functions. Guidelines for the design of the power converter and feedback loop are given in appendices 4 and 5. Appendix 6 lists the C-program for the analysis of multi-resonant boost converters and appendix 7 presents the list of the 13 published papers relating to this research project.

2. Switched Mode Dc-Dc Power Converters

2.1. Introduction

Electronic power processing technology has evolved around two fundamentally different circuit schemes: duty-cycle modulation, commonly known as Pulse-Width-Modulation (PWM), and resonance.

The PWM technique processes power by interrupting the power flow and controlling the duty cycle, thus, resulting in pulsating current and voltage. Due to circuit simplicity and ease of control, the PWM technique has been used predominantly in today's power electronics industry.

With available devices and circuit technologies, PWM converters have been designed to operate generally with a switching frequency up to 100kHz. In the frequency range of 30-50 kHz, the equipment is deemed optimal in weight, size, efficiency, reliability and cost [24].

During turn-on and turn-off of the switches, the voltages and currents exhibit abrupt increases and decreases of their values, and, therefore, the converters are referred to as "hard-switching".

The resonant techniques process power in a sinusoidal form. The switches are commutated at zero-current and/or zero-voltage. Therefore, resonant converters are referred to as "soft-switching" converters. Compared with PWM converters, the switching losses of resonant converters are reduced.

Soft-switching converters are suitable for operation at high switching frequencies. Numerous converters operating at frequencies in the MHz range have been reported in the literature [18,24,39,63,64,65].

This chapter presents the main classes of switched-mode dc-dc power converters: PWM, quasi-resonant and multi-resonant converters. The rules to obtain the resonant converters from their PWM counterparts are given and the theorems that are satisfied by each family of converters are stated.

2.2. PWM Power Converters

The term "PWM" is used here as a means of distinguishing converters with quasi-rectangular waveforms rather than to indicate any particular control scheme. The three main categories of PWM dc-dc converters are: buck (or step-down), boost (step-up) and buck-boost (step-down/step-up). Their circuit diagrams are shown in figures 2-1 to 2-3.

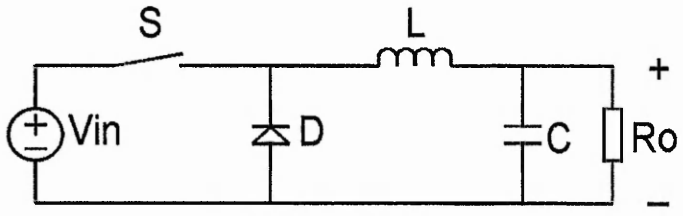

Figure 2-1: Buck converter.

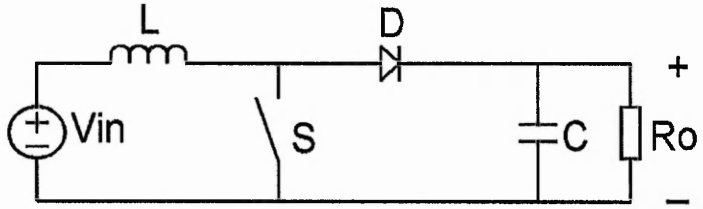

Figure 2-2: Boost converter.

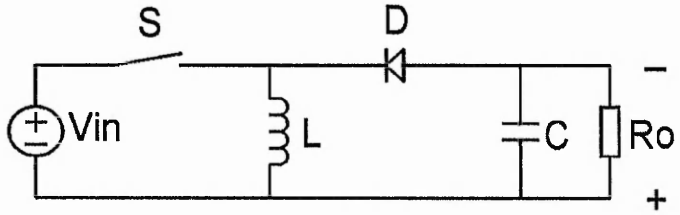

Figure 2-3: Buck-boost converter.

The three different switching converters employ the same three elements: inductor L, power switch S and diode D, but arranged in a different manner. The output capacitor C is a filter element, not part of the switching circuit. Theoretically, there are three other circuits possible using the same three elements with T configuration, but these are simply mirror images of the first three and couple power in the opposite direction [66].

One common principle that applies to all three topologies, regardless of operational mode or control method is that, in steady-state operation, the voltage across the inductor, averaged over each switching cycle, must be equal to zero. Otherwise, the average inductor current would change, violating the steady-state premise.

Each of the three basic circuit families has a unique set of relationships between input and output voltages, currents and duty cycle. The buck converter functions only with output voltage V_{out} less than the input voltage V_{in} and with the same polarity. The boost converter requires a greater output voltage than V_{in} and with the same polarity. The buck-boost converter functions with V_{out} either greater or less than V_{in}, but with opposite polarity.

A PWM converter always satisfies [22]:

Theorem 1: The power switch S, the diode D and a set of capacitors with total voltage V_{off} form a loop. The source V_{in} may also be included in the loop, with its voltage included in V_{off}.

Theorem 2: The power switch S, the diode D and a set of inductors with total current I_{on} form a cut-set.

A number of components in a circuit form a cut-set if they have a common node and the sum of the currents flowing into the common node is equal to the sum of all currents flowing out of the same node.

The quantities V_{off} and I_{on} are easy to find in any particular topology: V_{off} is the peak voltage across and I_{on} is the peak current through the switch S. The expressions for V_{off} and I_{on} for the basic dc-dc converters are given in table 2-1.

Table 2-1: Expressions for V_{off} and I_{on} for the three basic dc-dc converter topologies.

	V_{off}	I_{on}
Buck	V_{in}	I_{out}
Boost	V_{out}	I_{in}
Buck-Boost	$V_{in}+V_{out}$	$I_{in}+I_{out}$

Application of Kirchhoff's laws to the loop and cut-set of theorems 1 and 2 gives:

$v_S + v_D = V_{off}$ and $i_S + i_D = I_{on}$.

2.3. Quasi-Resonant Power Converters

With the progress in power MOSFET manufacturing technology, switching times of fractions of microseconds are now possible. When using PWM converters, the operation at high switching frequencies is accompanied with increased switching losses due to the simultaneous presence of high voltage and high current. On the other hand, when the switch turns on at a high voltage level, the energy stored in the device's output capacitance is dissipated internally. Furthermore, turn-on at high voltage levels induces a severe switching noise through the Miller capacitor coupled into the drive circuit, which leads to significant noise and instability in the drive circuit. The detrimental effects of parasitic elements become more pronounced as the switching frequency is increased. To improve switching behaviour of semiconductor devices in power processing circuits, two techniques were proposed. The zero-current-switching (ZCS) technique was introduced [15] in 1984 by Liu and Lee from Virginia Polytechnic Institute and State University, USA, and the zero-voltage-switching (ZVS) technique was introduced [18] in 1986 by the same authors.

2.3.1. Resonant Switches

For a better understanding of quasi-resonant converters, the concept of resonant switches is introduced. A resonant switch represents a subcircuit consisting of a semiconductor switching device S and resonant elements L_r and C_r. For a zero-current (ZC) resonant switch, as shown in figure 2-4, inductor L_r is in series with the switch S to achieve zero-current switching. In a zero-voltage (ZV) resonant switch, as shown in figure 2-5, capacitor C_r is in parallel with switch S to achieve zero-voltage switching.

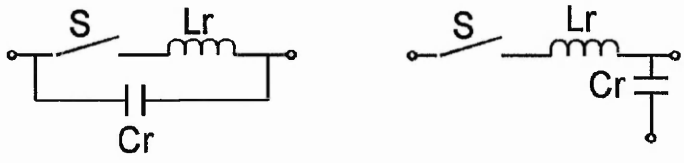

Figure 2-4: Zero-current resonant switches.

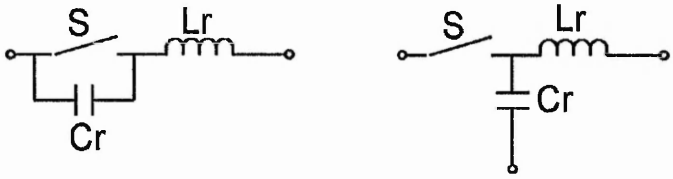

Figure 2-5: Zero-voltage resonant switches.

Zero-Current resonant switches: If the ideal switch S is implemented by a unidirectional switch, as in figure 2-6, the resonant switch is confined to operate in a *half-wave mode*, in the sense that the switch current is permitted to resonate only in the positive half cycle. On the other hand, if diode D_s is connected in antiparallel with Q as shown in figure 2-7, the switch current can flow bidirectionally and the resonant switch now operates in *full-wave mode*.

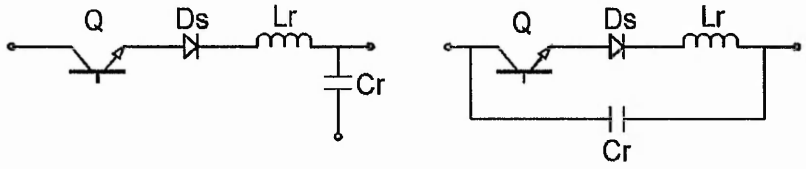

Figure 2-6: Half-wave ZCS configurations.

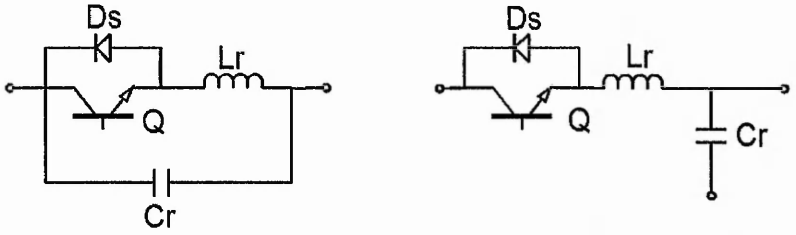

Figure 2-7: Full-wave ZCS configurations.

Zero-Voltage resonant switches: As in the case of a ZC resonant switch, the structure of S determines the operation mode of the ZV resonant switch. If an ideal switch S is implemented by a transistor Q and an antiparallel diode D_s, as shown in figure 2-8, the voltage across capacitor C_r is clamped by D_s at zero during the negative half of the resonant cycle. The resonant switch is operating in half-wave mode. On the other hand, if S is implemented by Q in series with D_s (figure 2-9) and the voltage across C_r can oscillate freely, then the resonant switch is operating in a full-wave mode.

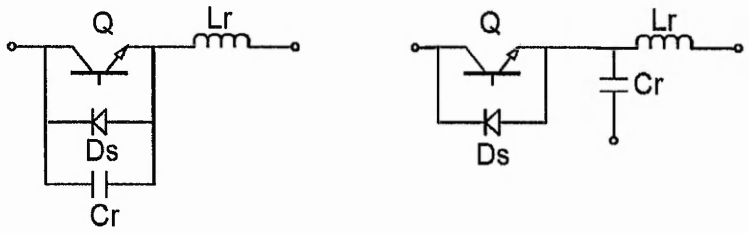

Figure 2-8: Half-wave ZVS configurations.

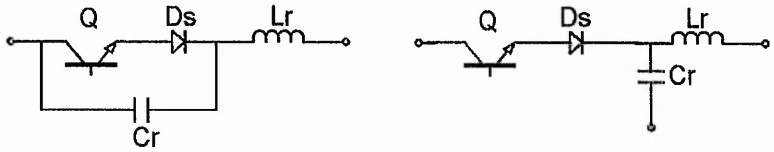

Figure 2-9: Full-wave ZVS configurations.

The switching trajectory [24] of PWM switching behaviour is shown as trajectory A in figure 2-10. The switching device is subjected to simultaneous high voltage and high current. The trajectory of a resonant switch is trajectory B. No simultaneous high voltage and high current are exerted on the switch and the switching losses and stresses are minimal.

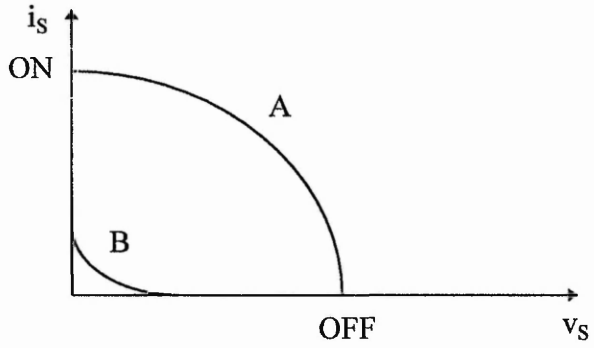

Figure 2-10: Switching trajectory: (A) conventional PWM switching; (B) resonant switching.

2.3.2. Zero-Current-Switching Quasi-Resonant Converters

A ZCS converter is obtained by replacing the switch S in the conventional PWM topology with a zero-current resonant switch, presented in section 2.3.1. The objective of the auxiliary LC resonant elements is to shape the switching device's current waveform during the on-time in order to create a zero-current condition for the device to turn off. The switching losses created by the simultaneous presence of high voltage and high current are eliminated, but turn-on losses due to the output capacitance discharge are not eliminated. The ZCS boost converter topologies are shown in figure 2-11.

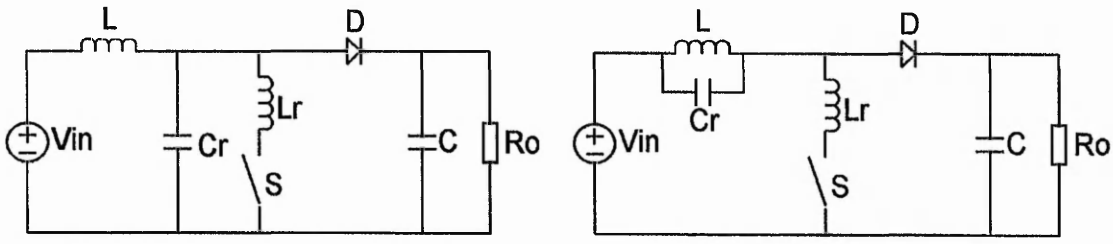

Figure 2-11: ZCS boost converters.

A ZCS converter can operate in a half-wave mode or full-wave mode, depending whether the switch S is a half-wave switch or a full-wave switch.

The following two rules generate all zero-current-switching quasi-resonant topologies [22]:

Rule 1: The resonant capacitor C_r must form a loop with the diode D and a (possibly empty) set of "stiff" capacitors and voltage sources.

Rule 2: The resonant inductor L_r must form a cut-set with the power switch S and a (possibly empty) set of "stiff" inductors.

A "stiff" capacitor or inductor is one with a small switching ripple. All non-resonant capacitors and inductors are assumed "stiff", as in the original PWM converter.

For dc-to-dc converter applications, the zero-current-switching technique is very effective up to 1 MHz, since it can eliminate the switching losses created by the simultaneous presence of high voltage and current. However, to operate the semiconductor switches above one megahertz, the capacitive turn-on loss associated with the discharging of the energy stored in the parasitic junction capacitance of the MOSFET becomes the primary limiting factor. The ZCS QRCs have another drawback at high switching frequencies. The turn-on of the power MOSFET at high voltage levels induces a severe dv/dt noise, which is coupled through the drain-to-gate capacitance to the gate drive circuit. This effect, known as the switching Miller effect, can lead to significant noise and instability in the drive circuit. Turning the switch on at zero voltage eliminates this effect.

2.3.3. Zero-Voltage-Switching Quasi-Resonant Converters

A ZVS converter is obtained by replacing the switch S in the conventional PWM topology with a zero-voltage resonant switch, presented in section 2.3.1. The objective of the auxiliary LC resonant elements is to shape the switching device's voltage waveform during the off-time in order to create a zero-voltage condition for the device to turn on. This technique eliminates the turn-on loss associated with the parasitic junction capacitances. Figure 2-12 shows the ZVS boost topologies.

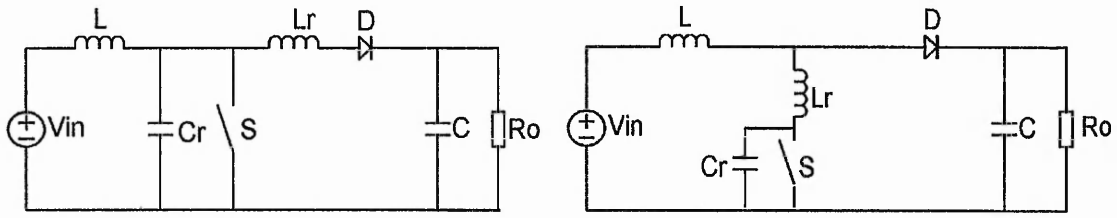

Figure 2-12: ZVS boost converters.

The switch S can be either a full-wave or a half-wave switch. Since ZCS and ZVS converters have in their operation both resonant and non-resonant stages they are referred to as *quasi-resonant converters*.

The following two rules generate all zero-voltage-switching quasi-resonant topologies [22]:

Rule 3: The resonant inductor L_r must form a cut-set with the diode D and a (possibly empty) set of "stiff" inductors.

Rule 4: The resonant capacitor C_r must form a loop with the power switch S and a (possibly empty) set of "stiff" capacitors and voltage sources.

Every quasi-resonant converter, if ZCS or ZVS, satisfies the following theorems:

Theorem 3: The elements S, D, L_r and the elements producing the voltage V_{off} together form a loop.

Theorem 4: The elements S, D, C_r and the inductors producing I_{on} together form a cut-set.

Parasitic capacitances and inductances can be absorbed into the LC resonant circuit. These converters are the most suitable for high-frequency operation and it is shown [30] how the greatest possible number of parasitic reactances are included harmlessly in the resonant circuit.

2.4. Multi-Resonant Power Converters

In quasi-resonant converters a resonant switch with a two-element resonant network (quasi-resonant switch) is used to achieve zero-current-switching or zero-voltage-switching of the main semiconductor switching device. The quasi-resonant switch also effects the switching waveforms of the passive switch [39]. In ZCS-QRCs, the passive switch operates with zero-voltage-switching, while in ZVS-QRCs it operates with zero-current-switching. The concept of multi-resonance explores the possibility of using a resonant switch with a three element resonant network (multi-resonant switch) to achieve either zero-voltage-switching of both the active and passive devices, or zero-current-switching for both devices. There are two families of multi-resonant converters, ZCS-MRCs and ZVS-MRCs.

Multi-resonant converters have been introduced [40] in 1988 by Tabisz and Lee from Virginia Polytechnic Institute and State University, USA.

2.4.1. Multi-Resonant Switches

The zero-current multi-resonant switch is shown in figure 2-13. The resonant circuit is formed in a T-network with resonant inductors L_S and L_D in series with the switching devices and resonant capacitor C_r.

The zero-voltage multi-resonant switch, shown in figure 2-14, is formed in a Π-network with resonant capacitors C_S and C_D connected in parallel with the switching devices and resonant inductor L_r.

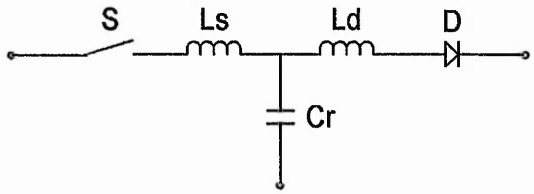

Figure 2-13: ZC multi-resonant switch.

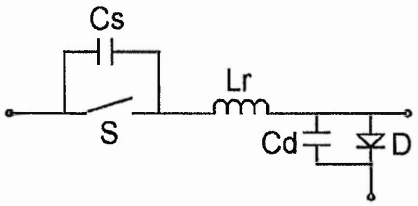

Figure 2-14: ZV multi-resonant switch.

During operation of a MRC, three different resonant circuits can be formed, depending on whether the active switch and diode are open or closed. This results in operation of the converter with three resonant stages in one cycle of operation, hence the term "multi-resonant".

2.4.2. Zero-Current-Switching Multi-Resonant Converters

A ZCS-MRC is obtained by the addition of the zero-current multi-resonant network to the related PWM converter. As an example, the boost ZCS multi-resonant converter is shown in figure 2-15. For optimal operation, the parasitic capacitances of the switching devices should be ideally zero. However, in practical high-frequency applications, these capacitances cannot be reduced to negligible values and, as a result, oscillations are present in the waveforms [43].

In ZCS-MRCs the on-time is maintained constant and the off-time is adjusted to obtain regulation of the output. During the off-time of the power MOSFET a high-frequency oscillation is superimposed to the voltage across the MOSFET due to the parasitic capacitance of the device. When the MOSFET is turned on, the energy stored in its output capacitance is dissipated, just as in PWM converters or ZCS-QRCs. During off-time of the output diode D, an oscillation is superimposed on the voltage across the diode. The oscillation occurs because of the parasitic capacitance of the diode.

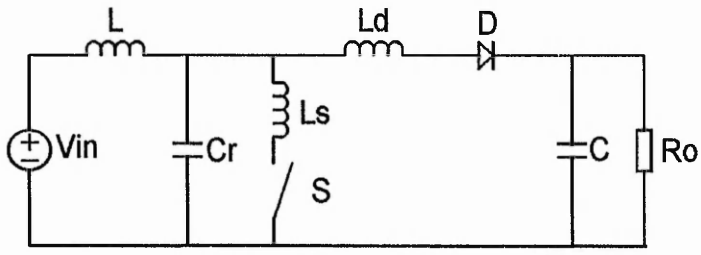

Figure 2-15: ZCS multi-resonant boost converter.

This technique is not suitable for high-frequency applications. In fact, ZCS-MRCs exhibit the major problems of both ZCS-QRCs (capacitive turn-on) and ZVS-QRCs (parasitic oscillation of the diode voltage). However, the ZCS-MRC technique could be useful in high-power high-current converters. In this thesis the ZCS-MRC technology is not addressed in more detail.

2.4.3. Zero-Voltage-Switching Multi-Resonant Converters

A ZVS-MRC is obtained by the addition of the zero-voltage multi-resonant network to the corresponding PWM converter. As an example, the boost ZVS multi-resonant converter is shown in figure 2-16.

The arrangement of the multi-resonant network results in the absorption in the resonant circuit of all major parasitic components, including power MOSFET output capacitance, diode junction capacitance and leakage inductances. This allows the multi-resonant converters to operate at high frequencies with favourable switching conditions (zero-voltage switching) for all semiconductor devices. If the converter is operated at a sufficiently high switching frequency, the resonant elements can be formed exclusively by the parasitic components [43].

In ZVS-MRCs the off-time is constant and the on-time is adjusted to regulate the output.

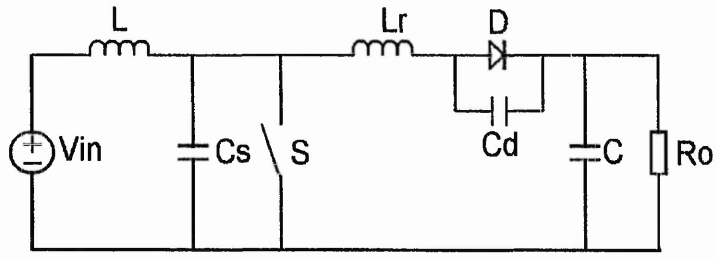

Figure 2-16: ZVS multi-resonant boost converter.

The ZVS-MRCs can be operated in either a half-wave mode, with a diode connected in antiparallel to the MOSFET, or a full-wave mode, with the diode in series with a MOSFET.

ZVS-MRCs are superior to ZVS-QRCs due to reduced switch voltage stress and improved load range. MRCs also eliminate the oscillations which appear in the ZVS

QRCs when the output diode turns off. Its parasitic junction capacitance oscillates with the resonant inductance. If damped, these oscillations cause significant power dissipation at high frequencies; undamped, they adversely affect the voltage gain of the converter and, thus, the stability of the closed-loop system [40].

Multi-resonant and quasi-resonant converters have one more advantage over PWM converters - the electromagnetic interference is reduced due to soft-switching [67,68].

ZVS multi-resonant converters can be obtained from PWM converters by adding two resonant capacitors C_S and C_D and a resonant inductor L_r according to the following three rules [52]:

Rule 5: The resonant capacitor C_S must form a loop with the power switch S and a (possibly empty) set of "stiff" capacitors and voltage sources.

Rule 6: The resonant capacitor C_D must form a loop with the diode D and a (possibly empty) set of "stiff" capacitors and voltage sources.

Rule 7: The resonant inductor L_r must form a cut-set with the diode D, the capacitor C_D and a (possibly empty) set of "stiff" inductors.

A MRC converter satisfies theorems 3 and 4a:

Theorem 4a: The elements S, D, C_S, C_D and the inductors producing I_{on} together form a cut-set.

2.5. Conclusions

To enable the operation of dc-dc converters at high switching frequencies and to reduce the switching stresses and losses of PWM converters, the two-element resonant switch is introduced and implemented in the forms of zero-current-switching and zero-voltage-switching. By direct application of the resonant switches into PWM converters, the

family of quasi-resonant converters is obtained. This family of converters allows numerous topological variations. It can be divided into two classes, one class is referred to as ZCS-QRCs, the other referred to as ZVS-QRCs. ZCS-QRCs and ZVS-QRCs again can be subdivided into two categories: half-wave mode and full-wave mode, depending upon whether the resonant switch is unidirectional or bidirectional.

The three-element multi-resonant switch is introduced and implemented in the forms of zero-current-switching and zero-voltage-switching. By direct application of multi-resonant switches into PWM converters, the family of multi-resonant converters is obtained, which can be divided in ZCS-MRCs and ZVS-MRCs. ZCS-MRCs are not used in high-frequency applications and will not be analysed further in this thesis.

3. Steady-State Modelling of Boost Converters

3.1. Introduction

To understand the operation of a converter and to be able to obtain its dc characteristics, the steady-state analysis has to be undertaken.

A switching cycle in the PWM boost converter is divided into two stages, depending on the on-state and off-state of the switching devices. In quasi-resonant converters, for which the resonant tank consists of two resonant elements, a switching cycle is divided into four stages, three of which are linear and one is resonant. In multi-resonant converters, for which the resonant tank consists of three resonant elements, a switching cycle is divided in four stages as well, but only one is linear and the other three are resonant.

This chapter presents the analysis of each of the stages of a switching cycle in steady-state operation. The variation of the output voltage with respect to the switching frequency is determined.

A method for the dc modelling of boost converters is presented. The dc modelling of boost resonant converters is referred to the PWM converter. The averaging technique is used, which proves to be a very efficient method for the modelling of dc-dc converters. It allows the derivation of a general model to calculate the voltage conversion ratio of a converter.

The new concept of characteristic function is defined, which describes the average behaviour of a switch. For quasi-resonant converters, analytic expressions are obtained, but for multi-resonant converters a numerical method has to be used. The duration of one of the operating stages of the MRC is obtained by solving a transcendental equation, for which a numeric algorithm needs to be used.

3.2. Steady-State Operation and DC Modelling of PWM Converters

The boost or step-up converter has an output that is always of the same polarity but greater than the input voltage - hence the name "boost". One supply line must be common to both input and output. This may be either the positive or negative line, depending on the design.

The operation of the boost converter can be divided into two stages, which are described below. Figure 3-1 shows the equivalent circuit of each stage.

Stage 1: When the switch S turns on, the supply voltage is impressed across the input inductor L. The current i_L, which flows from the source through the inductor, the switch, and back around to the source, increases linearly. During this portion of the cycle the inductor stores energy. Diode D is reverse-biased and not conducting. At the same time, current flows from the output capacitor C into the load. Hence, capacitor C is discharging.

Stage 2: When the switch S turns off, the current in L continues to flow in the same direction, decaying linearly, and the voltage across the inductor reverses polarity. The current path is from the source through the inductor, through the now forward-biased diode, through the output capacitor in parallel with the load, and back to the source to complete the path. During this portion of the cycle, the energy stored in the inductor is transferred to the output capacitor and the load. This completes one cycle. At the start of a new cycle, when the switch turns on, the diode is reverse biased, and the capacitor alone must supply the current to the load.

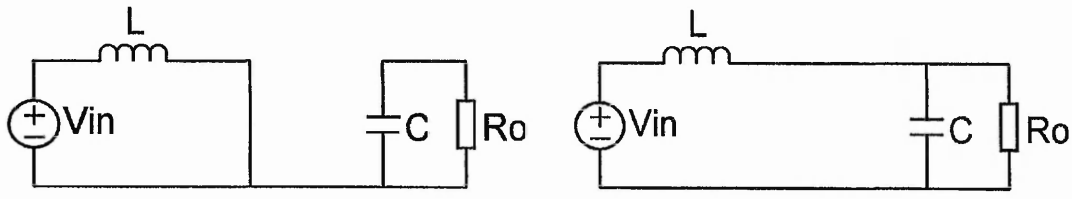

Figure 3-1: Equivalent circuits of the two stages of a operating cycle of a PWM boost converter.

The voltage conversion ratio x of a dc-dc converter is defined as the ratio of the output voltage and input voltage, $x = \frac{V_{out}}{V_{in}}$. For the boost converter the voltage conversion ratio is determined knowing that the average voltage across the inductor over one complete cycle is zero. During on-time, the voltage across the inductor is V_{in} and during off-time the voltage across L is equal to $(V_{in} - V_{out})$ and is negative.

Therefore,

$V_{in}T_{on} + (V_{in} - V_{out})T_{off} = 0.$

If the duty ratio of a PWM converter is defined as $d = \frac{T_{on}}{T_S}$, the voltage conversion ratio of the boost converter is

$$x = \frac{1}{1-d}. \tag{3.1}$$

Figure 3-2 shows the dependence of x on the duty ratio d.

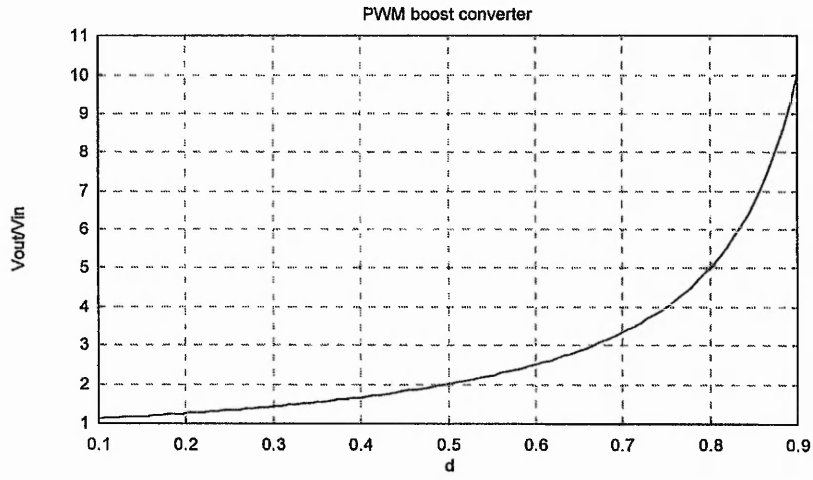

Figure 3-2: Voltage conversion ratio of a PWM boost converter.

The static and dynamic behaviour of many classes of power circuits can be analysed by using the averaging technique [69]. It represents a trade-off between accuracy and simplicity, which no doubt accounts for its widespread adoption.

The averaging technique has a solid mathematical basis. Averaged-circuit models have traditionally been derived mainly for switched-mode dc-dc converters.

A variable x(t) can be averaged, for a fixed T, as follows:

$$\bar{x}(t) = \frac{1}{T}\int_{t-T}^{t} x(\tau)d\tau .$$

This average at any time is taken over the preceding interval of length T. An appropriate choice of T is required and it is chosen to be equal to the shortest regular switching interval associated with the operation of the converter. Where $x(\tau)$ is periodic, the averaging interval T is equal to the period. The function $\bar{x}(t)$ is smoother than x(t) and is a continuous function of time. It can be easily verified that the derivative of the average of a variable equals the average of the derivative. Both Kirchoff's voltage and current laws are valid for averaged quantities as well as for instantaneous ones.

The average equivalent circuit can be constructed as follows. All instantaneous voltages and currents are replaced by their averages and all linear-time-invariant components remain unchanged. Nonlinear or time-varying components in the original circuit, however, do not map into the same components in the averaged circuit. For example, switches in the original circuit become elements in the averaged circuit that simultaneously have a nonzero (average) voltage and nonzero (average) current - and so are no longer switches.

The assumptions that are made [69] to obtain an averaged model are:
- a small ripple assumption, namely, that the voltage across the capacitor C and the current through the inductor L at time t are well approximated by their average values;
- a slow variation assumption, namely, that these two average values do not vary significantly over any interval of length T, that is, they vary more slowly than one half the switching frequency.

Both assumptions are satisfied in well-designed high-frequency switching converters operating in continuous conduction.

The averaging technique is exemplified using a PWM boost converter. The average values of the reverse voltage across the output diode v_D and the current through the power switch i_S are, respectively:

$$\bar{v}_D = \frac{1}{T_S}\int_0^{T_s} v_D(t)dt \quad \text{and} \tag{3.2}$$

$$\bar{i}_S = \frac{1}{T_S}\int_0^{T_s} i_S(t)dt, \tag{3.3}$$

where T_S is the switching period value.

From the steady-state analysis it is calculated that:

$$\bar{v}_D = dV_{out}; \tag{3.4}$$

$$\bar{i}_S = dI_{in}. \tag{3.5}$$

Figure 3-3 presents the averaged circuit of a boost converter. Considering that $\bar{v}_S = V_{out} - \bar{v}_D$ and $\bar{i}_D = I_{in} - \bar{i}_S$, an equivalent averaged circuit is presented in figure 3-4.

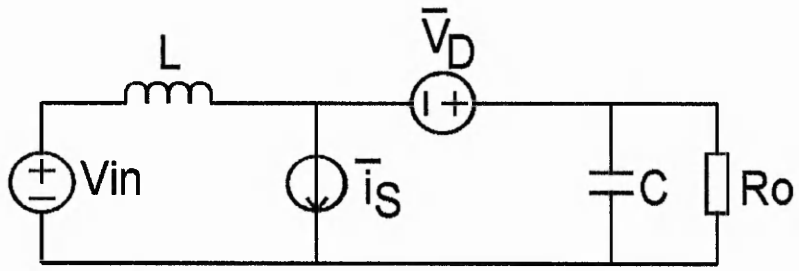

Figure 3-3: Averaged circuit of a PWM boost converter.

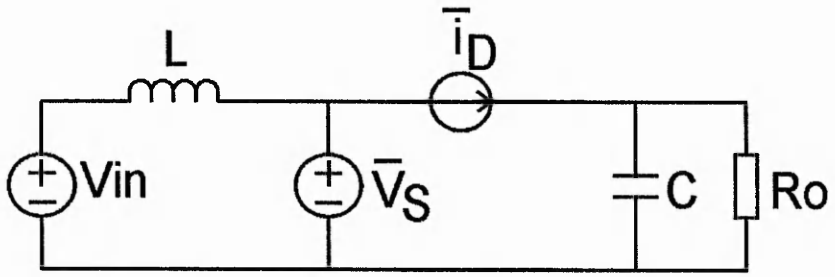

Figure 3-4: Averaged circuit equivalent to the one in figure 3-3.

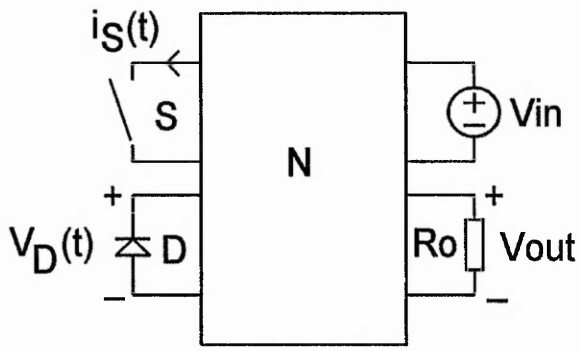

Figure 3-5: Dc-dc converter model.

The PWM converter can be considered as a linear and time invariant network N connected to the time varying devices switch and diode [22], as shown in figure 3-5. The network N has three inputs - reverse voltage across the diode D, $v_D(t)$, current through the switch S, $i_S(t)$ and input voltage V_{in} - and a single output V_{out}, the voltage across the load. Since the network N is linear, the average of its output can be found by driving the network with only the averages of its inputs. Specifically, the voltage conversion ratio x is unchanged if S and D are replaced with sources generating the averages of i_S and v_D. The averaged model of a dc-dc PWM converter is shown in figure 3-6.

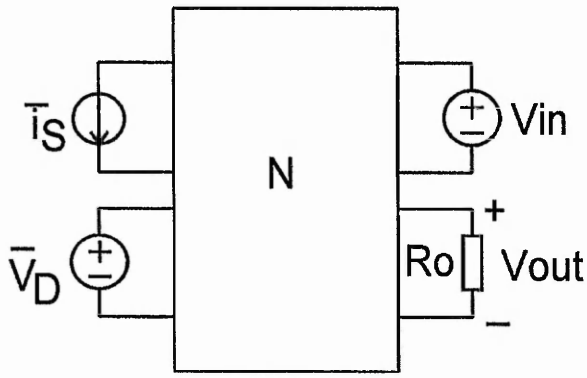

Figure 3-6: Average model of dc-dc converter.

3.3. Steady-State Operation of Quasi-Resonant Converters

In order to simplify the steady-state analysis of the boost converters, the following assumptions are made:

- the input inductor L is sufficiently large so that the input source can be treated as a constant current source I_{in};

- the output capacitor C is sufficiently large so that the output load can be treated as a constant voltage load V_{out};

- the power switches and diodes are ideal (no forward voltage drops in the on-state, no leakage currents in the off-state, no time delays at turn-on and turn-off, no parasitic capacitances);

- the reactive elements of the tank circuit are ideal.

Since the circuit's behaviour is largely determined by the values of the resonant elements L_r and C_r, the following parameters are defined as:

- characteristic impedance: $Z_r = \sqrt{\frac{L_r}{C_r}}$; (3.6)

- resonant angular frequency: $\omega_r = \frac{1}{\sqrt{L_r C_r}}$; (3.7)

- resonant frequency: $f_r = \frac{\omega_r}{2\pi}$; (3.8)

- normalised load resistance: $r = \frac{R_0}{Z_r}$. (3.9)

3.3.1. Zero-Current-Switching Boost Converters

In a zero-current-switching (ZCS) converter the switch uses auxiliary LC resonant elements to shape the switching device's current waveform during the on time in order to create a zero-current condition for the switch to turn off. The on-time is therefore determined by the natural frequency of the resonant tank and is constant. To regulate the output voltage against line and load variations, the off-time is varied. The switching

losses created by the simultaneous presence of high voltage and high current are eliminated.

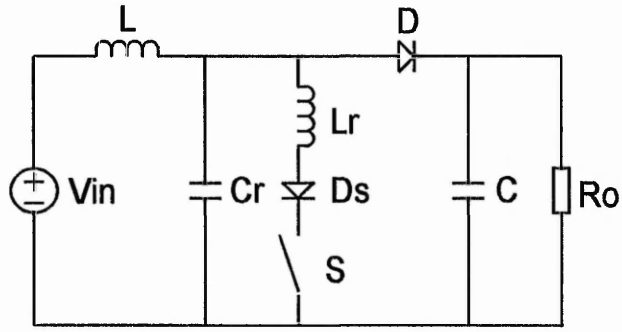

Figure 3-7: Zero-current-switching quasi-resonant boost converter.

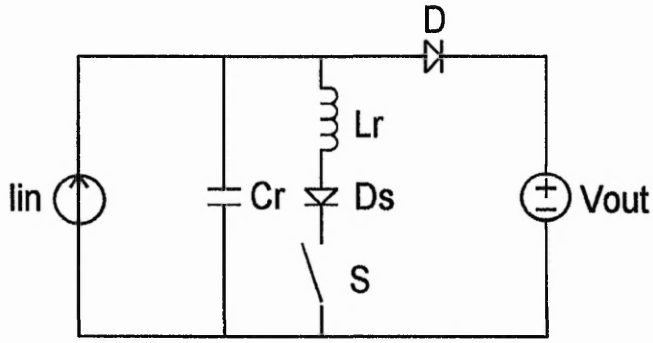

Figure 3-8: Simplified equivalent circuit.

The ZCS quasi-resonant boost converter is shown in figure 3-7 and the simplified equivalent circuit is shown in figure 3-8. For the half-wave implementation, diode D_S is connected in series with the power switch to provide reverse blocking capability, as shown in figure 3-7. To implement a full-wave ZCS converter, diode D_S is connected in anti-parallel with the power switch to provide reverse conduction capability.

In steady-state operation, a complete switching cycle can be divided into four stages starting from the moment diode D turns on. Before the beginning of a commutation cycle, the topological state of the circuit is as follows:

- the output diode D is in the off state;
- the power switch S is in the off state;
- the resonant capacitor voltage is increasing to V_{out}.

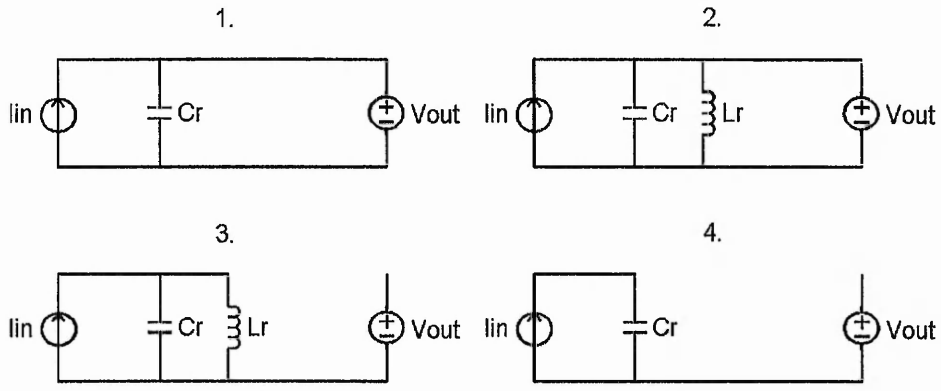

Figure 3-9: Equivalent circuits of the four stages.

The following description summarises the circuit operation during each of the four stages.

1. *Energy Transfer Stage* [T_0, T_1]:

Diode D is conducting and switch S is off. The input current I_{in} flows through D and transfers energy to the load, represented by the constant voltage source V_{out}. This stage finishes at time T_1 when switch S is turned on. The duration T_{01} of this stage is variable and determines the output voltage.

2. *First Linear Stage (Inductor-Charging Stage)* [T_1, T_2]:

At $t=T_1$ the switch is turned on. The resonant inductor current i_{Lr} rises linearly and is represented by the following equation:

$$i_{Lr} = \frac{V_{out}\, t}{L_r}. \tag{3.10}$$

This stage finishes at the time $t=T_2$ when $i_{Lr}=I_{in}$. The diode D is turned off and the resonant stage begins. The duration T_{12} of the first linear stage is given by:

$$T_{12} = \frac{I_{in}\, L_r}{V_{out}}. \tag{3.11}$$

3. *Resonant Stage* [T_2, T_3]:

The current i_{Lr} increases in a sinusoidal manner, reaches the maximum and then decreases until zero. The resonant capacitor is discharged and it holds at the end of this stage a negative value. The state equations are:

$$C_r \frac{dv_{Cr}}{dt} = I_{in} - i_{Lr},$$

$$L_r \frac{di_{Lr}}{dt} = v_{Cr}.$$

The initial conditions are:

$i_{Lr}(0)=I_{in}$ and $v_{Cr}(0)=V_{out}$.

Solving the above system the following time solutions are obtained:

$$i_{Lr}(t) = I_{in} + \frac{V_{out}}{Z_r} \sin \omega_r t; \tag{3.12}$$

$$v_{Cr}(t) = V_{out} \cos \omega_r t. \tag{3.13}$$

At time $t=T_3$ the current i_{Lr} is equal to zero and S is turned off.

The duration of this stage is $T_{23}=a_{zcs}/\omega_r$, (3.14)

where

$$a_{zcs} = \arcsin\left(-\frac{Z_r I_{in}}{V_{out}}\right) = \arcsin\left(-\frac{x}{r}\right). \tag{3.15}$$

It is shown in appendix 1 that for half-wave mode

$$a_{zcs} = \pi + \arcsin\left(\frac{x}{r}\right)$$

and for full-wave mode

$$a_{zcs} = 2\pi - \arcsin\left(\frac{x}{r}\right).$$

4. *Second Linear Stage (Capacitor Charging Stage)* [T_3, T_4]:

At time $t=T_3$ the resonant capacitor is charged linearly by the input current I_{in}, the initial condition being: $v_{Cr}(0)=V_{out}\cos a_{zcs}$.

The state equation is:

$$C_r \frac{dv_{Cr}}{dt} = I_{in}.$$

The time solution is:

$$v_{Cr}(t) = V_{out}\cos a_{zcs} + \frac{I_{in}}{C_r}t. \tag{3.16}$$

This stage finishes at time $t=T_4$ when the resonant capacitor voltage reaches the output voltage and the diode D is turned on.

The duration of this stage is:

$$T_{34} = \frac{1}{\omega_r}\frac{V_{out}}{Z_r I_{in}}(1-\cos a_{zcs}). \tag{3.17}$$

The equivalent circuits of the converter in the four stages are shown in figure 3-9.

The mathematical description of the four stages of a operating cycle is summarised table 3-1. The voltages v and currents i are normalised as follows:

$$v^* = \frac{v}{V_{out}}; \tag{3.18}$$

$$i^* = \frac{iZ_r}{V_{out}}. \tag{3.19}$$

The normalised input current is

$$\alpha = \frac{I_{in}Z_r}{V_{out}} \tag{3.20}$$

and $a_{zcs} = \arcsin(-\alpha)$ for ZCS converters.

Table 3-1: Normalised equations for the ZCS boost converter.

	Stage 1	Stage 2	Stage 3	Stage 4
$i_S^*(t)$	0	$\omega_r t$	$\alpha+\sin(\omega_r t)$	0
$i_D^*(t)$	α	$\alpha-\omega_r t$	0	0
$v_S^*(t)$	1	0	0	$\alpha\omega_r t+\cos(a_{zcs})$
$v_D^*(t)$	0	0	$1-\cos(\omega_r t)$	$1-\alpha\omega_r t-\cos(a_{zcs})$
duration	T_{01}	$\frac{\alpha}{\omega_r}$	$\frac{a_{zcs}}{\omega_r}$	$\frac{1}{\omega_r}\frac{1}{\alpha}(1-\cos(a_{zcs}))$

The waveforms of the normalised currents and voltages are shown in figures 3-10 and 3-11.

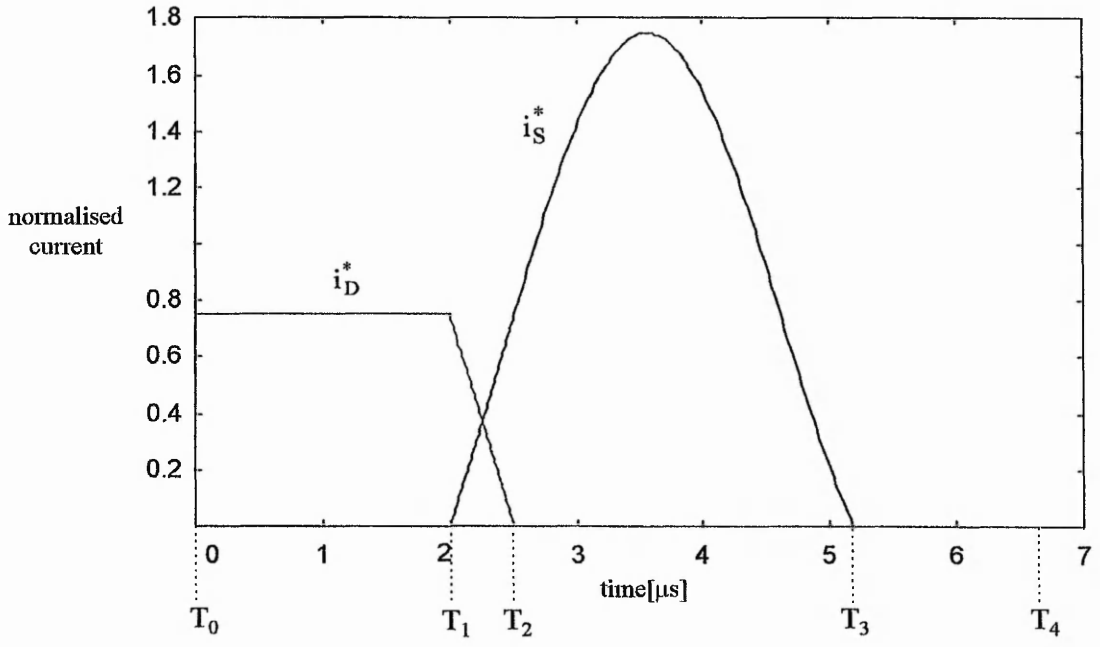

Figure 3-10: Current waveforms of the boost ZCS quasi-resonant converter.

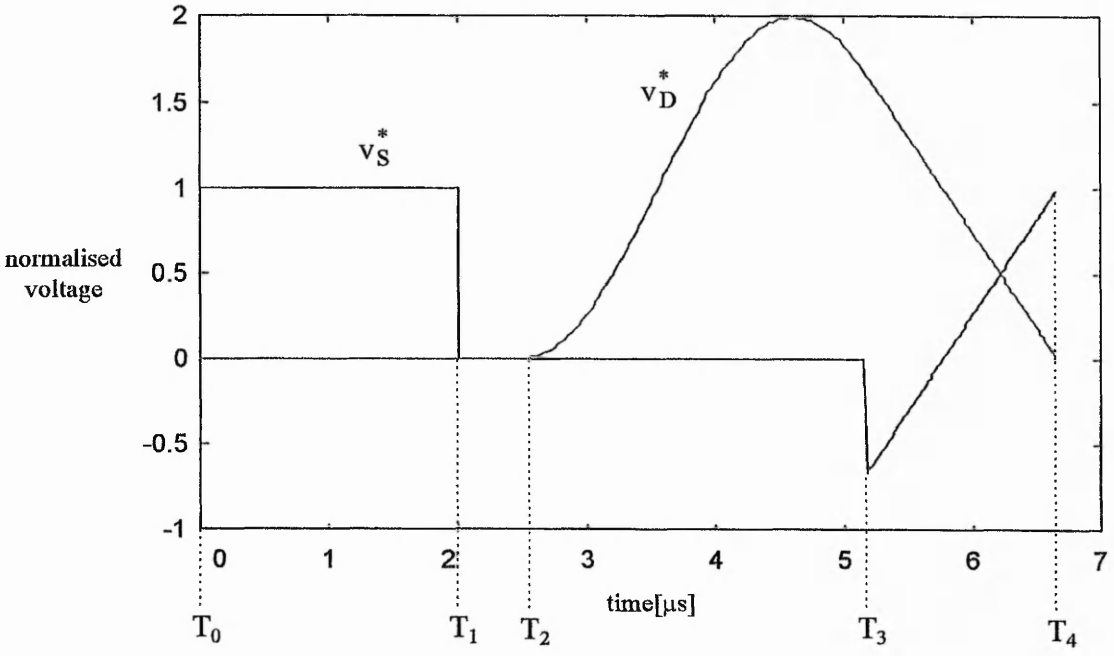

Figure 3-11: Voltage waveforms of the boost ZCS quasi-resonant converter.

The steady-state behaviour of the ZCS converter can be obtained simply by solving the state equations of the four stages in a switching cycle. The dc voltage conversion ratio $x=V_{out}/V_{in}$ depends on the normalised load resistance and switching frequency. It is shown in appendix 2 that for the half-wave ZCS boost converter:

$$\frac{f_S}{f_r} = 2\pi \frac{(x-1)}{x} \frac{1}{\frac{x}{2r} + \pi + \arcsin\left(\frac{x}{r}\right) + \frac{r}{x}\left(1+\sqrt{1-\frac{x^2}{r^2}}\right)}. \tag{3.21}$$

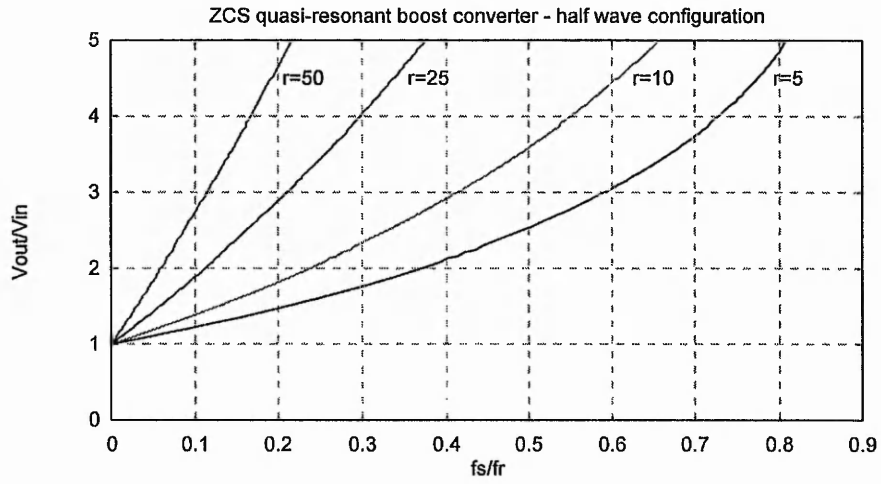

Figure 3-12: Voltage conversion ratio versus normalised switching frequency for the half-wave configuration.

For converters having a full-wave switch:

$$\frac{f_S}{f_r} = 2\pi \frac{(x-1)}{x} \frac{1}{\frac{x}{2r} + 2\pi - \arcsin\left(\frac{x}{r}\right) + \frac{r}{x}\left(1-\sqrt{1-\frac{x^2}{r^2}}\right)}. \tag{3.22}$$

The dc voltage conversion ratio versus normalised switching frequency is plotted for different loads in figure 3-12 for half-wave converters and in figure 3-13 for full-wave converters.

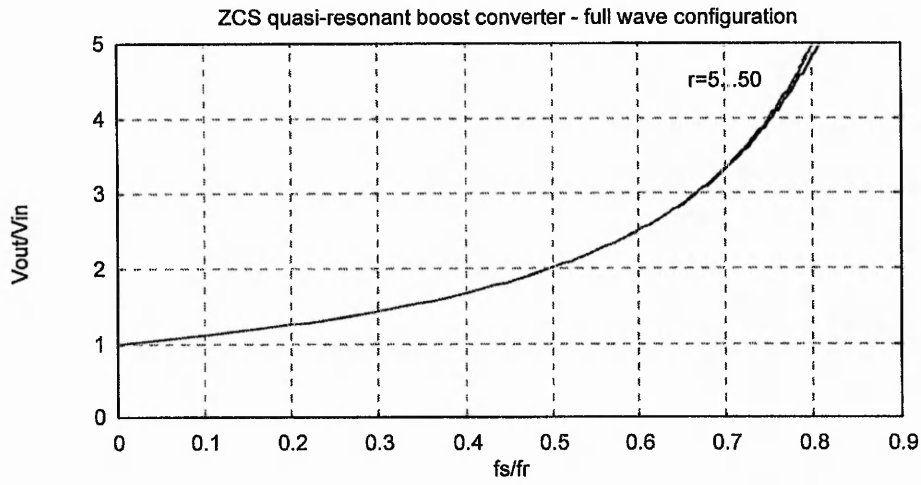

Figure 3-13: Voltage conversion ratio versus normalised switching frequency for the full-wave configuration.

Comparison of half-wave and full-wave mode quasi-resonant converter topologies is based mainly on the sensitivity of the voltage conversion ratio (V_{out}/V_{in}) to load variations. Full-wave mode topologies are less sensitive to load variations since they are able to return excessive tank energy to the source. This results in a narrower frequency range operation under varying line voltage and load. Half-wave converters, on the other hand, operate with a wide frequency range since the voltage conversion ratio is sensitive to load variations.

Half-wave ZCS-QRCs are usually operated at higher efficiencies than full-wave ZCS-QRCs due to the additional circulating current in the full-wave operation. A practical limitation [17] exists which makes the full-wave mode topologies rather unattractive for high-frequency applications. The limitation is due to the reverse recovery characteristic of the anti-parallel diode D_S which, in conjunction with the resonant inductor, gives rise to a high voltage spike and oscillations. The spike causes severe stress and power dissipation in the switch. The spike magnitude can be reduced by using a snubber across the switch. However, this approach is not recommended since it results in a significant drop in efficiency. The half-wave ZCS-QRCs do not suffer from the described problem.

The peak current of the power switch is

$$I_{Speak} = I_{in} + \frac{V_{out}}{Z_r} \text{ or}$$

$I_{Speak}=I_{out}(x+r)$.

The peak voltage of the switch during off-state is $V_{Speak}=V_{out}$.

The peak current through the output diode is $I_{Dpeak}=I_{in}$.

The peak voltage of diode D is $V_{Dpeak}=2V_{out}$.

The load range is limited, from a minimum load resistance $R_{loadmin}=xZ_r$ to a infinite load resistance (open circuit). When the load current is increased beyond the limit set by $R_{loadmin}$, the zero-current switching property will be lost.

3.3.2. Zero-Voltage-Switching Boost Converters

In a zero-voltage-switching (ZVS) converter the switch uses auxiliary LC resonant elements to shape the switching device's voltage waveform during off time in order to create a zero-voltage condition for the device to turn on. The off-time is therefore determined by the natural frequency of the resonant tank and is constant. To regulate the output voltage against line and load variations the on-time is varied. The switching losses, both at turn-on and turn-off are negligible.

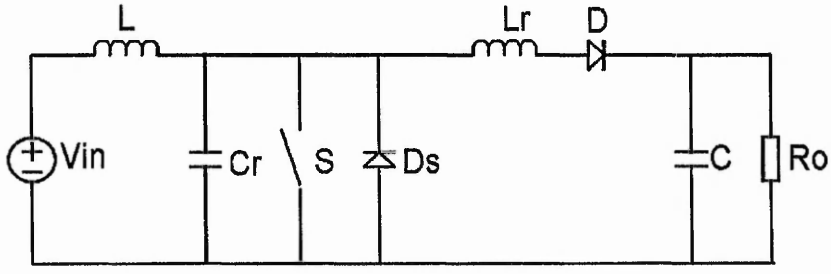

Figure 3-14: Zero-voltage-switching quasi-resonant boost converter.

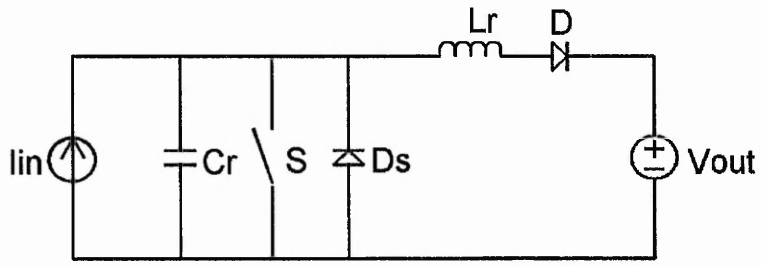

Figure 3-15: Simplified equivalent circuit.

The ZVS quasi-resonant boost converter is shown in figure 3-14 and the simplified equivalent circuit is shown in figure 3-15. For the half-wave implementation, diode D_S is connected in anti-parallel with the power switch to provide reverse conduction capability, as shown in figure 3-14. To implement a full-wave ZVS converter, diode D_S is connected in series with the power switch to provide reverse blocking capability.

In steady-state operation, a complete switching cycle can be divided into four stages starting from the moment the output diode D turns off. Before the beginning of a commutation cycle, the topological state of the circuit is as follows:

- diode D is on;
- switch S is on;
- the current i_{Lr} through the resonant inductor drops until it reaches zero.

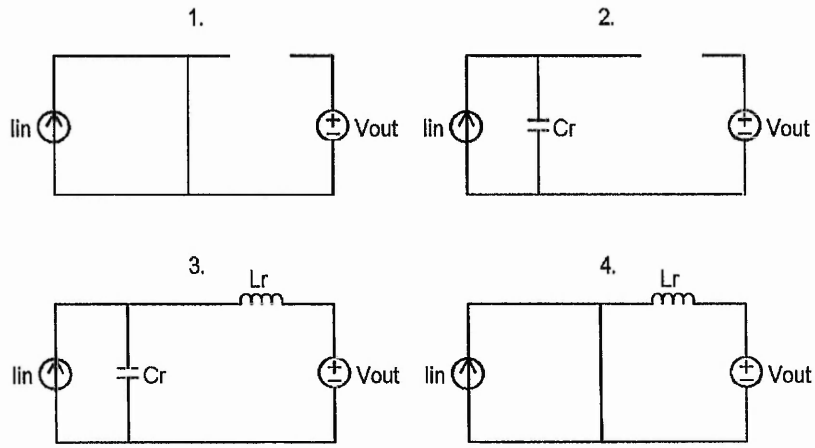

Figure 3-16: Equivalent circuit of the four stages.

The following description summarises the circuit operation during each of the four stages.

1. *Energy Transfer Stage* $[T_0, T_1]$:

At time T_0, the entire input current I_{in} flows through switch S until S is turned off again at T_1. Diode D is off. The duration of this stage T_{01} is an independent variable and determines the output voltage.

2. *First Linear Stage (Capacitor Charging Stage)* $[T_1, T_2]$:

At $t=T_1$ the switch is turned off. The input current I_{in} flows into C_r and the voltage $v_{Cr}(t)$ across C_r rises linearly.

Initial condition:

$$v_{Cr}(0)=0.$$

State equation:

$$C_r \frac{dv_{Cr}}{dt} = I_{in}.$$

The time solution is:

$$v_{Cr}(t) = \frac{I_{in}}{C_r} t. \tag{3.23}$$

At time T_2, v_{Cr} reaches V_{out} and diode D begins to conduct. The duration T_{12} of this stage can be determined from:

$$T_{12} = C_r \frac{V_{out}}{I_{in}}. \tag{3.24}$$

3. *Resonant Stage* $[T_2,T_3]$:

Diode D turns on at T_2 and a portion of I_{in} starts to flow into V_{out}.

Initial conditions:

$$i_{Lr}(0) = 0 \text{ and } v_{Cr}(0) = V_{out}.$$

State equations:

$$L_r \frac{di_{Lr}}{dt} = v_{Cr} - V_{out};$$

$$C_r \frac{dv_{Cr}}{dt} = I_{in} - i_{Lr}.$$

The state equations are solved, obtaining the time solutions:

$$i_{Lr}(t) = I_{in}(1-\cos\omega_r t)\,; \tag{3.25}$$

$$v_{Cr}(t) = V_{out} + Z_r I_{in}\sin\omega_r t\,. \tag{3.26}$$

Normally, in the half wave mode of operation, switch S shall turn on after v_{Cr} drops to zero at T_3 and before the current through D_s drops to zero. Otherwise, capacitor C_r will begin to recharge and S will lose the opportunity to turn on under zero-voltage conditions.

The duration of this stage T_{23} is determined by setting $v_{Cr}(T_{23})=0$ and is

$$T_{23} = \frac{a_{zvs}}{\omega_r}, \tag{3.27}$$

where

$$a_{zvs} = \arcsin(-\frac{V_{out}}{Z_r I_{in}}) = \arcsin(-\frac{r}{x})\,. \tag{3.28}$$

It is shown in appendix 1 that for half-wave mode

$$a_{zvs} = \pi + \arcsin(\frac{r}{x})$$

and for full-wave mode

$$a_{zvs} = 2\pi - \arcsin(\frac{r}{x})\,.$$

4. Second Linear Stage (Inductor Discharging Stage) [T_3, T_4]:

After time T_3 current i_{Lr} drops linearly and reaches zero at time T_4.

Initial condition:

$i_{Lr}(0)=I_{in}(1-\cos a_{zvs})$.

State equation:

$$L_r\frac{di_{Lr}}{dt} = -V_{out}\,.$$

Time solution:

$$i_{Lr}(t) = -\frac{V_{out}}{L_r}t + I_{in}(1-\cos a_{zvs}) \tag{3.29}$$

The duration of this stage is:

$$T_{34} = L_r I_{in}\frac{1-\cos a_{zvs}}{V_{out}}\,. \tag{3.30}$$

The equivalent circuits of the zero-voltage-switching quasi-resonant boost converter for the four stages are shown in figure 3-16.

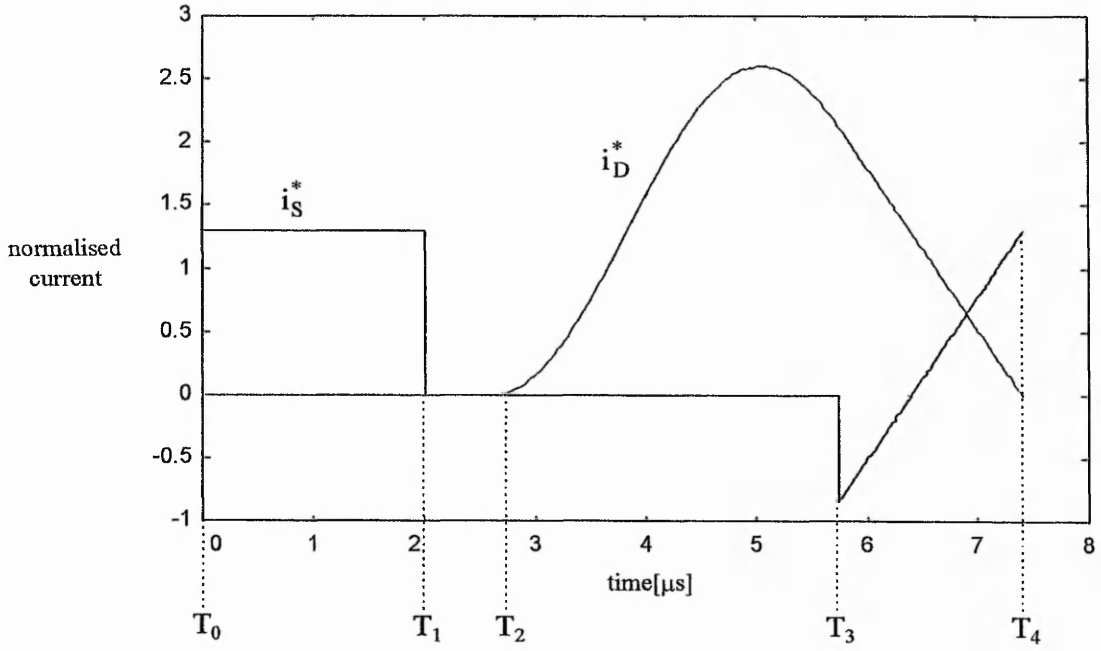

Figure 3-17: Current waveforms of the boost ZVS quasi-resonant converter.

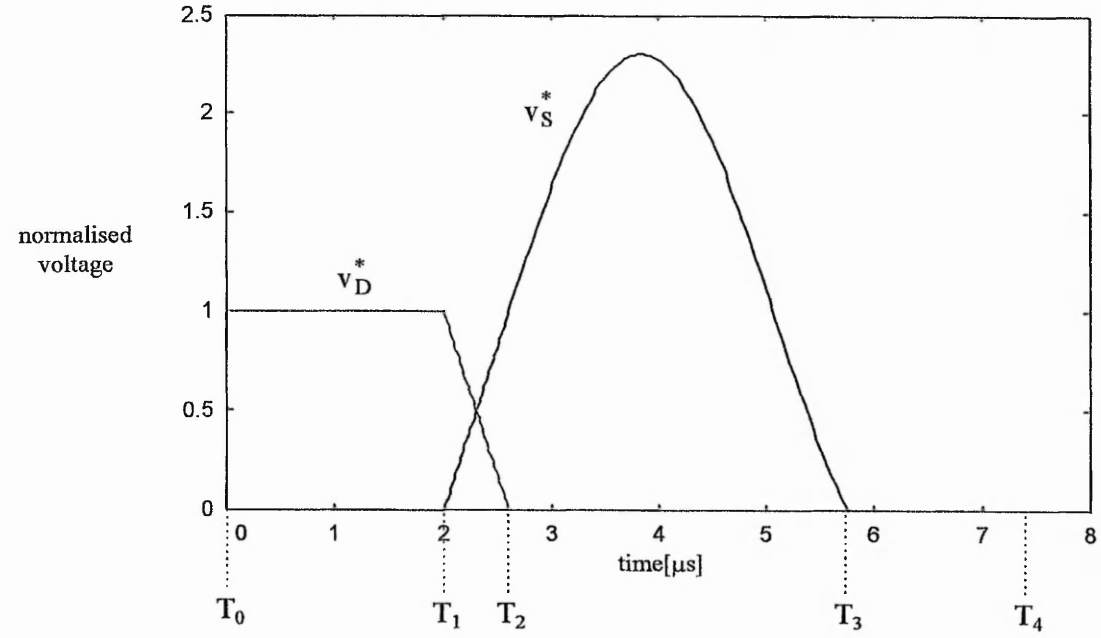

Figure 3-18: Voltage waveforms of the boost ZVS quasi-resonant converter.

The voltages are normalised by V_{out} and the currents are normalised by V_{out}/Z_r, as shown in equations (3.18) and (3.19). Table 3-2 summarises the equations for the four stages of a operating cycle. The value of the parameter a_{zvs} is $a_{zvs} = \arcsin\left(-\frac{1}{\alpha}\right)$.

Table 3-2: Normalised equations for the ZVS boost converter.

	Stage 1	Stage 2	Stage 3	Stage 4
$i_S^*(t)$	α	0	0	$\omega_r t + \alpha\cos(a_{zvs})$
$i_D^*(t)$	0	0	$\alpha - \alpha\cos(\omega_r t)$	$\alpha - \omega_r t - \alpha\cos(a_{zvs})$
$v_S^*(t)$	0	$\alpha\omega_r t$	$1 + \alpha\sin(\omega_r t)$	0
$v_D^*(t)$	1	$1 - \alpha\omega_r t$	0	0
duration	T_{01}	$\frac{1}{\omega_r \alpha}$	$\frac{a_{zvs}}{\omega_r}$	$\frac{\alpha}{\omega_r}(1-\cos(a_{zvs}))$

The waveforms of the normalised currents and voltages are shown in figures 3-17 and 3-18.

The steady-state circuit behaviour can be obtained by solving the state equations of the four stages in a switching cycle. The dc voltage conversion ratio $x=V_{out}/V_{in}$ is a function of load resistance and switching frequency. It is shown in appendix 2 that for the half-wave implementation of the ZVS boost converter:

$$\frac{f_S}{f_r} = \left(\frac{2\pi}{x}\right)\frac{1}{\left[\frac{r}{2x} + \pi + \arcsin\frac{r}{x} + \frac{x}{r}\left(1+\sqrt{1-\frac{r^2}{x^2}}\right)\right]}. \qquad (3.31)$$

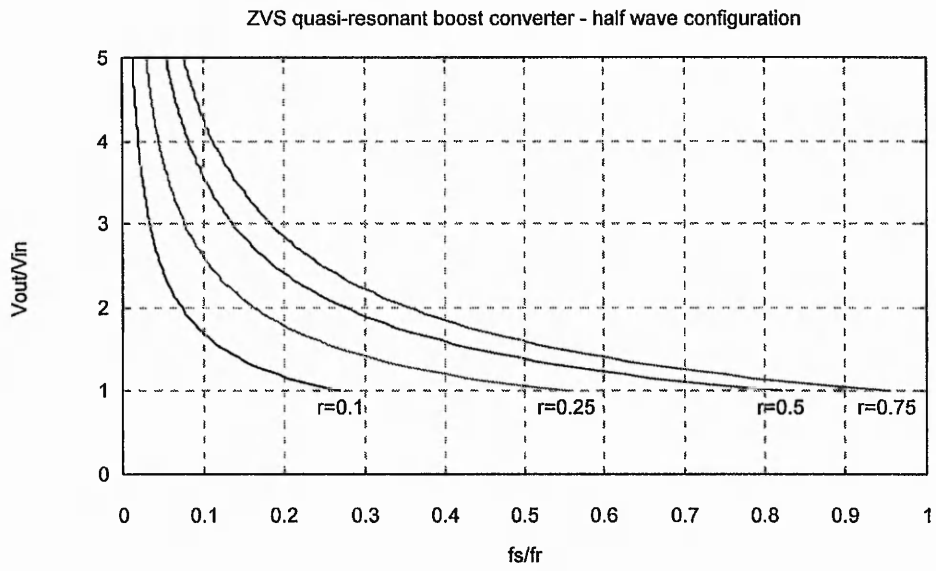

Figure 3-19: Voltage conversion ratio versus normalised switching frequency for the half-wave configuration.

For converters having a full-wave switch:

$$\frac{f_S}{f_r} = \left(\frac{2\pi}{x}\right) \frac{1}{\left[\frac{r}{2x} + 2\pi - \arcsin\frac{r}{x} + \frac{x}{r}\left(1 - \sqrt{1 - \frac{r^2}{x^2}}\right)\right]}. \tag{3.32}$$

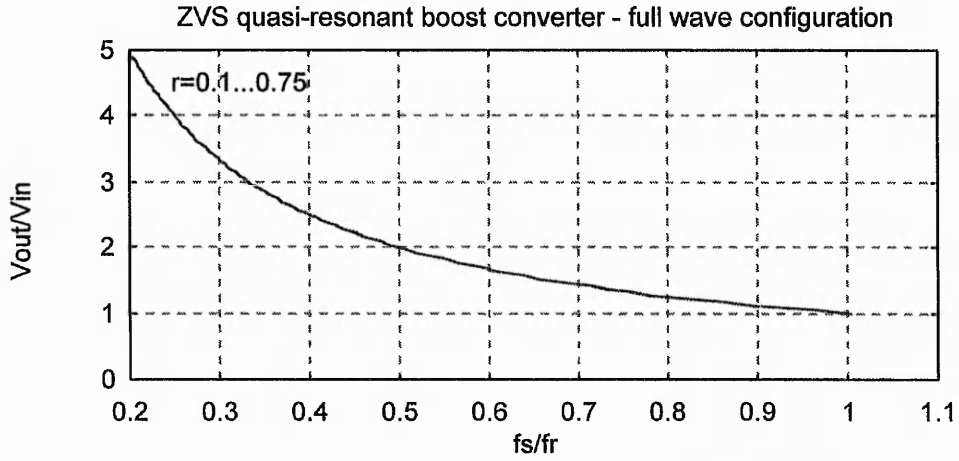

Figure 3-20: Voltage conversion ratio versus normalised switching frequency for the full-wave configuration.

The dc conversion ratio versus normalised switching frequency is plotted for different loads in figure 3-19 for half-wave converters and in figure 3-20 for full-wave converters..

The half-wave ZVS converter is sensitive to load variations, while the full-wave implementation is almost insensitive to load variations. However, the full-wave operation suffers from conduction losses due to the forward drop of the series diode. In addition [39], the series diode hinders the resonant discharge of the output capacitance of the power MOSFET, which no longer achieves a true zero-voltage-switching. This problem can be alleviated by adding a capacitance across the series diode. This additional capacitance will restore the zero-voltage-switching of the power MOSFET, but will result in a resonant network of increased complexity. Due to the above reasons, full-wave mode converters are rarely used. In this thesis only ZVS-MRCs operating in half-wave mode are addressed in detail.

The peak current through the power switch is $I_{Speak}=I_{in.}$
The peak voltage of the switch during off-state is $V_{Speak}=V_{out}+Z_rI_{in}$
or $V_{Speak}=V_{out}(1+x/r)$.
The peak current through the diode is $I_{Dpeak}=2I_{in}$.
The peak voltage of diode D is $V_{Dpeak}=V_{out}$.

The load range is limited from zero load resistance (short circuit) to a maximum load resistance equal to $R_{loadmax}=xZ_r$. When the load current is too small, the zero-voltage switching property will be lost. For both ZCS and ZVS topologies, variations in line and load are shown to have an adverse effect on stresses [27].

It should be noted that the value of the resonant capacitor must be significantly larger than the parasitic junction capacitance across the output diode D. This parasitic capacitance is a limiting factor in operating the converter at very high frequencies.

3.4. DC Modelling of Quasi-Resonant Converters

The averaging technique is effective for modelling quasi-resonant and multi-resonant dc-dc converters. It exploits the fact that the average voltage of the resonant inductor and the average currents of the resonant capacitors are all zero.

The averaged circuits of the ZCS and ZVS boost converters obtained as described in section 3.2 are presented in figure 3-21 and figure 3-22, respectively.

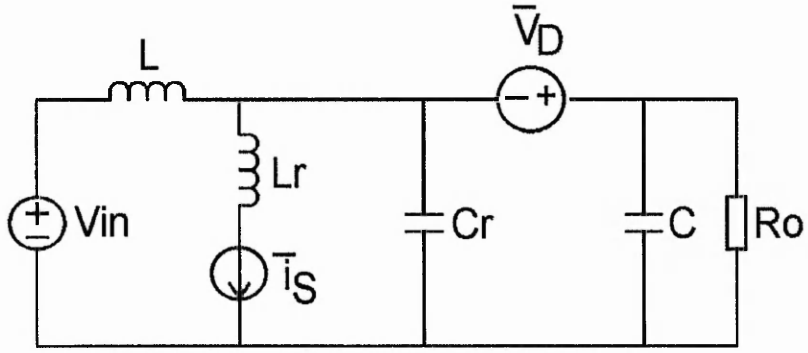

Figure 3-21: Averaged circuit of ZCS boost converter.

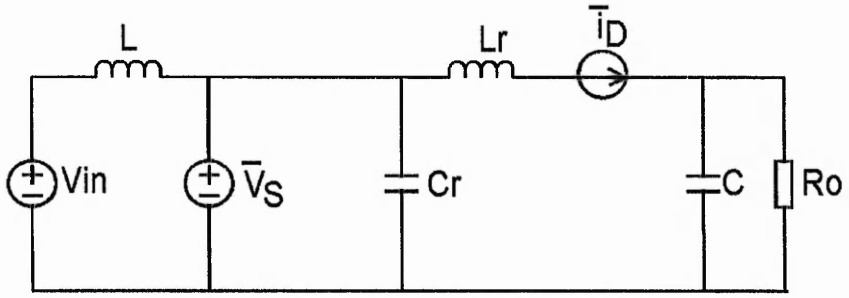

Figure 3-22: Averaged circuit of ZVS boost converter.

For the ZCS boost converter, the resonant capacitor C_r forms a loop with the voltage sources representing diode D and the "stiff" output capacitor C, which has a voltage with a negligible switching ripple. The voltage across C_r is determined by $\overline{v}_D$ and V_{out}

and, consequently, C_r has no effect on the model and can be removed. The resonant inductor L_r is in series with the ideal current source $\bar{i}_S$ and the current through L_r is determined by the current source. Therefore, the resonant inductor has no influence on the averaged model and can be removed. The averaged equivalent circuit in figure 3-3 is valid for ZCS boost converters as well as for PWM converters.

Applying the averaging procedure to the ZVS boost converter, it is seen that the resonant capacitor C_r appears across an ideal voltage source $\bar{v}_S = V_{out} - \bar{v}_D$, representing the average voltage across the power switch. The resonant capacitor has no influence on the averaged model and can be removed. So can be the resonant inductor L_r, which is in series with the current source $\bar{i}_D = I_{in} - \bar{i}_S$. The circuit in figure 3-4 can be considered as the averaged model. By manipulating the voltage and current sources the equivalent model in figure 3-3 is obtained. It should be noted that this circuit is the equivalent nonlinear averaged model for PWM, ZCS and ZVS boost converters. What is different from topology to topology is the procedure of calculating the values of $\bar{i}_S$ and $\bar{v}_D$.

In quasi-resonant converters one resonant capacitor and one inductor are included in accord with rules 1 and 2 for ZCS converters and rules 3 and 4 for ZVS converters, rules which are presented in section 2.3. A new linear network N^Q is obtained. The network N^Q of the quasi-resonant converter is the same as the PWM network N with the exception of the addition of L_r in series and C_r in parallel with the elements of N. At dc, however, the networks N and N^Q are equivalent, because the average voltage across L_r is zero and the average current through C_r is also zero. The averaged model of a QRC is shown in figure 3-23.

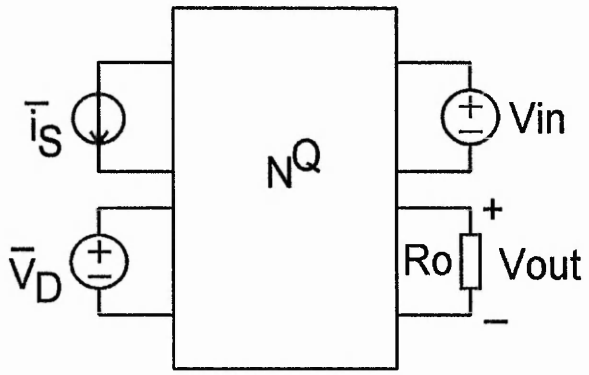

Figure 3-23: Average model of dc-dc quasi-resonant converter.

A function $G(f_S, I_{in}, V_{out})$ is introduced which characterises the average values of the switch waveforms over one switching period. This function G is referred to as *characteristic function* of the converter.

Mathematically, the characteristic function of a boost quasi-resonant converter is defined as follows:

$$\bar{v}_D = G(f_S, I_{in}, V_{out}) V_{out} . \tag{3.33}$$

It is shown in appendix 3 that

$$\bar{i}_S = G(f_S, I_{in}, V_{out}) I_{in} . \tag{3.34}$$

By comparing equations (3.4) and (3.5) valid for the PWM boost converter with equations (3.33) and (3.34) valid for quasi-resonant converters, it is noted that the characteristic function G can be seen as the equivalent steady-state duty ratio of quasi-resonant converters.

The derivation of G for both zero-current-switching and zero-voltage-switching boost converters is done in appendix 3. It is obtained that:

$$G_{ZCS}(f_S, I_{in}, V_{out}) =$$

$$= \frac{1}{2\pi}\frac{f_S}{f_r}\left[\frac{Z_r I_{in}}{2V_{out}} + \pi + \arcsin\left(\frac{Z_r I_{in}}{V_{out}}\right) + \frac{V_{out}}{Z_r I_{in}}\left(1 + \sqrt{1 - \left(\frac{Z_r I_{in}}{V_{out}}\right)^2}\right)\right];$$

$$G_{ZVS}(f_S, I_{in}, V_{out}) =$$

$$= 1 - \frac{1}{2\pi}\frac{f_S}{f_r}\left[\frac{V_{out}}{2Z_r I_{in}} + \pi + \arcsin\left(\frac{V_{out}}{Z_r I_{in}}\right) + \frac{Z_r I_{in}}{V_{out}}\left(1 + \sqrt{1 - \left(\frac{V_{out}}{Z_r I_{in}}\right)^2}\right)\right].$$

Considering that $\frac{x}{r} = \frac{Z_r I_{in}}{V_{out}}$, the characteristic functions can be written as:

$$G_{ZCS} = \frac{1}{2\pi}\frac{f_S}{f_r}\left[\frac{x}{2r} + \pi + \arcsin\left(\frac{x}{r}\right) + \frac{r}{x}\left(1 + \sqrt{1 - \frac{x^2}{r^2}}\right)\right]; \tag{3.35}$$

$$G_{ZVS} = 1 - \frac{1}{2\pi}\frac{f_S}{f_r}\left[\frac{r}{2x} + \pi + \arcsin\frac{r}{x} + \frac{x}{r}\left(1 + \sqrt{1 - \frac{r^2}{x^2}}\right)\right]. \tag{3.36}$$

The normalised switching frequency f_n is defined as the ratio of the switching frequency f_S and the resonant frequency f_r, $f_n = \frac{f_S}{f_r}$. The normalised input current is defined by equation (3.20) as $\alpha(V_{out}, I_{in}) = \frac{Z_r I_{in}}{V_{out}}$.

If the normalised variables α and f_n are considered, the characteristic functions become, respectively:

$$G_{ZCS}(f_n, \alpha) = \frac{1}{2\pi} f_n\left[\frac{\alpha}{2} + \pi + \arcsin\alpha + \frac{1}{\alpha}\left(1 + \sqrt{1 - \alpha^2}\right)\right], \tag{3.37}$$

$$G_{ZVS}(f_n, \alpha) = 1 - \frac{1}{2\pi} f_n\left[\frac{1}{2\alpha} + \pi + \arcsin\frac{1}{\alpha} + \alpha\left(1 + \sqrt{1 - \frac{1}{\alpha^2}}\right)\right]. \tag{3.38}$$

It is noted that the relationship between the characteristic functions of the ZCS and ZVS boost quasi-resonant converters is the following one:

$$G_{ZVS}(f_n,\alpha) = 1 - G_{ZCS}(f_n,\frac{1}{\alpha}). \tag{3.39}$$

The normalised switching frequency f_n is always less than one, since the switching frequency f_S is lower than the resonant frequency f_r. The normalised input current α is less than one for ZCS converters and greater than one for ZVS converters. The value of α is limited due to the limited load range of quasi-resonant converters, for which zero-current-switching or zero-voltage-switching conditions are achieved.

The dc voltage conversion ratio of the boost quasi-resonant converters can be referred to the boost PWM converter.

Since the linear networks N and N^Q are equivalent at dc, PWM converters and QRCs have the same voltage conversion ratio whenever the average values of i_S and v_D are the same in both cases. Therefore, the voltage conversion ratio for QRCs is obtained from equation (3.1) by replacing the duty ratio d with the characteristic function G.

For the ZCS boost converter,

$$x = \frac{1}{1 - G_{ZCS}(f_n,\alpha)}. \tag{3.40}$$

For the ZVS boost converter,

$$x = \frac{1}{1 - G_{ZVS}(f_n,\alpha)}. \tag{3.41}$$

The assumption made above is validated by the theoretical steady-state analysis undertaken in paragraphs 3.2.1 and 3.2.2 and by calculating the voltage conversion ratio using equations (3.40) and (3.37) and comparing it to (3.21) for ZCS converters and equation (3.41) and (3.38) compared to (3.31) for ZVS converters.

3.5. Steady-State Operation of Multi-Resonant Converters

The multi-resonant converters operate with zero-voltage-switching for both switching devices. During one cycle of operation of the MRC, three different resonant circuits are formed compared to only one for QRCs. This results in operation of the converter with three different resonant stages in one cycle of operation. Another significant difference compared to quasi-resonant converters is that two modes of operation are possible due to the more complicated structure of the multi-resonant network. The modes of operation of a MRC are determined by the sequence of topological stages during one cycle of circuit operation. During one of the resonant stages, both switch S and diode D are in the off-state and the voltages across both devices are sinusoidal. The sequence of topological stages and operating modes depends on which of the two voltages reduces first to zero, as it is described below in this section.

To gain insight into the operation and performance of the boost ZVS-MRC, a theoretical steady-state analysis is undertaken. In order to simplify the analysis, the assumptions stated in section 3.2. are made. Figure 3-24 shows the half-wave boost ZVS-MRC and figure 3-25 its simplified equivalent circuit. The full-wave ZVS-MRCs have the same problems as the ZVS-QRCs and will not be analysed in this thesis.

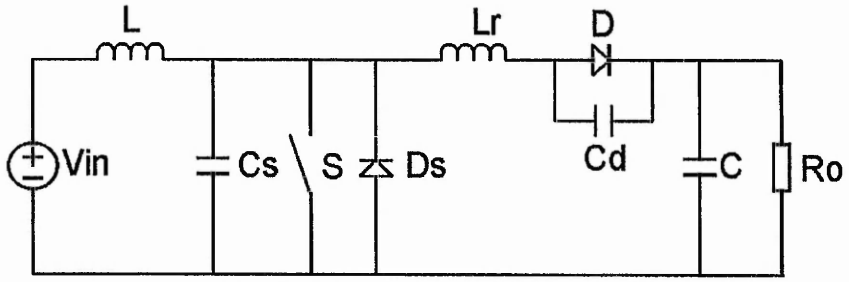

Figure 3-24: Half-wave ZVS-MRC.

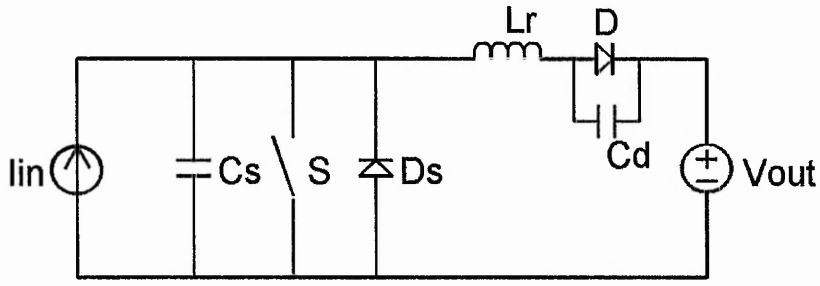

Figure 3-25: Simplified equivalent circuit for boost MRC.

The following parameters are defined as:

- resonant angular frequencies:

$$\omega_D = \frac{1}{\sqrt{L_r C_D}}; \tag{3.42}$$

$$\omega_S = \frac{1}{\sqrt{L_r C_S}}; \tag{3.43}$$

$$\omega_{SD} = \frac{1}{\sqrt{L_r \dfrac{C_S C_D}{C_S + C_D}}}; \tag{3.44}$$

- resonant frequency: $f_r = \dfrac{1}{2\pi\sqrt{L_r C_S}}$; (3.45)

- characteristic impedance: $Z_r = \sqrt{\dfrac{L_r}{C_S}}$; (3.46)

- normalised ratio of resonant capacitances: $C_N = \dfrac{C_D}{C_S}$. (3.47)

The definion of the normalised load resistance in equation (3.9) is valid for multi-resonant converters.

A complete switching cycle can be divided into four stages, starting from the moment when the output diode D turns off and switch S is conducting.

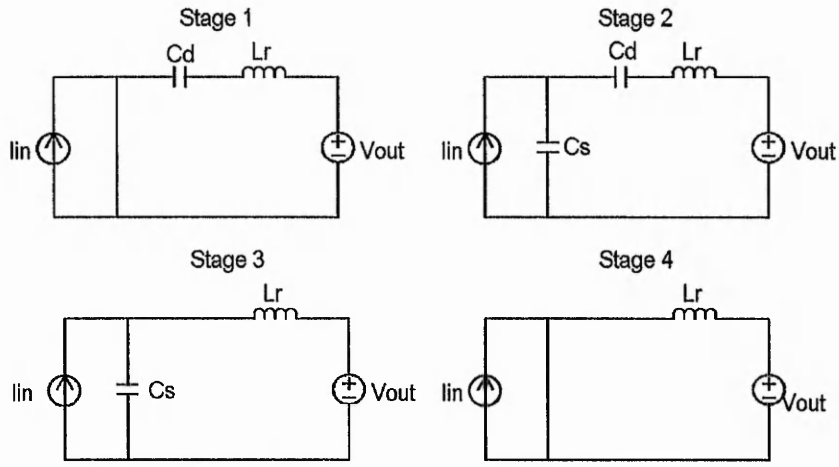

Figure 3-26: Equivalent circuit of the four stages in operation mode 1.

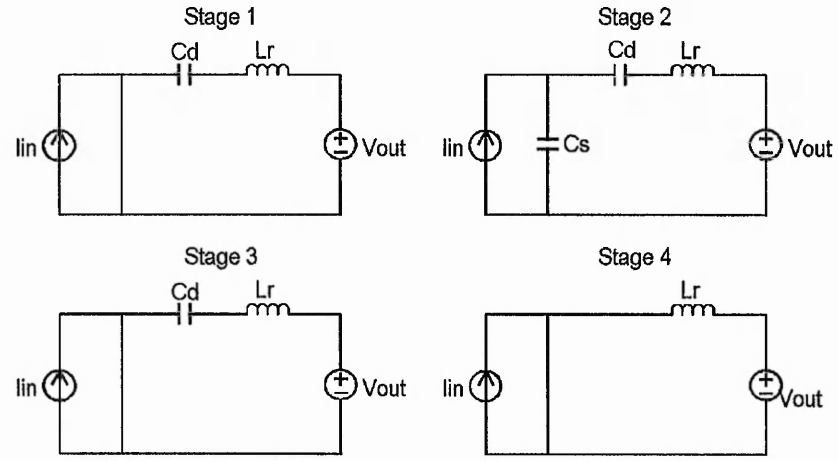

Figure 3-27: Equivalent circuit of the four stages in operation mode 2.

1. First Resonant Stage [T_0, T_1]

Switch S is conducting: $v_S(t)=0$.

Initial conditions: $i_{Lr}(0)=0$, $i_S(0)=I_{in}$, $v_D(0)=0$.

State equations: $i_{Lr}+i_S=I_{in}$,

$$L_r\frac{di_{Lr}}{dt}-v_D+V_{out}=0,$$

$$i_{Lr}=-C_D\frac{dv_D}{dt}.$$

Time expressions: $v_D(t) = V_{out}(1-\cos\omega_D t)$ (3.48)

$i_{Lr}(t) = -\omega_D C_D V_{out} \sin\omega_D t$. (3.49)

This stage ends when the switch S is turned off. The duration T_{01} of the stage is variable and determines the output voltage.

2. Second Resonant Stage [T_1, T_2]

Both switch and diode are off.

Initial conditions: $i_{Lr}(0)=I_{LT1}$, $v_S(0)=0$, $v_D(0)=V_{DT1}$.

State equations: $i_{Lr} + C_S \frac{dv_S}{dt} = I_{in}$,

$L_r \frac{di_{Lr}}{dt} - v_S - v_D + V_{out} = 0$,

$i_{Lr} = -C_D \frac{dv_D}{dt}$.

The parameter c is defined as $c = \frac{C_D}{C_S + C_D}$. (3.50)

Time expressions: $i_{Lr}(t) = cI_{in} + (I_{LT1} - cI_{in})\cos\omega_{SD}t + \frac{V_{DT1} - V_{out}}{\omega_{SD} L_r}\sin\omega_{SD}t$ (3.51)

$$v_D(t) = cV_{DT1} + (1-c)V_{out} - \frac{I_{in}}{C_S + C_D}t + \frac{cI_{in} - I_{LT1}}{\omega_{SD} C_D}\sin\omega_{SD}t + \\ +(1-c)(V_{DT1} - V_{out})\cos\omega_{SD}t \quad (3.52)$$

$$v_S(t) = -cV_{DT1} + cV_{out} + \frac{I_{in}}{C_S + C_D}t + \frac{cI_{in} - I_{LT1}}{\omega_{SD} C_S}\sin\omega_{SD}t + \\ +c(V_{DT1} - V_{out})\cos\omega_{SD}t \quad (3.53)$$

Stage 2 ends when either v_D reduces to zero and the output diode D turns on (*operation mode 1*) or when v_S reduces to zero and the antiparallel diode D_S of the switch turns on and the switch S is turned on (*operation mode 2*).

The duration T_{12} of this stage is determined by setting either $v_D(T_{12})=0$ or $v_S(T_{12})=0$ and solving the corresponding nonlinear equation using the Newton-Raphson method.

3. Third Resonant Stage [T_2, T_3] - Operating Mode 1

Diode D is conducting: $v_D(t)=0$.

Initial conditions: $i_{Lr}(0)=I_{LT2}$, $v_S(0)=V_{ST2}$.

State equations: $i_{Lr} + C_S \frac{dv_S}{dt} = I_{in}$,

$$L_r \frac{di_{Lr}}{dt} - v_S + V_{out} = 0.$$

Time expressions: $i_{Lr}(t) = I_{in} + (I_{LT2} - I_{in})\cos\omega_S t + \frac{V_{ST2} - V_{out}}{\omega_S L_r}\sin\omega_S t$ (3.54)

$$v_S(t) = V_{out} - \omega_S L_r (I_{LT2} - I_{in})\sin\omega_S t + (V_{ST2} - V_{out})\cos\omega_S t. \quad (3.55)$$

Stage 3 ends when the switch S is turned on (determined by the moment when the voltage across the switch reaches zero). The duration T_{23} of this stage is calculated by setting $v_S(T_{23})=0$.

3. Third Resonant Stage [T_2, T_3] - Operating Mode 2

Switch S is conducting: $v_S(t)=0$.

Initial conditions: $i_{Lr}(0)=I_{LT2}$, $v_D(0)=V_{DT2}$.

State equations:

$$L_r \frac{di_{Lr}}{dt} - v_D + V_{out} = 0,$$

$$i_{Lr} = -C_D \frac{dv_D}{dt}.$$

Time expressions: $i_{Lr}(t) = I_{LT2}\cos\omega_D t + (V_{DT2} - V_{out})\omega_D C_D \sin\omega_D t$, (3.56)

$$v_D(t) = V_{out} - \frac{I_{LT2}}{\omega_D C_D}\sin\omega_D t + (V_{DT2} - V_{out})\cos\omega_D t. \quad (3.57)$$

Stage 3 ends when diode D is turned on (determined by the moment when the reverse voltage across the diode reaches zero). The duration T_{23} of this stage is calculated by setting $v_D(T_{23})=0$.

4. Linear Stage [T_3, T_4]

This stage is common to both modes of operation.

At time $t=T_3$ switch S and diode D are conducting: $v_S(t)=0$ and $v_D(t)=0$.

Initial condition: $i_{Lr}(0)=I_{LT3}$.

State equation: $L_r \frac{di_{Lr}}{dt} + V_{out} = 0$.

Time expressions: $i_{Lr}(t) = I_{LT3} - \frac{V_{out}}{L_r} t$ (3.58)

$i_S(t) = I_{in} - I_{LT3} + \frac{V_{out}}{L_r} t$.

This stage ends when i_{Lr} equals zero and diode D turns off.

The duration T_{34} of this stage is:

$$T_{34} = \frac{I_{LT3} L_r}{V_{out}}. \quad (3.59)$$

The sequences of topological states are presented in tables 3-3 and 3-4 and the equivalent circuits for each stage in figures 3-26 and 3-27. The waveforms of the boost MRC are shown in figures 3-28 to 3-31 for the two operation modes.

Table 3-3: Sequence of topological states for operating mode 1.

	1	2	3	4
S	ON	OFF	OFF	ON
D	OFF	OFF	ON	ON

Table 3-4: Sequence of topological states for operating mode 2.

	1	2	3	4
S	ON	OFF	ON	ON
D	OFF	OFF	OFF	ON

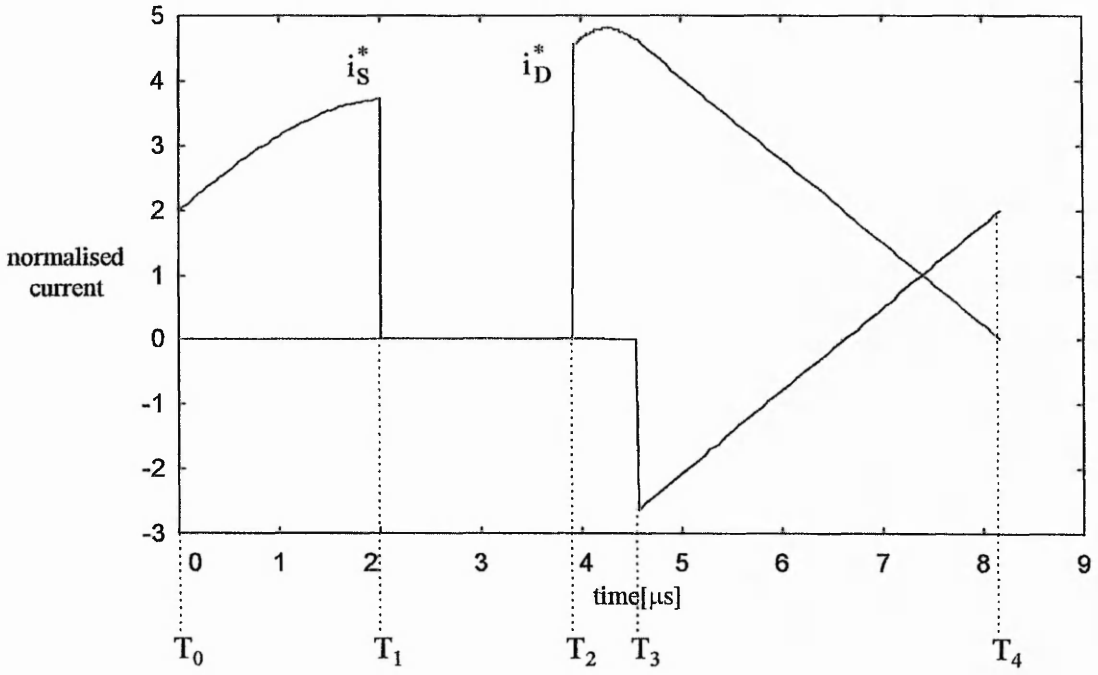

Figure 3-28: Current waveforms of boost ZVS multi-resonant converter for operating mode 1.

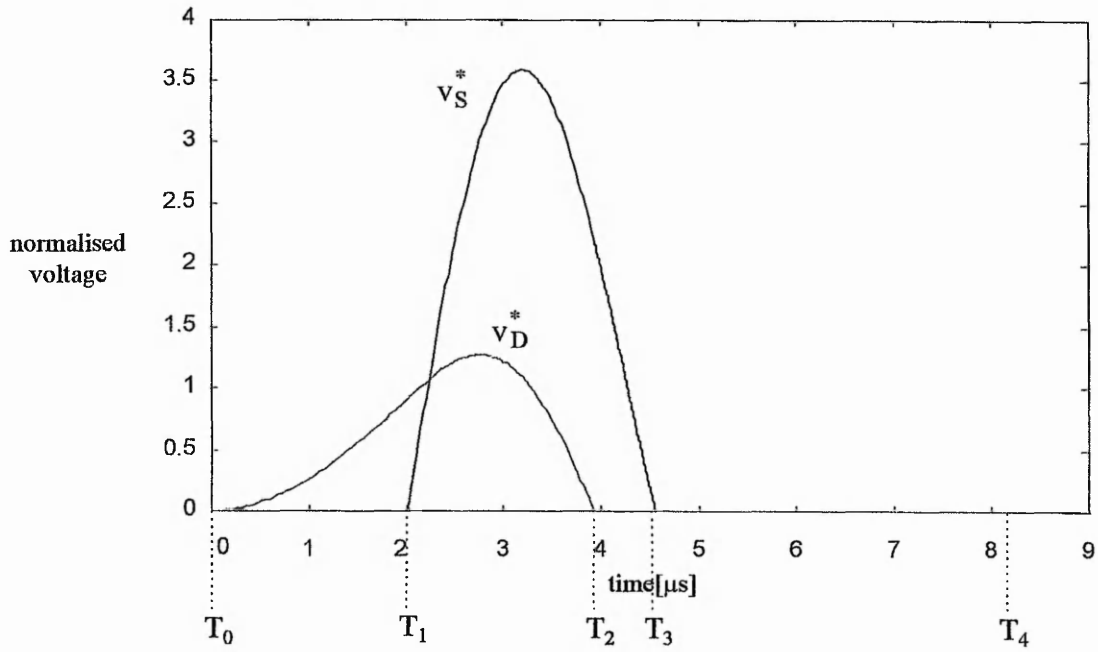

Figure 3-29: Voltage waveforms of boost ZVS multi-resonant converter for operating mode 1.

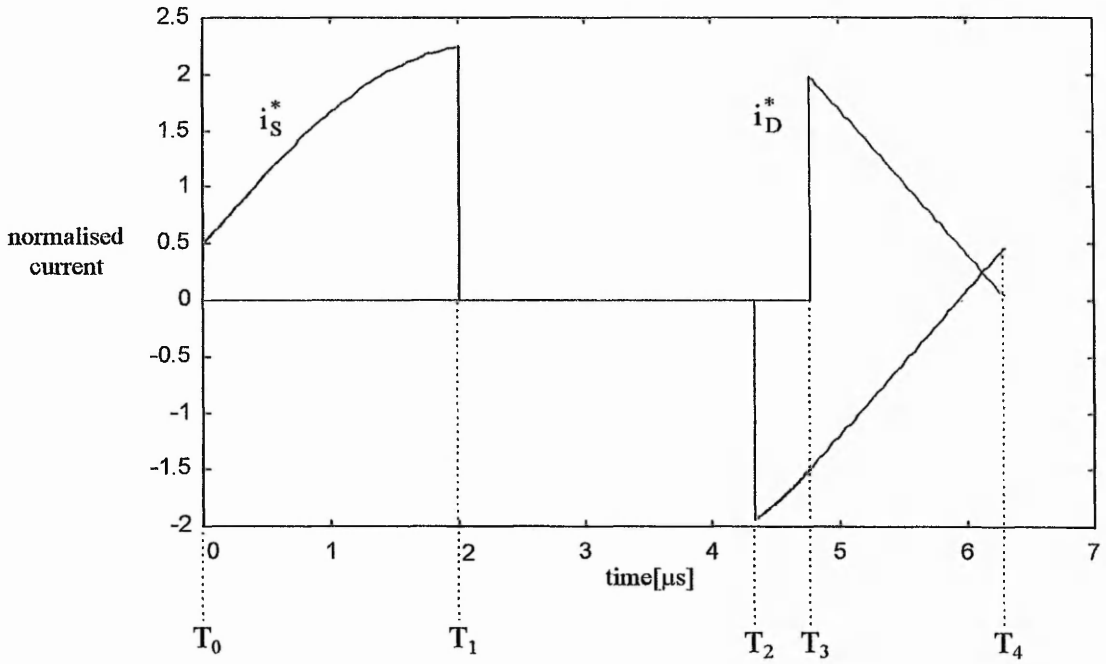

Figure 3-30: Current waveforms of boost ZVS multi-resonant converter for operating mode 2.

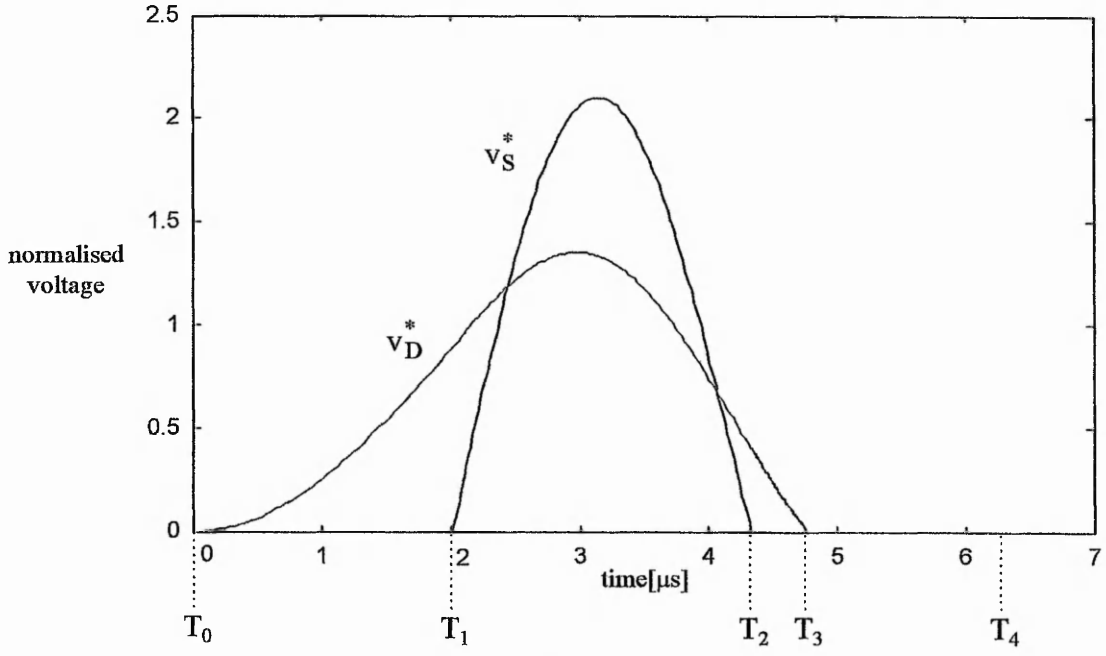

Figure 3-31: Voltage waveforms of boost ZVS multi-resonant converter for operating mode 2.

The normalised equations describing each stage of operation are obtained by the same procedure as described in section 3.4 and are given below.

1. First Resonant Stage [T_0, T_1]

$$v_S^*(t) = 0 \tag{3.60}$$

$$v_D^*(t) = 1 - \cos\omega_D t \tag{3.61}$$

$$i_{Lr}^*(t) = -\sqrt{C_N}\sin\omega_D t \tag{3.62}$$

2. Second Resonant Stage [T_1, T_2]

$$v_S^*(t) = -cV_{DT1}^* + c + \alpha\sqrt{c}(1-c)\omega_{SD}t + \sqrt{c}(c\alpha - I_{LT1}^*)\sin\omega_{SD}t + \\ +c(V_{DT1}^* - 1)\cos\omega_{SD}t \tag{3.63}$$

$$v_D^*(t) = cV_{DT1}^* + (1-c) - \alpha\sqrt{c}(1-c)\omega_{SD}t + \sqrt{c}(c\alpha - I_{LT1}^*)\frac{1}{C_N}\sin\omega_{SD}t + \\ +(1-c)(V_{DT1}^* - 1)\cos\omega_{SD}t \tag{3.64}$$

$$i_{Lr}^*(t) = c\alpha + (I_{LT1}^* - c\alpha)\cos\omega_{SD}t + \sqrt{c}(V_{DT1}^* - 1)\sin\omega_{SD}t \tag{3.65}$$

3A. Third Resonant Stage [T_2, T_3] - Operating Mode 1

$$v_S^*(t) = 1 - (I_{LT2}^* - \alpha)\sin\omega_S t + (V_{ST2}^* - 1)\cos\omega_S t \tag{3.66}$$

$$v_D^*(t) = 0 \tag{3.67}$$

$$i_{Lr}^*(t) = \alpha + (I_{LT2}^* - \alpha)\cos\omega_S t + (V_{ST2}^* - 1)\sin\omega_S t \tag{3.68}$$

3B. Third Resonant Stage [T_2, T_3] - Operating Mode 2

$$v_S^*(t) = 0 \tag{3.69}$$

$$v_D^*(t) = 1 - \frac{I_{LT2}^*}{\sqrt{C_N}}\sin\omega_D t + (V_{DT2}^* - 1)\cos\omega_D t \tag{3.70}$$

$$i_{Lr}^{*}(t) = I_{LT2}^{*}\cos\omega_D t + (V_{DT2}^{*} - 1)\sqrt{C_N}\sin\omega_D t \tag{3.71}$$

4. Linear Stage [T_3,T_4]

$$v_S^{*}(t) = 0 \tag{3.72}$$

$$v_D^{*}(t) = 0 \tag{3.73}$$

$$i_{Lr}^{*}(t) = I_{LT3}^{*} - \omega_S t \tag{3.74}$$

Note that parameter c defined in equation (3.50) can be expressed as a value of the normalised capacitance C_N,

$$c = \frac{C_N}{1 + C_N}. \tag{3.75}$$

3.6. DC Modelling of Multi-Resonant Converters

The averaged circuit of the boost ZVS-MRC is obtained as described in section 3.2 and shown in figure 3-32.

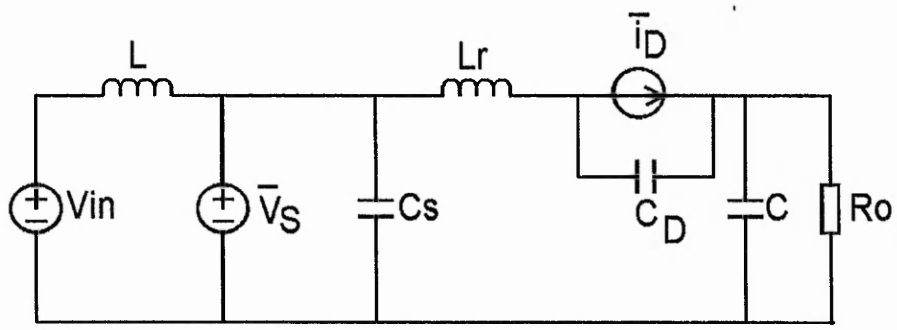

Figure 3-32: Averaged circuit of boost ZVS-MRC.

The resonant capacitor C_S appears across the ideal voltage source $\bar{v}_S$ and has no influence on the averaged circuit. Therefore, it can be removed. The voltage across the resonant capacitor C_D depends on the voltage across the "stiff" capacitor C, which is

assumed constant, and on the voltage source $\bar{v}_S$. The voltage across the resonant inductor L_r is zero, because the above circuit is an averaged circuit and the average voltage across an inductor is zero. Capacitor C_D has no influence on the averaged circuit and can be removed. So can be inductor L_r, which is in series with the current source $\bar{i}_D$.

The circuit in figure 3-32 is equivalent to the one in figure 3-4 and to the averaged circuit in figure 3-3. Therefore, the circuit shown in figure 3-3 is the averaged circuit of the boost ZVS-MRC.

In multi-resonant converters two resonant capacitors and one inductor are included in accord with rules 5 to 7 presented in paragraph 2.4. A new linear network N^M is obtained, as shown in figure 3-33. The network N^M of the multi-resonant converter is the same as the PWM network N (as defined in paragraph 3.4.) with the exception of the addition of L_r in series and C_S and C_D in parallel with the elements of N. At dc, however, the networks N and N^M are equivalent, because the average voltage of L_r is zero and the average currents of the resonant capacitors are also zero.

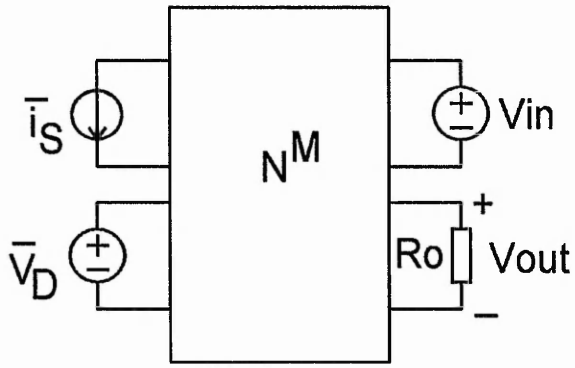

Figure 3-33: Average model of dc-dc multi-resonant converter.

To characterise the average behaviour of the switching devices, the characteristic functions G_v and G_i of a multi-resonant boost converter are introduced. Mathematically, they are defined as follows:

$$\bar{v}_D = G_v(f_S, I_{in}, V_{out})V_{out}; \tag{3.76}$$

$$\bar{i}_S = G_i(f_S, I_{in}, V_{out})I_{in}. \tag{3.77}$$

If normalised quantities are used:

$$\bar{v}_D = G_v(f_n, \alpha)V_{out}; \tag{3.78}$$

$$\bar{i}_S = G_i(f_n, \alpha)I_{in}. \tag{3.79}$$

The expressions of the characteristic functions of a boost MRC are derived in appendix 3.

The voltage conversion ratio in the boost multi-resonant converter can be referred to the related PWM converter. Since the linear networks N and N^M are equivalent at dc, PWM converters and MRCs have the same voltage conversion ratio whenever the average values of the inputs are the same in both cases. Therefore, the voltage conversion ratio for MRCs is obtained from equation (3.1) by replacing the duty ratio d with the characteristic function G_v.

The voltage conversion ratio of the boost ZVS-MRC is:

$$x = \frac{1}{1 - G_v(\alpha, f_n)}. \tag{3.80}$$

To determine the characteristic function G_v and the voltage conversion ratio x of the multi-resonant converter, a numeric algorithm has to be used. This numeric procedure is necessary because the duration of stage 2 for both operating modes is determined from either equation (3.63) or (3.64), which are both transcendental equations of the type

$A\sin\omega t + B\cos\omega t + Ct + D = 0$.

This type of equation is solved numerically by using the Newton-Raphson method.

The numerical algorithm uses the normalised equations of the MRC and the normalised input current α as a free running parameter. The algorithm is implemented in the C-programming language and the computer program is listed in appendix 6.

The main steps of the numeric method are described below.

Step 1.

The input parameters are specified:

- resonant inductor L_r
- resonant capacitor C_S
- resonant capacitor C_D
- normalised input current α
- duration of stage 1 T_{01}

Step 2.

The resonant angular frequencies -equations (3.42) to (3.44), resonant frequency - equation (3.45), characteristic impedance - equation (3.46) and normalised capacitance - equation (3.47) are calculated.

Step 3.

From equations (3.61) and (3.62) the values of V^*_{DT1} and I^*_{LT1}, which are the initial conditions for stage 2, are determined by setting $t=T_{01}$.

Step 4.

The operating mode has to be determined by calculating which voltage (across the switch, v_S, or across the diode, v_D) reaches first zero. From equation (3.63) the time T_{12mod1} after which v^*_S decreases to zero is determined. Similarly, from equation (3.64), the time T_{12mod2} after which v^*_D reaches zero is calculated. Both equations are solved using the Newton-Raphson method.

If T_{12mod1} is less than T_{12mod2}, then the converter operates in mode 1.

If T_{12mod1} is greater than T_{12mod2}, then the converter operates in mode 2.

The duration T_{12} of stage 2 is $T_{12} = \min(T_{12mod1}, T_{12mod2})$.

Step 5 - operating mode 1.

The initial values for stage 3, V^*_{ST2} and I^*_{LT2}, are calculated using equations (3.63) and (3.65) with $t=T_{12}$.

The duration T_{23} of the third resonant stage is determined stage from equation (3.66) by setting $v_S(t)=0$. The solution T_{23} can be obtained either in an analytic form or the using the Newton-Raphson method. The second method is adopted for the present program.

The value of I^*_{LT3} is calculated from equation (3.68).

Step 5 - operating mode 2.

The initial values for stage 3, V^*_{DT2} and I^*_{LT2}, are calculated using equations (3.64) and (3.65) with $t=T_{12}$.

The duration T_{23} of the third resonant stage is determined stage from equation (3.70) by setting $v_D(t)=0$. The solution T_{23} can be obtained either in an analytic form or the using the Newton-Raphson method. The second method is adopted for the present program.

The value of I^*_{LT3} is calculated from equation (3.71).

Step 6 (optional).

The peak values of the voltages across switch S and diode D are reached during the second operating stage of the converter. The maximum value occurs when the derivative of the voltage with respect to time equals zero.

The procedure to obtain the peak normalised voltage V^*_{Smax} across switch S in operating mode 1 is described below. To obtain the peak voltage across the output diode D in mode 1 and both peak voltages in mode 2, a similar procedure to the one described is used.

The value of V^*_{Smax} is obtained as follows:

- the derivative with respect to time of v^*_S is calculated from equation (3.63);
- the time t_{vsmax} for which the maximum value occurs is calculated using the Newton-Raphson method for equation $\frac{dv^*_S}{dt} = 0$;
- the peak voltage is calculated from (3.63), $V^*_{Smax} = v^*_S(t_{vsmax})$.

Step 7.

This step is common for both operating modes, since stage 4 of operation is common. The duration of stage 4 is easily determined from (3.74) by setting $i_L^*(t) = 0$.

Step 8.

The duration of all stages is known and the value of the switching period is determined, $T_S = T_1 + T_2 + T_3 + T_4$.

The switching frequency is

$f_S = 1/T_S$.

The normalised switching frequency is $f_n = f_S/f_r$.

Step 9.

The characteristic function G_v is determined using the expressions presented in appendix 3. It can be calculated from either of two equations,

$\bar{v}_D = G_v V_{out}$ or $\bar{v}_S = (1 - G_v) V_{out}$.

Optional, the characteristic function G_i is determined using the expressions in appendix 3. It can be calculated from one of the following equations:

$\bar{i}_S = G_i I_{in}$ or $\bar{i}_D = (1 - G_i) I_{in}$ or $\bar{i}_{Lr} = (1 - G_i) I_{in}$.

Step 10.

The voltage conversion ratio is determined from equation (3.80).

Step 11.

The normalised load resistance is calculated, $r = \frac{x}{\alpha}$.

The characteristic function G_v of a boost ZVS-MRC is shown in figures 3-34 and 3-35.

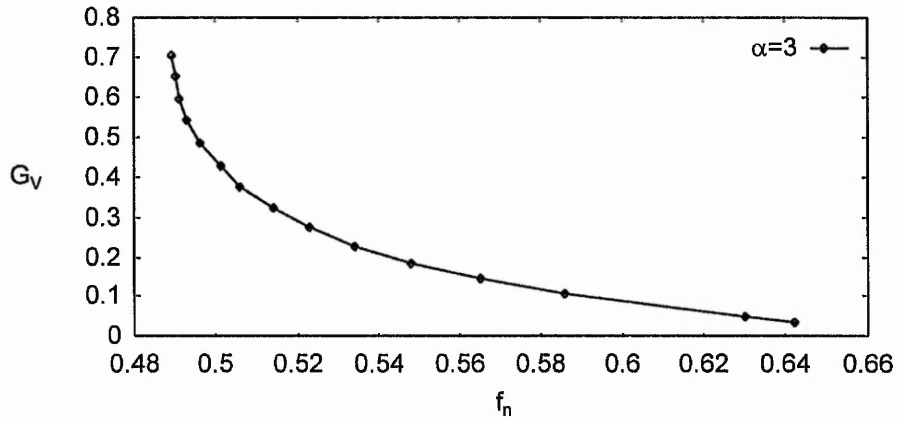

Figure 3-34: Characteristic function G_v of a MRC for a value of the normalised input current of $\alpha=3$.

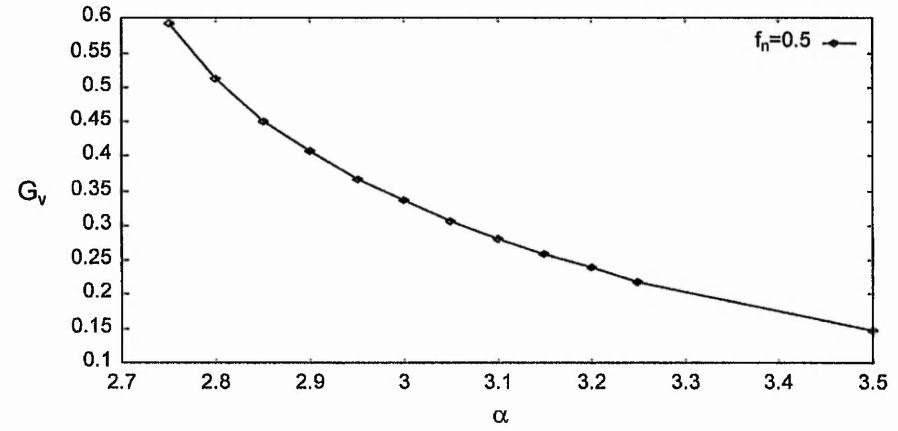

Figure 3-35: Characteristic function G_v of a MRC for a value of the normalised switching frequency of $f_n=0.5$.

The graphical representation of the voltage conversion ratio $x=V_{out}/V_{in}$ versus the normalised switching frequency $f_n=f_S/f_r$ with the normalised input current as running parameter and $C_N=3$ is shown in figure 3-36.

For the design of the converter the dependence of x to the normalised load resistance r is useful. It is shown in figure 3-37 for $C_N=3$ and r as running parameter and in figure 3-38 for the constant value of r=0.5 and C_N as running parameter.

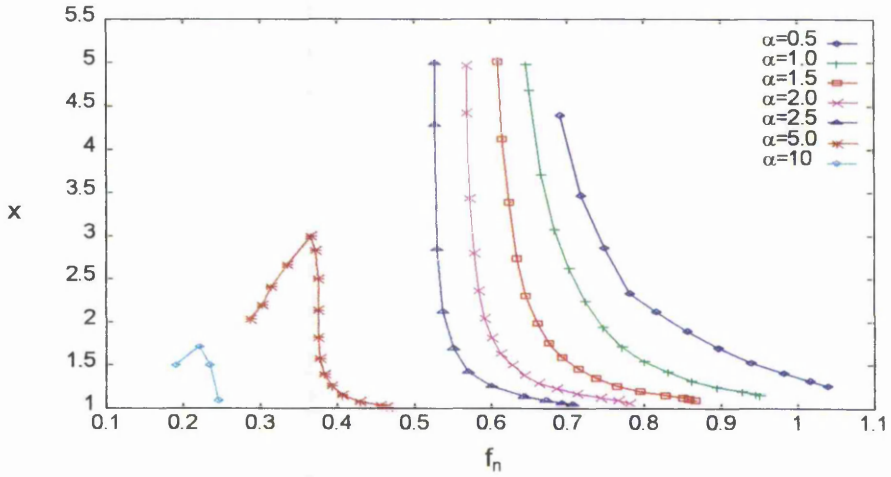

Figure 3-36: Voltage conversion ratio for boost ZVS MRC, C_N=3.

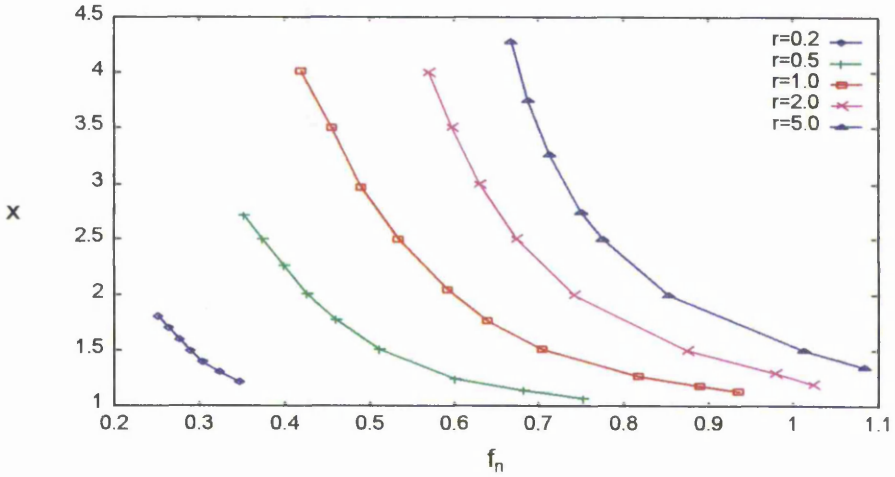

Figure 3-37: Voltage conversion ratio for boost ZVS MRC, C_N=3.

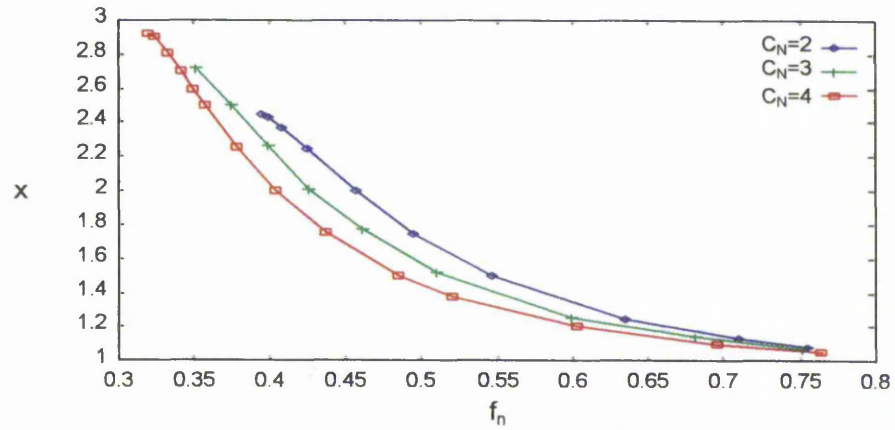

Figure 3-38: Voltage conversion ratio for boost MRC, r=0.5.

The peak voltage across the power switch S is shown in figure 3-39 for C_N=3 and r as a running parameter and in figure 3-40 for r=0.5 and C_N as a running parameter.

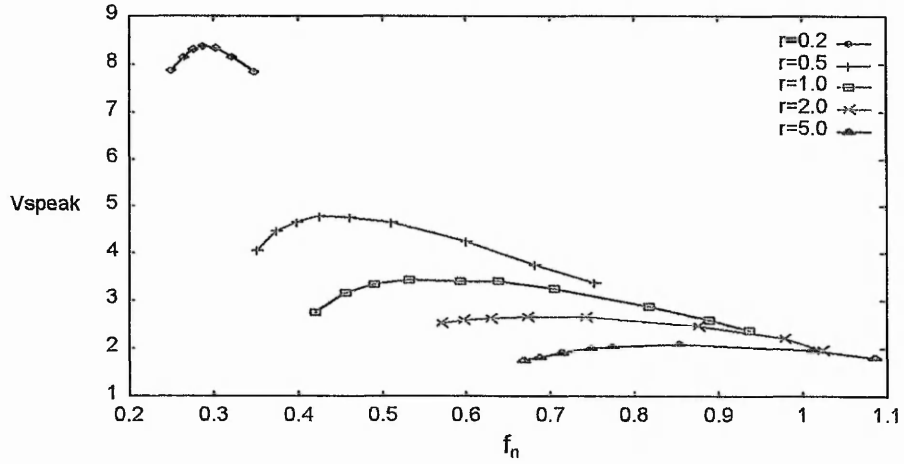

Figure 3-39: Peak switch voltage for boost ZVS MRC, C_N=3.

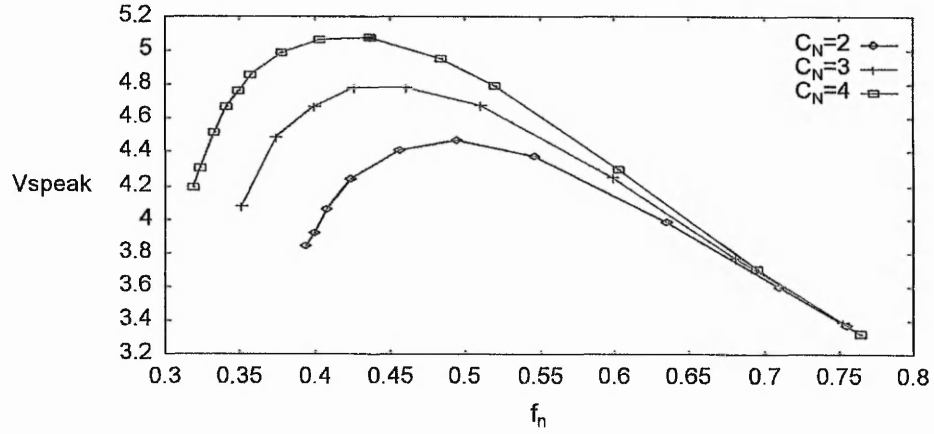

Figure 3-40: Peak switch voltage for r=0.5.

Note that the load range is improved compared to the boost ZVS-QRC. As the value of C_N increases, the peak switch voltage increases while the voltage conversion ratio decreases. A low C_N will produce a reduced voltage stress on the switching device. On the other side, the operating range in terms of voltage conversion ratio is more reduced with a low value of C_N.

Considerations on the values of the peak diode voltage and peak currents through D and S are made by Tabisz [41]. It is shown that for the boost ZVS-MRC,

$$V_{Dpeak} \leq 2V_{out};$$

$$I_{Speak} \leq \frac{\sqrt{C_N}}{Z_r} V_{out} + I_{in};$$

$$I_{Dpeak} \leq \frac{\sqrt{C_N}}{Z_r} V_{out} + 2I_{in}.$$

Interesting operating conditions exist when α=1, C_N=1 and f_n=0.5. Both active and passive switches operate with both zero-current-switching and zero-voltage-switching. These switching conditions can be considered ideal. However, this type of operation does not seem to be suitable for practical applications due to the high sensitivity to operating conditions [43].

3.7. Conclusions

The steady-state analysis of boost quasi-resonant converters is undertaken and the major characteristics of the zero-current-switching and zero-voltage-switching techniques are summarised in table 3-5.

A numeric method for the steady-state analysis of the boost ZVS-MRCs is described. The voltage waveforms of both switching devices are quasi-sinusoidal and the current waveforms are quasi-square waveforms. The voltage stress on the main switch is higher than in PWM converters, but reduced compared to QRCs. The voltage conversion ratio decreases with the increase of the switching frequency. The ZVS-MRCs operate with constant off-time and variable on-time. The load range of MRCs is improved compared to QRCs.

The dc modelling of QRCs and MRCs is undertaken. The averaging technique is used and the concept of characteristic functions is introduced, which describe the average behaviour of the switching devices. The characteristic functions G_v and G_i are calculated

using a numeric algorithm for MRCs. For QRCs, the two characteristic functions are equal, $G_v=G_i=G$, and the expression of G is analytically determined.

It is shown that the average equivalent circuit of all classes of boost converters is the one presented in figure 3-3. But the values of the voltage source $\bar{v}_D$ and current source $\bar{i}_S$ are different and depend on the characteristic function.

The voltage conversion ratio of the boost resonant converters is referred to the one of the PWM converter and is determined by replacing the duty ratio in the expression of the conversion ratio of the PWM converter with the characteristic function.

Table 3-5: A comparative analysis of ZCS and ZVS quasi-resonant converters.

	ZCS	ZVS
Switch's current waveform	quasi-sinusoidal waveform	quasi-square waveform
Switch's voltage waveform	quasi-square waveform	quasi-sinusoidal waveform
Diode's current waveform	quasi-square waveform	quasi-sinusoidal waveform
Diode's voltage waveform	quasi-sinusoidal waveform	quasi-square waveform
Current stress on switch	higher than corresponding PWM converter	same as in corresponding PWM converter.
Voltage stress on switch	same as corresponding PWM converter	higher than corresponding PWM converter
Voltage conversion ratio vs. switching frequency	increasing the switching frequency increases the voltage-conversion ratio	increasing the switching frequency decreases the voltage-conversion ratio
Regulation scheme	constant on-time ; variable off-time	constant off-time ; variable on-time
Load range	R_{0min} to ∞	0 to R_{0max}
Sensitivity of output voltage to load variations	sensitive in half-wave mode of operation; insensitive in the full-wave mode of operation	sensitive in half-wave mode of operation; insensitive in the full-wave mode of operation

4. Small-Signal Modelling of Boost Converters

4.1. Introduction

Quasi-resonant and multi-resonant converters are controlled by varying the switching frequency. Closed-loop regulation is most commonly achieved by feedback of the output voltage through an error-amplifier circuit and voltage-controlled-oscillator.

To design a stable and high-performance feedback control loop for a dc-dc converter, it is important to know the frequency responses of its power stage due to excitations at the control and source inputs. The open loop control-to-output transfer function is used for the analytical design of the control circuit to obtain the desired dynamic performance and system stability. To study the influence of the perturbations in the input voltage, the line-to-output transfer function, also referred to as audio susceptibility transfer function, is required.

Depending on the complexity of the converter power stage, these frequency responses (or transfer functions) may be obtained experimentally, numerically or analytically. Experimental measurements of the converter frequency responses become necessary when the converter power stage is known as a black box. If the circuit topology as well as the control technique of the converter are known, the power stage responses can be simulated numerically, thus avoiding the costly construction of the converter power stage. However, due to highly intensive computations, this method is time consuming. Hence, it is worthwhile to derive the analytical solutions so that excessive time and expense in the experimental approach can be avoided. It is more efficient to use analytical solutions for the power stage responses in the systematic design of a control circuit.

The previous chapter presents the dc or steady-state analysis of QRCs and MRCs. When evaluating a converter for an application, not only the dc design must be considered, but also the small-signal ac characteristics. The small-signal design affects the control loop

configuration and dynamic specifications and is a key parameter for feedback control implementation.

This chapter presents a review of small-signal modelling techniques for dc-dc switching converters. The averaging technique is used to derive the small-signal model of quasi-resonant and multi-resonant boost converters. It is first exemplified for the PWM boost converter and then extended to QRCs and MRCs. A general expression of the control-to-output and line-to-output transfer function of boost converters is given.

4.2. Small-Signal Modelling Techniques

Several techniques are described in the literature for the small-signal modelling of dc-dc switching converters, namely:

- the averaging technique;
- the sampled-data modelling technique;
- the harmonic balance technique;
- the time-varying transfer function technique;
- the extended describing function technique;
- the Volterra series modelling technique;
- empirical small-signal modelling technique using PSPICE.

4.2.1. The Averaging Technique

The averaging technique is a popular approach to model switching converters. It is valuable because it provides a method of analysing both the dc and ac behaviour of a large number of converters in a systematic manner. This method was originally proposed to model PWM converters [70-72]. Extensions of the method from hard-switching PWM converters to those employing various soft-switching techniques are proposed [73-79]. These methods use similar mathematical principles and share a common theoretical basis [80-87].

First the averaged models are obtained by replacing the instantaneous values of all state and control variables by their one-cycle averages. Using the perturbation and linearisation theory, the small-signal equivalent circuit is obtained and the control-to-output and line-to-output transfer functions are derived. The form of circuit models of QRCs and MRCs thus obtained is quite different from that of the PWM circuits. However, the end results of the analysis, the transfer functions of QRCs and MRCs, are similar to the PWM converters and suggest that all classes of converters can be analysed using a unified method. The properties of QRCs and MRCs can be linked to the properties of their related PWM converters. Therefore, the primary advantage of the averaging technique is that it permits a systematic and unified analysis of MRCs, QRCs and PWM converters and the large body of existing knowledge concerning PWM converters can be extended to QRCs and MRCs.

4.2.2. The Sampled-Data Modelling Technique

The sampled-data technique is one of the most mathematically detailed techniques for the small-signal modelling of converters [88]. One of the main assumptions is that the steady-state topological evolution of the converter may be represented by a sequence of piece-wise linear differential equations. On this basis the state-vector at the end of the $(k+1)^{th}$ cycle, X_{k+1}, may be expressed in terms of the state-vector at the end of the previous cycle, X_k:

$$X_{k+1} = F(U_k,T_k)X_k + G(U_k,T_k), \tag{4.1}$$

where:

U_k are the converter inputs at the end of the k^{th} cycle;

T_k is a vector of transition times, the instants in the cycle at which the converter switches from one configuration to the next;

F and G are functions of the vectors U_k and T_k.

The large signal, non-linear, discrete time representation of the converter in equation (4.1) is linearised by introducing small perturbations in all variables including the transition times, expanding the equation using a Taylor series and then neglecting the nonlinear terms. A small-signal discrete-time model results. Standard techniques may then be used to transform the discrete-time model into the continuous-time frequency domain for comparison with measurements.

To derive the small-signal sampled-data model, the converter steady-state operating conditions must be known accurately. The derivation procedure summarised above may then be undertaken. The complexity of the equations usually prevents explicit expressions being determined and the model must be calculated by computer.

Sampled data models have the shortcomings of discrete-time modelling. It is more desirable to have a continuous-time model, which is more adequate for designing an analogue compensator (fast, simple and low cost). A discrete time model is inconvenient because it has to be handled with z transformations and the model prediction is not directly supported by the measurements of a network analyser.

4.2.3. The Harmonic Balance Technique

The harmonic balance method [89,90] imitates the approach of a network analyser when measuring the transfer function of a real circuit. The piece-wise linear time-domain equations describing the system operation are first transformed into the frequency domain as a set of nonlinear equations that describe the harmonics of the system, typically one equation for each harmonic considered. This system representation is called the method of harmonic balance. A set of linearised, small-signal, frequency domain equations may be found by perturbing the set of nonlinear equations. The set of small-signal equations describe the harmonics of the system response to a periodic small-signal input. A laboratory network analyser emits a small-signal stimulus, and displays a ratio of two measurements that have been bandpass filtered, with the bandpass being very narrow and centred around the stimulus frequency. Thus, we may solve this set of small-signal equations for the harmonics of the response, select the

harmonics at the frequency of the stimulus, compute the appropriate ratios, and have the desired transfer functions.

4.2.4. The Time-Varying Transfer Function Technique

The time-varying transfer function technique [91,92] is similar to the harmonic balance method. It combines the time domain and frequency domain techniques. First, it is investigated how the injected control signal influences the duration of each stage, then it is evaluated how the perturbed waveforms propagate. Finally the spectral component of the output which has the same frequency with the injected signal is calculated.

Both methods can predict small-signal frequency response accurately up to one-half of the switching frequency. These methods can be applied to any piece-wise linear circuit and there is no theoretical limitation to apply them to resonant type converters. But so far only examples of PWM converters have been reported. One disadvantage is the fact that they cannot provide a unified small-signal model but only Bode plots. Therefore it is difficult to evaluate the closed-loop small-signal behaviour of the circuit. The main disadvantage is that they present an increased complexity even for simple circuits.

4.2.5. The Extended Describing Function Technique

The extended describing function method [93-96] is a general approach for modelling switching converters. Continuous small-signal models are derived, which can be employed in the control-loop design of converters. The derivation of models starts from the non-linear differential equations of the converter. The nonlinear terms are approximated either by the fundamental component terms (for example for the resonant tank waveforms) or by the dc terms. This step is called harmonic approximation and the extended describing functions are defined. They are functions of the operating conditions and the harmonic coefficients of the state variables and can be calculated by making Fourier expansions of the nonlinear terms. A new system of nonlinear equations, called modulation equations is obtained. It is a nonlinear large-signal model

of the converter power stage. Under steady-state conditions, the new state variables of the modulation equations do not change with time. For a given operating point, the steady-state solution is obtained, which provides the results of the dc analysis. By perturbing the large-signal model around the operating point and by making linearisation under the small-signal assumption, an analytical model is obtained. Using controlled-sources the small-signal equivalent circuit is derived.

The extended describing function method proved to be very efficient for load resonant converters [97,98], like the series and parallel resonant converters and their derivations, but has never been applied to quasi-resonant converters.

4.2.6. The Volterra Series Modelling Technique

The Volterra series method for obtaining the nonlinear control-to-output response is applied for PWM [99] and quasi-resonant [100] converters. A multi-input system is considered which facilitates the examination of the output distortion due to both supply voltage and duty ratio disturbances. The expressions for the Volterra kernels are calculated, the perturbed nonlinear state-space model is obtained and the spectral components of the converter output waveform are predicted. The small-signal model developed using this technique is more complex than using other methods.

4.2.7. Empirical Small-Signal Modelling Technique Using PSPICE

A method for the empirical small-signal modelling of switching converters using PSPICE has been developed [101]. It adopts an input-output data analysis point of view. It presumably treats any converter as a black box and identifies the unknown small-signal model based on its input-output response. The approach is accurate up to one half of the switching frequency and suitable for identification of various types of converters. The small-signal procedure consists of three steps. Firstly, the converter is modelled using PSPICE for data generation. Secondly, an algorithm is performed on the data to approximate the equivalent auotregressive moving average model. Finally, the

conversion to small-signal transfer function is performed. The method is difficult to apply and complicated since the data obtained from the PSPICE simulation has to be transferred into MATLAB for the identification of the small-signal transfer functions.

4.3. Small-Signal Modelling of PWM Converters

The averaging technique is employed for the small-signal modelling of boost converters. The first step in obtaining the small-signal model of a converter is to derive the nonlinear circuit that describes the average behaviour of the power circuit, as described in section 3.4.

The averaged models of switching power electronic circuits are nonlinear. Assessing stability and designing or evaluating controllers with nonlinear models is usually difficult. The most common and generally successful approach to this task is linearisation. It yields linear models that approximately describe small deviations or perturbations from nominal operation of a system. Linearised models, also called small-signal models, are crucial to evaluating the stability of a system at nominal operating condition.

The small-signal model of a dc-dc converter is obtained by applying the perturbation theory [69]. The steady-state duty ratio d of the boost converter is pertubed by $\tilde{d}$. The corresponding perturbations in the output voltage V_{out} and average diode voltage $\overline{v}_D$ are $\tilde{v}_{out}$ and $\tilde{v}_D$, respectively. For any variable x of the averaged model of the converter it can be written that

$\overline{x}=X+\tilde{x}$,

where

$\overline{x}$ is the averaged value;

X is the dc steady-state value;

$\tilde{x}$ is the ac small-signal perturbation.

The superposition theorem is applied and the small-signal equivalent circuit of a boost converter is given in figure 4-1.

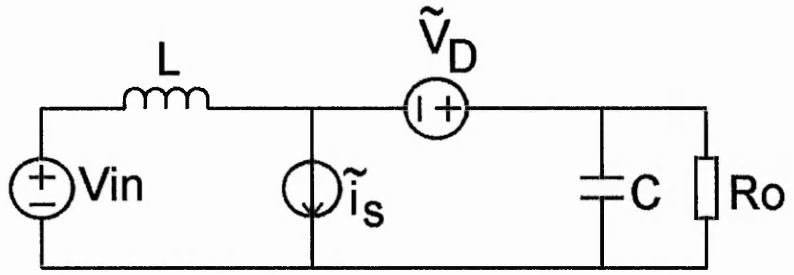

Figure 4-1: Equivalent small-signal circuit of a boost converter.

As a result of the perturbation, equation (3.4) becomes

$\bar{v}_D + \tilde{v}_D = (d + \tilde{d})(V_{out} + \tilde{v}_{out})$ or

$\bar{v}_D + \tilde{v}_D = dV_{out} + \tilde{d}\tilde{v}_{out} + \tilde{d}V_{out} + d\tilde{v}_{out}$.

The small signal approximations are made, namely that the departures from the steady-state values are small compared to the steady-state values themselves and nonlinear terms such as the second order or higher terms due to the product of two or more ac perturbations are neglected.

The dc and ac components are separated and the term $\tilde{d}\tilde{v}_{out}$ is neglected. It is obtained that:

$$\tilde{v}_D = \tilde{d}V_{out} + d\tilde{v}_{out}. \qquad (4.2)$$

Similarly by perturbing equation (3.5) it is calculated that

$$\tilde{i}_S = \tilde{d}I_{in} + d\tilde{i}_{in}. \qquad (4.3)$$

Kirchhoff's laws are satisfied for ac and dc quantities. The reason is that the derivations from nominal (or ac quantities) are obtained by taking the difference between two sets of voltages or currents - the perturbed set and the nominal set - that each satisfy the

same linear equations. Kirchhoff's laws for the equivalent small-signal circuit of a boost converter are:

$$\tilde{v}_{in} = L\frac{d\tilde{i}_{in}}{dt} - \tilde{v}_D + \tilde{v}_{out} \tag{4.4}$$

$$\tilde{i}_{in} = \tilde{i}_S + C\frac{d\tilde{v}_{out}}{dt} + \frac{\tilde{v}_{out}}{R}. \tag{4.5}$$

Equations (4.4) and (4.5) consist of ac perturbations in the time domain. They are transformed into the s-domain by using the Laplace transformation.

$$\tilde{v}_{in} = sL\tilde{i}_{in} - \tilde{v}_D + \tilde{v}_{out} \tag{4.6}$$

$$\tilde{i}_{in} = \tilde{i}_S + sC\tilde{v}_{out} + \frac{\tilde{v}_{out}}{R}. \tag{4.7}$$

For control design purposes, the transfer function from perturbation $\tilde{d}$ in the duty cycle, which constitutes the control input, to perturbation $\tilde{v}_{out}$ in the output voltage for a constant input voltage V_{in} must be known. This function, called control-to-output transfer function, is obtained by a straightforward computation setting $\tilde{v}_{in} = 0$ and is:

$$\frac{\tilde{v}_{out}(s)}{\tilde{d}(s)} = -\left(\frac{I_{in}}{C}\right)\frac{s - \frac{(1-d)V_{out}}{LI_{in}}}{s^2 + \frac{1}{R_0C}s + \frac{(1-d)^2}{LC}}. \tag{4.8}$$

The transfer function from a perturbation in the input voltage to the output voltage for a constant duty ratio d is called line-to-output transfer function and is determined by setting $\tilde{d} = 0$:

$$\frac{\tilde{v}_{out}(s)}{\tilde{v}_{in}(s)} = \frac{\frac{1-d}{LC}}{s^2 + \frac{1}{R_0C}s + \frac{(1-d)^2}{LC}}. \tag{4.9}$$

Figure 4-2 and figure 4-3 show the Bode plots of the small-signal transfer functions of a PWM boost converter.

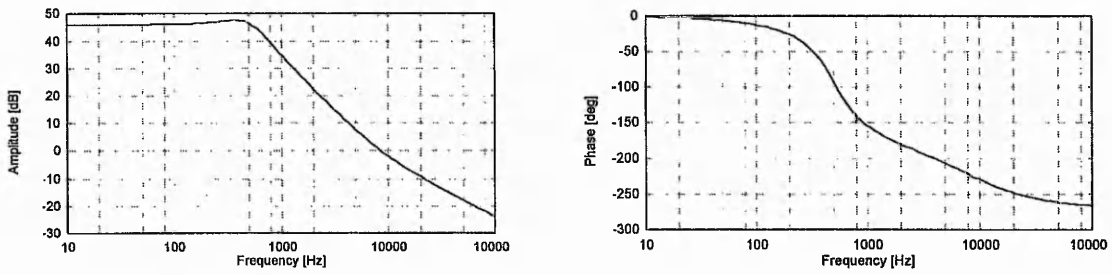

Figure 4-2: Bode plots of the control-to-output transfer function.

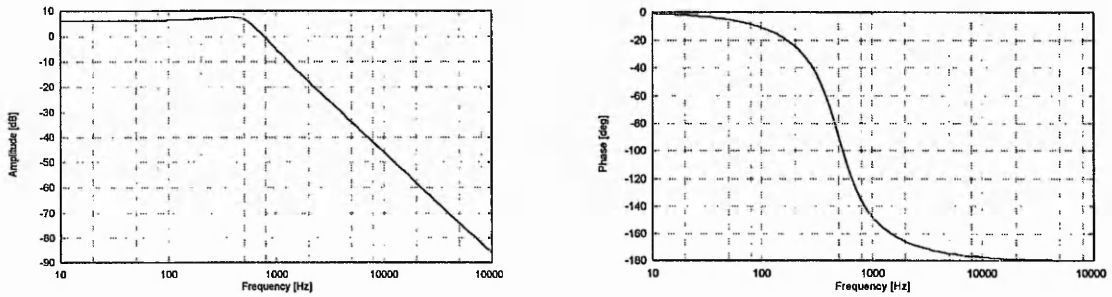

Figure 4-3: Bode plots of the line-to-output transfer function.

Equation (4.6) shows that a right-half-plane (RHP) zero appears in the small-signal control-to-output transfer function of the boost converter. A Bode plot of the RHP zero has the characteristic of a rising 20 dB/decade gain with 90 degrees phase lag instead of the more usual phase lead. This characteristic is difficult to compensate and the 90 degree phase lag severely constrains the loop gain crossover to a frequency much lower than the RHP zero. It limits the dynamic performance of the converter and it is difficult to obtain a good stability margin and a good transient response from a boost converter operating in continuous conduction mode.

Systems which have a RHP zero are referred to as *non-minimum phase systems*. RHP zeros do not usually give rise to instability, but they do give rise to responses which

initially tend to go in the opposite direction in the steady-state response, as shown in figure 4-4.

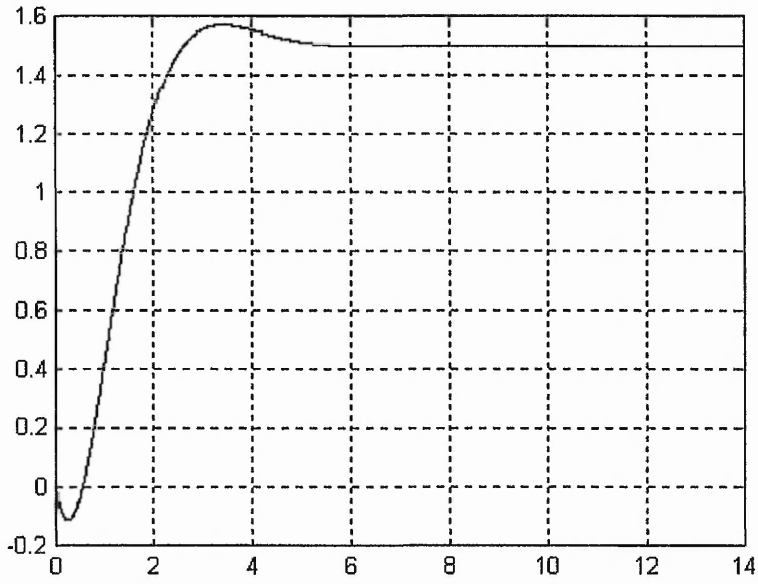

Figure 4-4: Transient response of boost converter.

In simple terms, the right-half-plane zero is best explained by considering the transient action of a PWM boost converter operating in continuous conduction mode. When a sudden decrease of the load occurs, the load current increases and the capacitor voltage immediately starts to drop. The resulting error voltage temporarily increases the duty cycle d, causing the inductor current to rise to accommodate the increased load current. However, it may take many cycles for the inductor current to complete its rise. During this time, increased d makes (1-d) smaller. Since $I_{out}=I_{in}(1-d)$, the output current is temporarily decreased, the opposite of what is desired. This additional lag because of the right-half-plane zero inevitably forces the loop gain crossover frequency to be much lower than otherwise desired.

It would seem that the only cure for this effect is to change the pulse width slowly over a large number of cycles, so that the inductor current can follow the change. Under these conditions, the dynamic output reversal does not occur; however, the transient response is rather poor. There is in addition a large signal problem with continuous mode circuits:

the inability to rapidly slew the inductor current as desired with large step changes in load. This is because of the large inductor values used in continuous mode circuits.

The right-half-plane zero never occurs in circuits of the buck family because the output current equals the inductor current. It is encountered only in boost and buck-boost circuits, and then only when these circuits are operated in the continuous conduction mode.

4.4. Small-Signal Modelling of Quasi-Resonant Converters

The small-signal model of a boost quasi-resonant converter is obtained by linearising the equivalent averaged circuit of the converter, which is shown in figure 3-3, around a steady-state operating point. If a perturbation is applied to the averaged circuit, as shown in section 4.3., the circuit in figure 4-1 is obtained. But, unlike for the PWM converter, this circuit is nonlinear for quasi-resonant boost converters because the voltage source $\bar{v}_D$ and the current source $\bar{i}_S$ are nonlinear. The average values of the diode voltage and switch current are given by equations (3.33) and (3.34). The characteristic function $G(f_S,I_{in},V_{out})$ depends nonlinearly on the switching frequency f_S, the input current I_{in} and the output voltage V_{out}.

To linearise a nonlinear equation around a static operating point, the Taylor series for a multi-variable function is used and the second and higher order terms are neglected. If f(x,y,z) is the multi-variable function which is linearised around the static point (x_0,y_0,z_0), it can be written that

$$f(x,y,z) = f(x_0,y_0,z_0) + \frac{\partial f}{\partial x}(x-x_0) + \frac{\partial f}{\partial y}(y-y_0) + \frac{\partial f}{\partial z}(z-z_0). \qquad (4.10)$$

All partial derivatives are calculated for the static point (x_0,y_0,z_0).

Each of the equations (3.33) and (3.34) are expanded as a function of the small-signal variation of the quantities $\tilde{i}_{in}$, $\tilde{v}_{out}$ and $\tilde{f}_S$, where ~ signifies the small-signal variation of a quantity as defined before.

The variation of the diode voltage $\bar{v}_D$ is:

$$\tilde{v}_D = \frac{\partial \bar{v}_D}{\partial I_{in}} \tilde{i}_{in} + \frac{\partial \bar{v}_D}{\partial V_{out}} \tilde{v}_{out} + \frac{\partial \bar{v}_D}{\partial f_S} \tilde{f}_S . \tag{4.11}$$

The small-signal variation of the switch current $\bar{i}_S$ is given by:

$$\tilde{i}_S = \frac{\partial \bar{i}_S}{\partial I_{in}} \tilde{i}_{in} + \frac{\partial \bar{i}_S}{\partial V_{out}} \tilde{v}_{out} + \frac{\partial \bar{i}_S}{\partial f_S} \tilde{f}_S . \tag{4.12}$$

Calculating the partial derivatives in (4.11) and (4.12), it is obtained:

$$\begin{aligned}
k_{vv} &= \frac{\partial \bar{v}_D}{\partial V_{out}} = G(f_n,\alpha) - \alpha \frac{\partial G(f_n,\alpha)}{\partial \alpha}; \\
k_{vi} &= \frac{\partial \bar{v}_D}{\partial I_{in}} = Z_r \frac{\partial G(f_n,\alpha)}{\partial \alpha}; \\
k_{vf} &= \frac{\partial \bar{v}_D}{\partial f_S} = \frac{V_{out}}{f_r} \frac{\partial G(f_n,\alpha)}{\partial f_n}; \\
k_{iv} &= \frac{\partial \bar{i}_S}{\partial V_{out}} = -\frac{1}{Z_r} \alpha^2 \frac{\partial G(f_n,\alpha)}{\partial \alpha}; \\
k_{ii} &= \frac{\partial \bar{i}_S}{\partial I_{in}} = G(f_n,\alpha) + \alpha \frac{\partial G(f_n,\alpha)}{\partial \alpha}; \\
k_{if} &= \frac{\partial \bar{i}_S}{\partial f_S} = \frac{I_{in}}{f_r} \frac{\partial G(f_n,\alpha)}{\partial f_n} .
\end{aligned} \tag{4.13}$$

All partial derivatives, or k-parameters, are expressed as a function of the normalised input current α, which is defined by equation (3.20) as $\alpha(I_{in}, V_{out}) = \frac{Z_r I_{in}}{V_{out}}$.

The units of each k-parameter can be found by imagining a fraction bar (/) between the two subscripts.

By taking into account equation (4.11) each term can be represented by a controlled voltage source of a value given by the appropriate k-parameter. These three sources

replace the diode D. Similarly from equation (4.12), the switch S can be replaced by three current sources. The equivalent small-signal model of the converter is shown in figure 4-5.

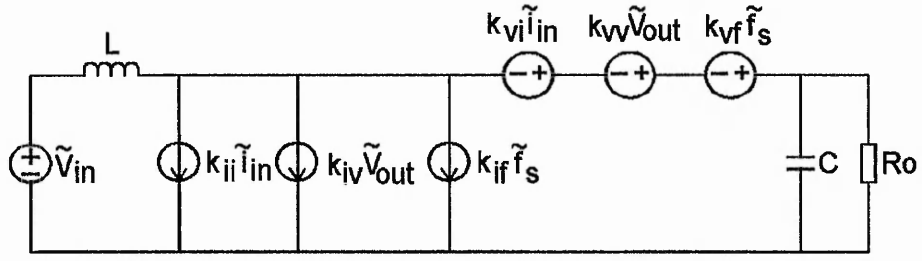

Figure 4-5: Small-signal linear equivalent circuits for boost QRCs.

The expressions of the characteristic function G_{ZCS} of the ZCS boost converter and G_{ZVS} of the ZVS boost converter are given by equations (3.37) and (3.38), respectively:

$$G_{ZCS}(f_n,\alpha)=\frac{1}{2\pi}f_n\left[\frac{\alpha}{2}+\pi+\arcsin\alpha+\frac{1}{\alpha}\left(1+\sqrt{1-\alpha^2}\right)\right],$$

$$G_{ZVS}(f_n,\alpha)=1-\frac{1}{2\pi}f_n\left[\frac{1}{2\alpha}+\pi+\arcsin\frac{1}{\alpha}+\alpha\left(1+\sqrt{1-\frac{1}{\alpha^2}}\right)\right].$$

The partial derivatives of the characteristic functions G_{ZCS} and G_{ZVS} are:

$$\frac{\partial G_{ZCS}(f_n,\alpha)}{\partial\alpha}=\frac{f_n}{2\pi}\left(\frac{1}{2}-\frac{1+\sqrt{1-\alpha^2}}{\alpha^2}\right); \tag{4.14}$$

$$\frac{\partial G_{ZCS}(f_n,\alpha)}{\partial f_n}=\frac{1}{2\pi}\left[\frac{\alpha}{2}+\pi+\arcsin\alpha+\frac{1}{\alpha}\left(1+\sqrt{1-\alpha^2}\right)\right]; \tag{4.15}$$

$$\frac{\partial G_{ZVS}(f_n,\alpha)}{\partial\alpha}=\frac{f_n}{2\pi}\left(\frac{1}{2\alpha^2}-1-\sqrt{1-\frac{1}{\alpha^2}}\right); \tag{4.16}$$

$$\frac{\partial G_{ZVS}(f_n,\alpha)}{\partial f_n}=-\frac{1}{2\pi}\left[\frac{1}{2\alpha}+\pi+\arcsin\frac{1}{\alpha}+\alpha\left(1+\sqrt{1-\frac{1}{\alpha^2}}\right)\right]. \tag{4.17}$$

Considering the relationship between G_{ZCS} and G_{ZVS} given by equation (3.39), the relationship between their partial derivatives is:

$$\frac{\partial G_{ZVS}(f_n,\alpha)}{\partial \alpha} = \frac{1}{\alpha^2}\frac{\partial G_{ZCS}(f_n,\frac{1}{\alpha})}{\partial(\frac{1}{\alpha})}; \tag{4.18}$$

$$\frac{\partial G_{ZVS}(f_n,\alpha)}{\partial f_n} = -\frac{1}{f_n}G_{ZCS}(f_n,\frac{1}{\alpha}). \tag{4.19}$$

Kirchhoff's laws are satisfied for small-perturbations and equations (4.4) to (4.7) are valid. In equation (4.6) $\tilde{v}_D$ is replaced by $\tilde{v}_D = k_{vi}\tilde{i}_{in} + k_{vv}\tilde{v}_{out} + k_{vf}\tilde{f}_S$ and in equation (4.7) $\tilde{i}_S$ is replaced by $\tilde{i}_S = k_{ii}\tilde{i}_{in} + k_{iv}\tilde{v}_{out} + k_{if}\tilde{f}_S$. The control-to-output transfer function is obtained by considering the input voltage constant or $\tilde{v}_{in} = 0$:

$$\frac{\tilde{v}_{out}}{\tilde{f}_s} = -\frac{k_{if}}{C}\frac{s - \frac{1}{Lk_{if}}[k_{vf}(1-k_{ii}) + k_{vi}k_{if}]}{s^2 + s\left(\frac{1}{R_0C} + \frac{k_{iv}}{C} - \frac{k_{vi}}{L}\right) + \frac{1}{LC}\left[(1-k_{ii})(1-k_{vv}) - k_{iv}k_{vi} - \frac{k_{vi}}{R_0}\right]}. \tag{4.20}$$

The line-to-output transfer function is obtained by considering the switching frequency constant or $\tilde{f}_S = 0$:

$$\frac{\tilde{v}_{out}}{\tilde{v}_{in}} = \frac{1-k_{ii}}{LC}\frac{1}{s^2 + s\left(\frac{1}{R_0C} + \frac{k_{iv}}{C} - \frac{k_{vi}}{L}\right) + \frac{1}{LC}\left[(1-k_{ii})(1-k_{vv}) - k_{iv}k_{vi} - \frac{k_{vi}}{R_0}\right]}. \tag{4.21}$$

For the voltage-mode control of QRCs, the voltage-controlled-oscillator can be modelled by a constant gain block [22]. If the voltage-controlled-oscillator is considered in the control-to-output transfer function, it becomes:

$$\frac{\tilde{v}_{out}}{\tilde{v}_{control}} = k_{VCO}\frac{\tilde{v}_{out}}{\tilde{f}_S}. \tag{4.22}$$

It should be noted that for QRCs the control quantity is the switching frequency f_S, since they operate with variable frequency, and for PWM converters the control quantity is the duty ratio d, since they operate with constant switching frequency. There is a similarity between the transfer functions of boost QRCs and PWM converters. All transfer functions are second order and the control-to-output transfer functions have a right-half-plane zero.

The transfer functions (4.8) and (4.9) of PWM converters can be obtained from equations (4.20) and (4.21), respectively, by replacing the switching frequency f_S with the duty ratio d and knowing that the characteristic function uniquely depends on d and has the expression G(d)=d. The k-parameters of the boost PWM converter will be the following:

$$
\begin{aligned}
k_{vv} &= \frac{\partial \bar{v}_D}{\partial V_{out}} = d; \\
k_{vi} &= \frac{\partial \bar{v}_D}{\partial I_{in}} = 0; \\
k_{vf} &= \frac{\partial \bar{v}_D}{\partial d} = V_{out}; \\
k_{iv} &= \frac{\partial \bar{i}_S}{\partial V_{out}} = 0; \\
k_{ii} &= \frac{\partial \bar{i}_S}{\partial I_{in}} = d; \\
k_{if} &= \frac{\partial \bar{i}_S}{\partial d} = I_{in}.
\end{aligned}
\tag{4.23}
$$

4.5. Small-Signal Modelling of Multi-Resonant Converters

The small-signal equivalent circuit presented in figure 4-5 is valid for boost MRCs as well as for boost QRCs. The evaluation of the k-parameters is different for the boost MRC.

The average values of the diode voltage and of the switch current are given by equations (3.76) and (3.77):

$$\bar{v}_D = G_v(f_S, I_{in}, V_{out})V_{out};$$
$$\bar{i}_S = G_i(f_S, I_{in}, V_{out})I_{in}.$$

They are expanded as a function of the small-signal variation of the quantities $\tilde{v}_{out}$, $\tilde{i}_{in}$ and $\tilde{f}_S$:

$$\tilde{v}_D = k_{vv}\tilde{v}_{out} + k_{vi}\tilde{i}_{in} + k_{vf}\tilde{f}_S; \tag{4.24}$$
$$\tilde{i}_S = k_{iv}\tilde{v}_{out} + k_{ii}\tilde{i}_{in} + k_{if}\tilde{f}_S. \tag{4.25}$$

The expressions of the k-coefficients are as follows:

$$k_{vv} = \frac{\partial \bar{v}_D}{\partial V_{out}} = G_v(f_n,\alpha) - \alpha\frac{\partial G_v(f_n,\alpha)}{\partial \alpha};$$
$$k_{vi} = \frac{\partial \bar{v}_D}{\partial I_{in}} = Z_r\frac{\partial G_v(f_n,\alpha)}{\partial \alpha};$$
$$k_{vf} = \frac{\partial \bar{v}_D}{\partial f_S} = \frac{V_{out}}{f_r}\frac{\partial G_v(f_n,\alpha)}{\partial f_n}; \tag{4.26}$$
$$k_{iv} = \frac{\partial \bar{i}_S}{\partial V_{out}} = -\frac{1}{Z_r}\alpha^2\frac{\partial G_i(f_n,\alpha)}{\partial \alpha};$$
$$k_{ii} = \frac{\partial \bar{i}_S}{\partial I_{in}} = G_i(f_n,\alpha) + \alpha\frac{\partial G_i(f_n,\alpha)}{\partial \alpha};$$
$$k_{if} = \frac{\partial \bar{i}_S}{\partial f_S} = \frac{I_{in}}{f_r}\frac{\partial G_i(f_n,\alpha)}{\partial f_n}.$$

It is shown in section 3.6. that the characteristic functions G_v and G_i are determined by using a numeric algorithm. To calculate the derivatives of G_v and G_i with respect to the normalised switching frequency f_n and normalised input current α, a numeric procedure has to be used as well. The partial derivative of G_v with respect to α is calculated from

$$\frac{\partial G_v}{\partial \alpha} = \frac{G_v(\alpha + \Delta\alpha, f_n) - G_v(\alpha, f_n)}{\Delta\alpha}, \tag{4.27}$$

where $\Delta\alpha$ is as small as possible.

The partial derivative of G_v with respect to f_n is calculated from

$$\frac{\partial G_v}{\partial f_n} = \frac{G_v(\alpha, f_n + \Delta f_n) - G_v(\alpha, f_n)}{\Delta f_n}, \tag{4.28}$$

where Δf_n is as small as possible.

The partial derivatives of the second characteristic function G_i are calculated in a similar manner.

The mathematical expressions of the control-to-output and line-to-output transfer functions of the boost ZVS-MRC are the same as for the boost QRC and are given by equations (4.20) and (4.21).

4.6. Conclusions

This chapter presents a method based on the averaging technique for the small-signal modelling of boost resonant converters. The small-signal equivalent circuits are obtained and the mathematical expressions of the control-to-output and line-to-output transfer functions are derived.

The boost QRCs and MRCs have the same small-signal equivalent model and the same mathematical expressions for the transfer functions. Although the equivalent small-signal circuit of resonant boost converters is different from the one of the PWM converter, the transfer functions of all classes of boost converters have the same order -

second order. The control-to-output transfer function has a right-half-plane zero, which restricts the dynamic performance of the converters.

The resonant elements do not increase the order of the model. Therefore, the existing knowledge for the design of the feedback loop of PWM converters can be applied to quasi-resonant and multi-resonant converters.

5. Simulation, Hardware Implementation and Experimental Results

5.1. Introduction

A power electronic system consists of two main parts: the power converter and the control system. The power converter consists of passive components (inductors, capacitors, resistors) and solid state switches. Accurate simulation of the power converter in the time domain is a necessity for minimising costly repetitions of designs and breadboarding. There are many benefits of simulation [102-104], some of which are listed below.

(i) The understanding of the circuit is improved.
(ii) The overall design process is shortened, since it is easier to study the influence of a parameter on the system behaviour in simulation, as compared to accomplishing the same in the laboratory on a hardware breadboard.
(iii) A simulation can discover possible problems and determine optimal parameters.
(iv) Simulated waveforms at different places in the circuit can be easily monitored without the hardware hindrance of measurement noise. As switching frequencies increase, the problem of laboratory measurement becomes more and more difficult.

For the design of the control system, the frequency-domain analysis is necessary. A linear equivalent circuit of the power processor or the frequency-domain transfer function needs to be available. Small-signal perturbations, for which the assumption of linearity is valid, are applied and the stability and dynamic performance of the overall system is analysed. It allows well-established control theory techniques to be used. Simulation capability in the frequency domain is now a standard feature of almost all general-purpose simulation packages.

After an electronic system has been designed and successfully simulated, it can be built and tested.

This chapter describes simulation techniques that can be used for quasi-resonant and multi-resonant converters. It also presents the hardware implementation of quasi-resonant and multi-resonant converters and shows the experimental results that have been obtained.

5.2. Simulation of Quasi-Resonant and Multi-Resonant Converters

For the present research project, two types of simulations need to be carried out:
- open-loop, large-signal simulations, and
- small-signal modelling and simulation.

The main software package used is MicroSim Design Center version 5.3. It consists of three programs: Schematics for entering the circuit diagram, PSpice to perform the actual simulations and Probe to view the simulated waveforms. Both time-domain and frequency-domain analysis can be undertaken.

5.2.1. Large-Signal Simulation

In order to get a better understanding of the behaviour of a system, the power converter is simulated with prespecified control signals. The objective of the simulation is to obtain various voltage and current waveforms of the converter and to verify that the circuit behaves properly, as predicted by the analytical calculations. This step provides the designer with a choice of circuit topology and the component values.

This simulation includes each switch opening and closing, and the simulation is carried out over a large number of switching cycles to reach steady-state. No benefit is gained by including very detailed models of the circuit components. Therefore, the switching devices should be represented by simple, idealised models. Because the design of the controller still remains to be carried out, it is not represented. Therefore, the simulation is called open-loop simulation.

The power switch S of the converters is modelled as a two-valued resistor: a low-resistance in the on-state and a high-resistance in the off-state. If an ideal switch is used (short circuit in its on-state and open-circuit in the off-state), there can be numerical problems in the simulation. The internal system of equations of the simulator will easily end up as a singular system, that is, a system with no solution. Accurate models of solid-state switches are usually not available, very difficult to obtain and increase the simulation time considerably (because they incorporate controlled sources or nonlinear capacitors).

Because only the steady-state waveforms are of interest, initial conditions are specified at the start of the simulation.

Two approaches are used to simulate QRCs and MRCs. The difference consists in the way the main switch S is controlled.

For the first method, a voltage pulse generator is used to directly control the switch S. No zero-current or zero-voltage detection is implemented. The advantage of this method is that the simulation is fast. The disadvantage is that either the on-time for ZCS converters or off-time for ZVS converters has to be accurately calculated before the start of the simulation. If the value of the on-time or off-time is different from the one required, the converter will not operate with zero-current or zero-voltage conditions.

The second method takes advantage of the mixed-mode simulation capability of PSpice 5.3. True zero-detection is achieved, but with the cost of an increased simulation time. For ZCS converters, a low-value resistor is connected in series with switch S to enable the detection of the moment when the current reaches zero. The signal proportional to the current is fed into a comparator. To consider the propagation delay between the instant the zero-value is sensed and the instant the switch is actually turned on, an offset voltage in the range 0.1...0.5 V is connected to the other input of the comparator. The output of the comparator is connected to a monostable multivibrator digital circuit, which is triggered on the falling edge of the comparator. The width of the pulse

generated by the monostable circuit is equal to the off-time of the switch, which in a practical circuit is variable and controlled by the voltage controlled oscillator.

A similar circuit is used for the simulation of ZVS converters, for which the voltage across the switch is fed to the comparator through a resistive divider. The width of the pulse generated by the monostable circuit is equal to the on-time of the switch, which in a practical circuit is variable and controlled by the VCO.

Guidelines for the design of quasi-resonant and multi-resonant converters are given in appendix 4 and will not be presented in this chapter.

The following converters are simulated:

(i) boost ZCS-QRC;
(ii) boost ZVS-QRC;
(iii) boost ZVS-MRC.

The component values, operating conditions and simulated waveforms of these converters are given below.

(i) Boost ZCS-QRC

The resonant elements are L_r=3μH, C_r=30nF, the resonant frequency is f_r=500kHz and the characteristic impedance Z_r=10Ω. The load resistance is R_0=100Ω and the normalised load resistance is r=10. The input inductor and output capacitor have the values of L=330μH and C=22μF, respectively.

Figures 5-1 and 5-2 show the simulated circuit of the boost ZCS-QRC for both methods described above. The waveforms for an input voltage V_{in}=20V and a switching frequency f_S=200 kHz are shown in figure 5-3.

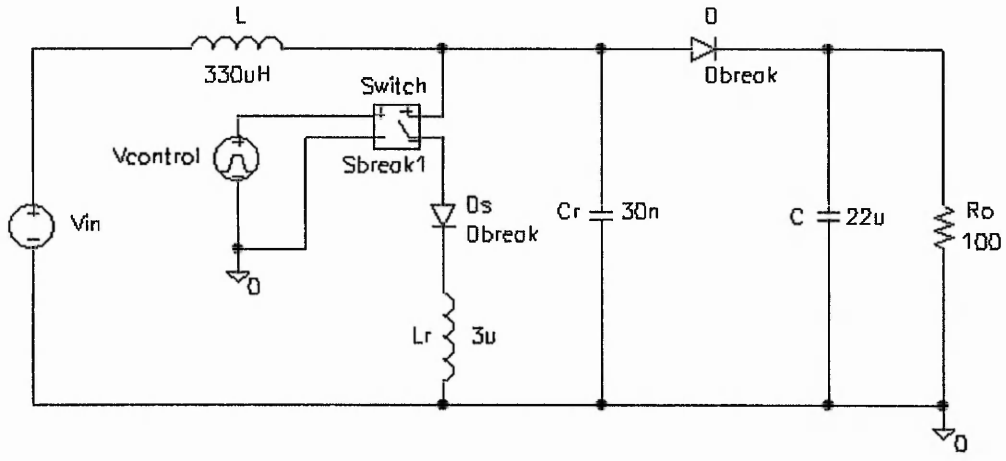

Figure 5-1: Simulation circuit of the boost ZCS-QRC.

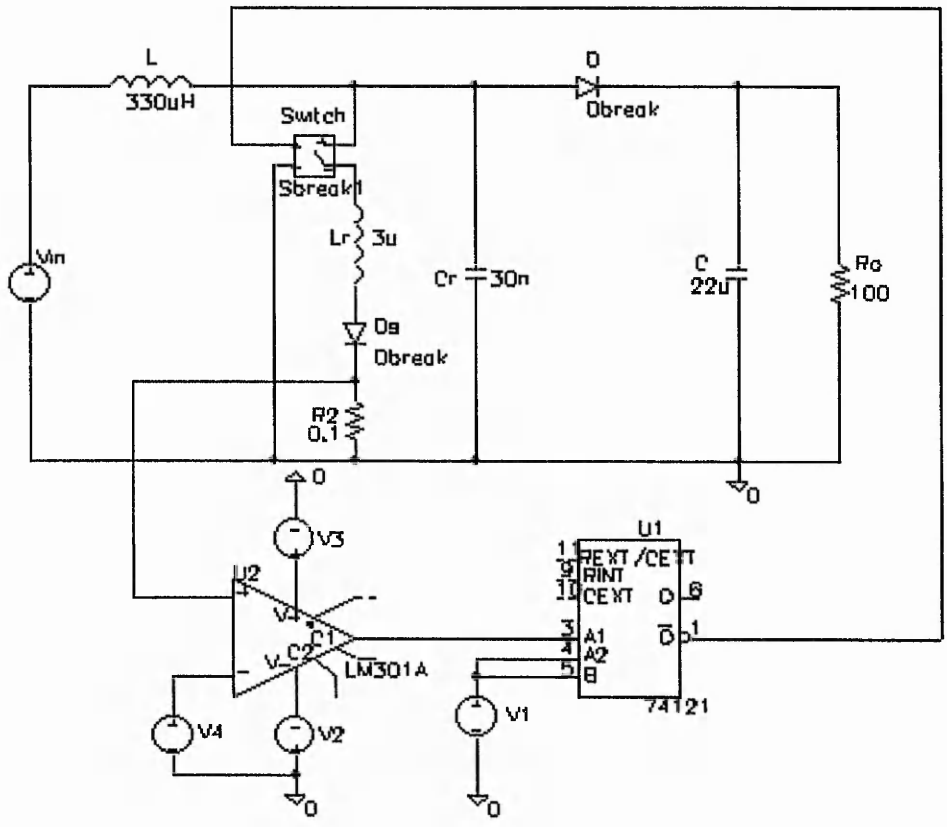

Figure 5-2: Simulation circuit of boost ZCS-QRC using zero-current detection.

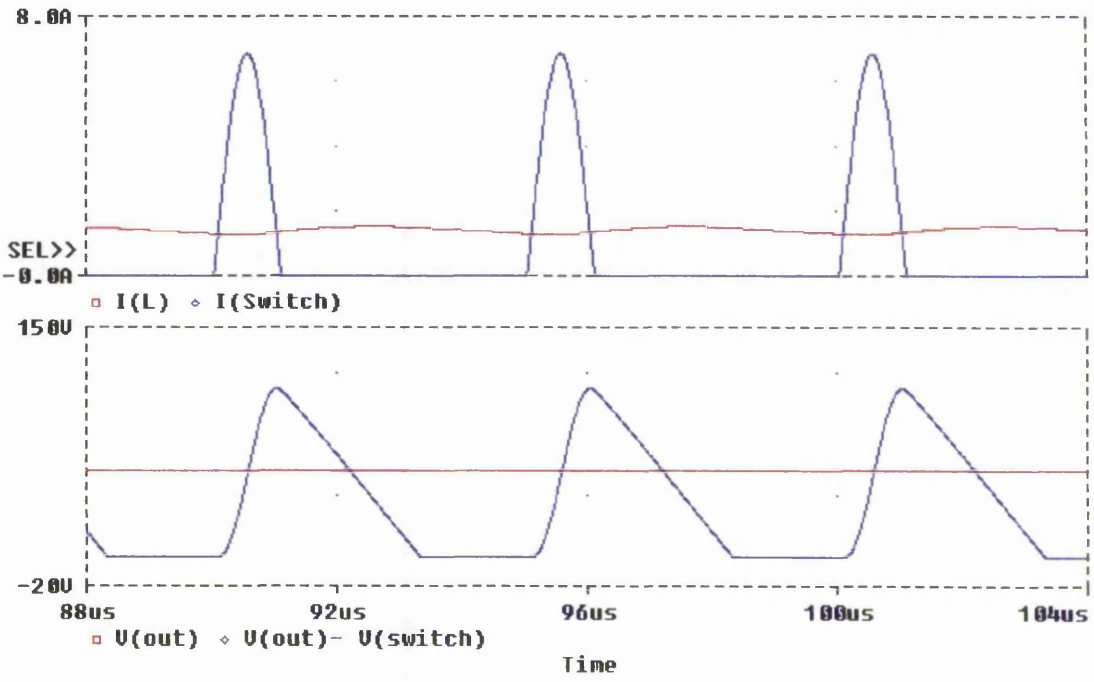

Figure 5-3: Simulated waveforms of boost ZCS-QRC: input inductor current I(L); switch current I(Switch); output voltage V(out); voltage across output diode V(out)-V(switch).

(ii) Boost ZVS-QRC

The resonant elements are L_r=47μH, C_r=13.3nF, the resonant frequency is f_r=200kHz and the characteristic impedance Z_r=60Ω. The load resistance is R_0=30Ω and the normalised load resistance is r=0.5. The input inductor and output capacitor have the values of L=390μH and C=22μF, respectively.

Figures 5-4 and 5-5 show the simulated circuit of the boost ZVS-QRC for both methods described above. The waveforms for an input voltage V_{in}=15V and a switching frequency f_S=100kHz are shown in figure 5-6.

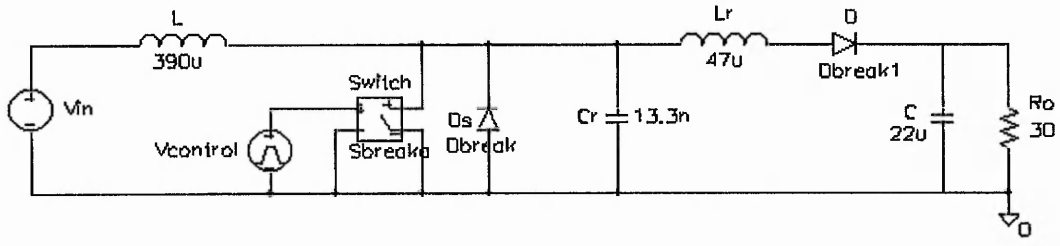

Figure 5-4: Simulation circuit of boost ZVS-QRC.

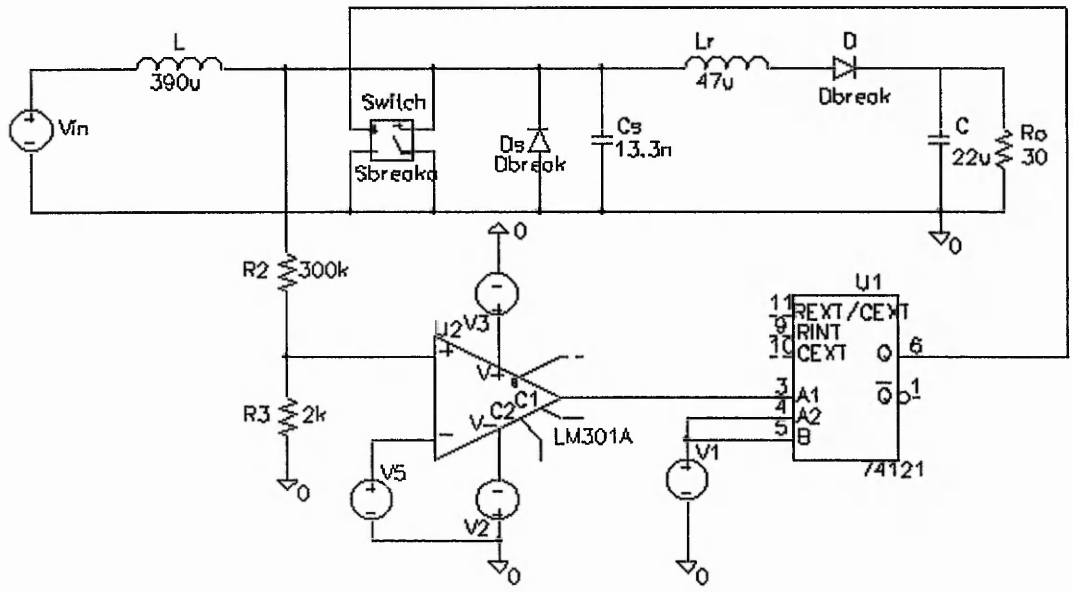

Figure 5-5: Simulation circuit of boost ZVS-QRC using zero-voltage detection.

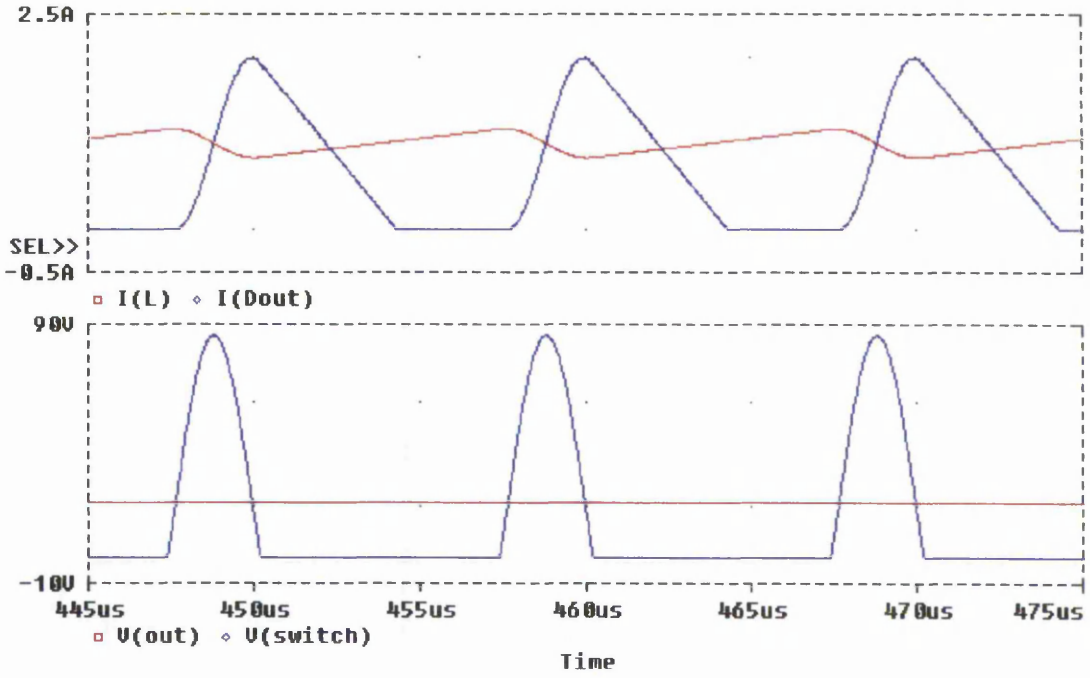

Figure 5-6: Simulated waveforms of boost ZVS-QRC: input inductor current I(L); output diode current I(Dout); output voltage V(out); voltage across main switch V(switch).

(iii) Boost ZVS-MRC

The resonant elements are L_r=47μH, C_S=13.3nF, C_D=39.8nF the resonant frequency is f_r=200kHz and the characteristic impedance Z_r=60Ω. The load resistance is R_0=30Ω and the normalised load resistance is r=0.5. The input inductor and output capacitor have the values of L=330μH and C=22μF, respectively.

Figures 5-7 and 5-8 show the simulated circuit of the boost ZVS-MRC for both methods described above. The waveforms for an input voltage V_{in}=15V and a switching frequency f_S=100kHz are shown in figure 5-9.

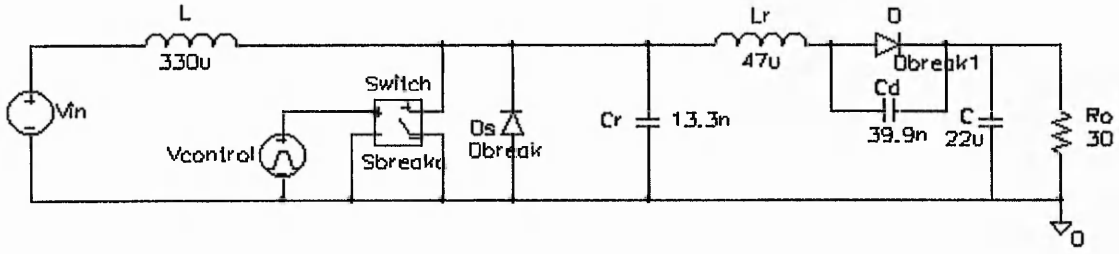

Figure 5-7: Simulation circuit of boost ZVS-MRC.

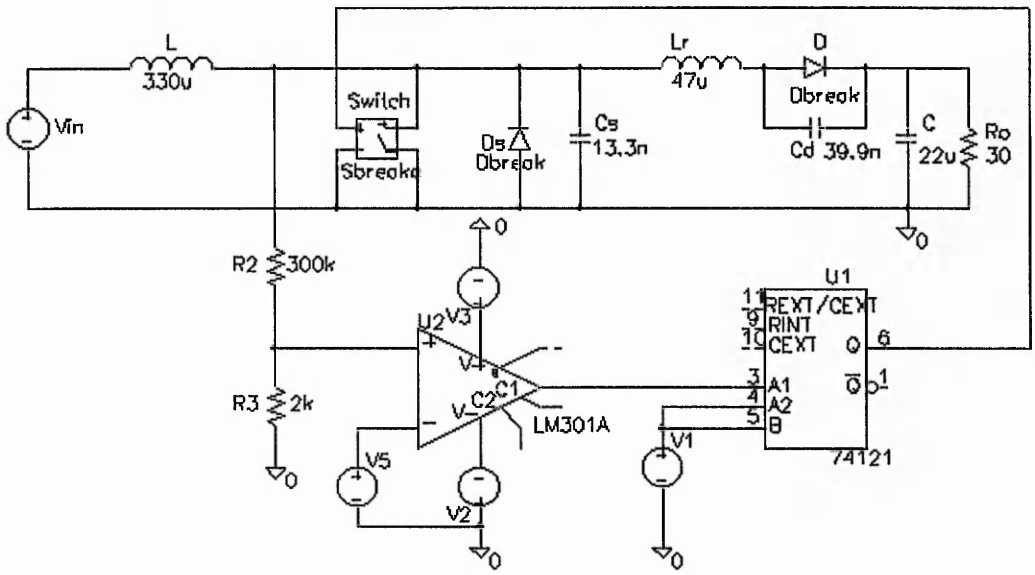

Figure 5-8: Simulation circuit of boost ZVS-MRC using zero-voltage detection.

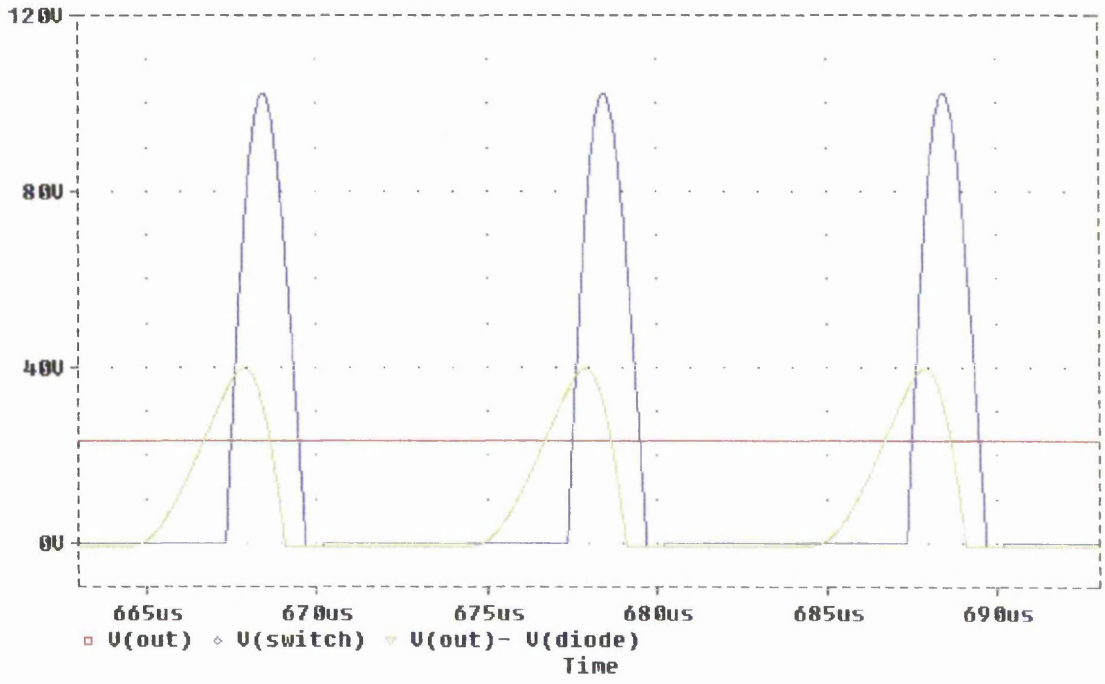

Figure 5-9: Simulated waveforms of boost ZVS-MRC: output voltage V(out); voltage across main switch V(switch); voltage across output diode V(out)-V(diode).

5.2.2. Small-Signal Simulation

With a chosen circuit topology and the component values calculated previously, the small-signal model of the converter needs to be developed as shown in chapter 4. The important item to note is that in such a model, the switches are represented by their averaged characteristics. Once the small-signal model is available, there are well-known methods from control theory for designing the feedback loop to ensure stability and the desired dynamic response. Appendix 5 describes the design of the feedback loop of a dc-dc converter.

The transfer function of a QRC or MRC can be obtained either from the simulation of the small-signal equivalent circuit of the converter shown in figure 4-5 or by directly calculating its expression using equations (4.21) and (4.22).

As an example, the boost ZVS-QRC described in section 5.2.1. is considered. The first step is to calculate the k-parameters of the converter using equations (4-13). The following values are obtained:

k_{ii}= -0.157 k_{vv}= 0.696

k_{iv}= 0.021 Ω^{-1} k_{vi}= -8.821 Ω

k_{if}= -12.709 A/MHz k_{vf}= -262.937 V/MHz.

The value of the gain k_{VCO} of the voltage-controlled-oscillator is calculated as described in [112] and is 43.1 kHz/V.

The equivalent circuit of figure 4-5 is implemented in PSpice. The output diode D of the boost QRC is represented by three voltage sources connected in series: the voltage-controlled voltage sources E_{dvout} and E_{dfs} and the current-controlled voltage source H_{din}. The voltage source E_{dvout} represents the term $k_{vv}\tilde{v}_{out}$ in figure 4-5. It is controlled by the output voltage $\tilde{v}_{out}$. The voltage source E_{dfs} represents the term $k_{vf}\tilde{f}_S$. It is controlled by the independent voltage source V_{fs}, whose coefficient is k_{vf}. In order to include the voltage-controlled-oscillator in the transfer function, as shown by equation (4.22), the coefficient k_{vf} of the source V_{fs} is multiplied by k_{VCO}. The voltage source H_{din} represents the term $k_{vi}\tilde{i}_{in}$ and is controlled by the input current $\tilde{i}_{in}$.

The power switch S is represented by three current sources connected in parallel: the voltage-controlled current sources G_{svout} and G_{sfs} and the current-controlled current source F_{sin}. The current source G_{svout} represents the term $k_{iv}\tilde{v}_{out}$ in figure 4-5. It is controlled by the output voltage $\tilde{v}_{out}$. The current source G_{sfs} represents the term $k_{if}\tilde{f}_S$. It is controlled by the independent voltage source V_{fs}, whose coefficient is k_{if}. In order to include the voltage-controlled-oscillator in the transfer function, as shown by equation (4.22), the coefficient k_{if} of the source V_{fs} is multiplied by k_{VCO}. The current source F_{sin} represents the term $k_{ii}\tilde{i}_{in}$ and is controlled by the input current $\tilde{i}_{in}$.

The simulation circuit is given in figure 5-10. Simulations in the frequency domain are undertaken by applying a small-signal perturbation to the source V_{fs} to obtain the Bode plots of the control-to-output transfer function and a perturbation to the input voltage V_{in} to obtain the line-to-output transfer function. Both transfer functions are shown in figure 5-11 and figure 5-12, respectively.

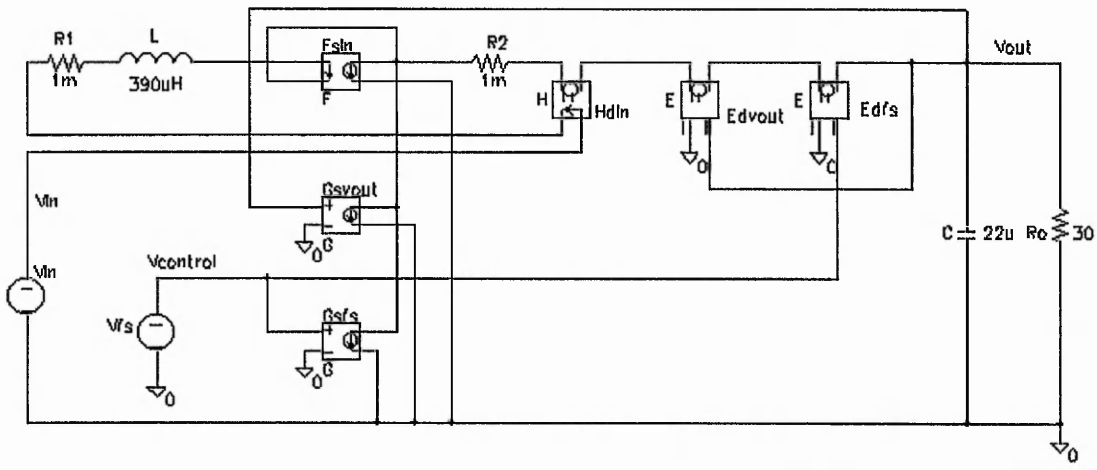

Figure 5-10: Simulation circuit for determining the transfer functions of a boost ZVS-QRC.

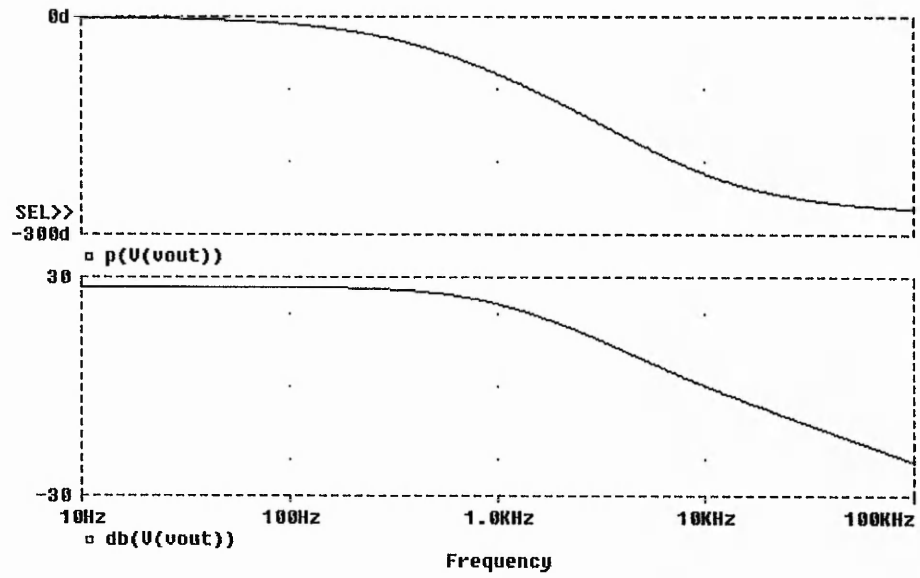

Figure 5-11: Control-to-output transfer function of boost ZVS-QRC.

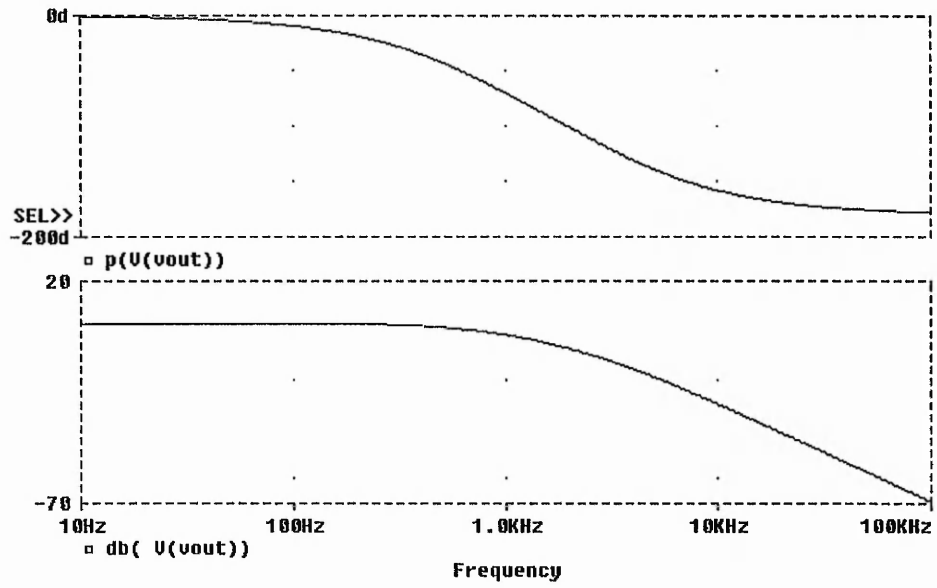

Figure 5-12: Line-to-output transfer function of boost ZVS-QRC.

The same frequency responses are obtained if equations (4.21) and (4.22) are used to calculate the analytic expressions of the transfer functions. The Bode diagrams can be plotted using Matlab or Gnuplot.

For the ZCS-QRC having the component values and operating conditions described in section 5.2.1., the Bode diagrams can be plotted using either of the two methods described above - frequency domain simulation in PSpice or analytic calculation of transfer function and Matlab or Gnuplot. They are shown in figure 5-13 and figure 5-14.

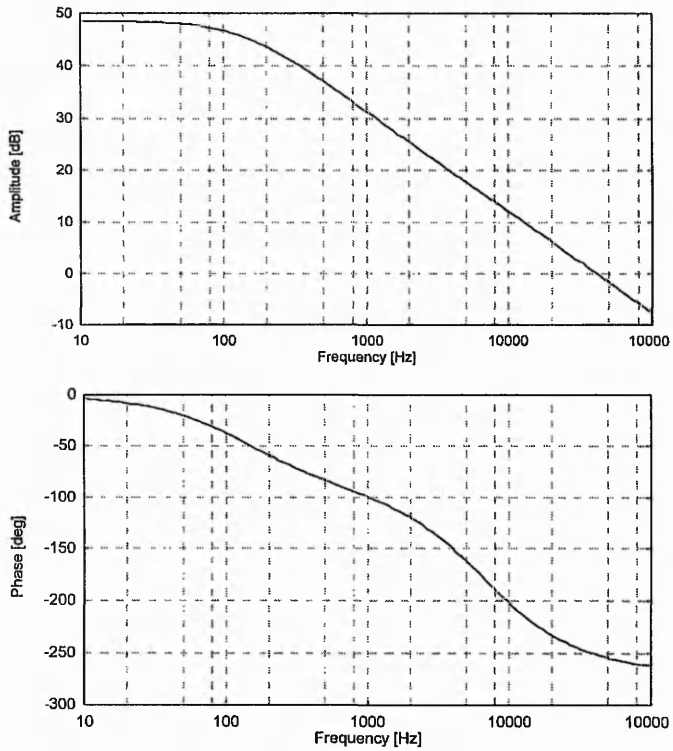

Figure 5-13: Control-to-output transfer function of boost ZCS-QRC.

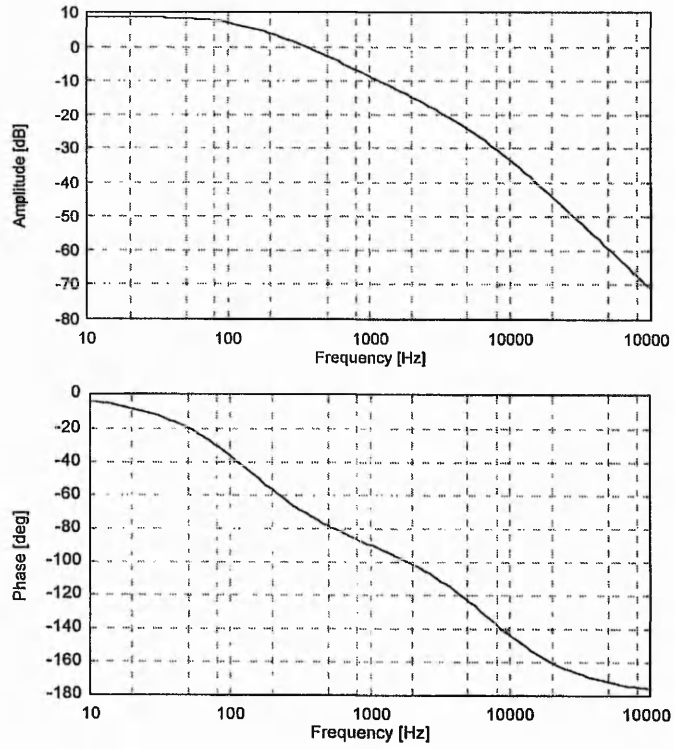

Figure 5-14: Line-to-output transfer function of boost ZCS-QRC.

For the multi-resonant converter described in the previous section, the characteristic functions are determined by the numeric algorithm presented in section 3.6 and are G_v=0.3401 and G_i=0.2014. The partial derivatives of the characteristic functions are calculated from equations (4.27) and (4.28) and have the following values:

$$\frac{\partial G_v}{\partial \alpha} = -0.64 \;; \qquad \frac{\partial G_v}{\partial f_n} = -6.9 \;; \qquad \frac{\partial G_i}{\partial \alpha} = -0.56 \;; \qquad \frac{\partial G_i}{\partial f_n} = -6 \;.$$

The k-parameters are calculated from equations (4.26):

k_{vv} = 2.26; k_{vi} = -38.04 Ω ; k_{vf} = -771.23 V/MHz;

k_{iv} = 84.79 $m\Omega^{-1}$; k_{ii} = -1.48; k_{if} = -34.02 A/MHz.

Considering a gain of the VCO of k_{VCO}=43.1 kHz/V, the small-signal transfer functions are plotted using equations (4.21) and (4.22) and are shown in figures 5-15 and 5-16, respectively.

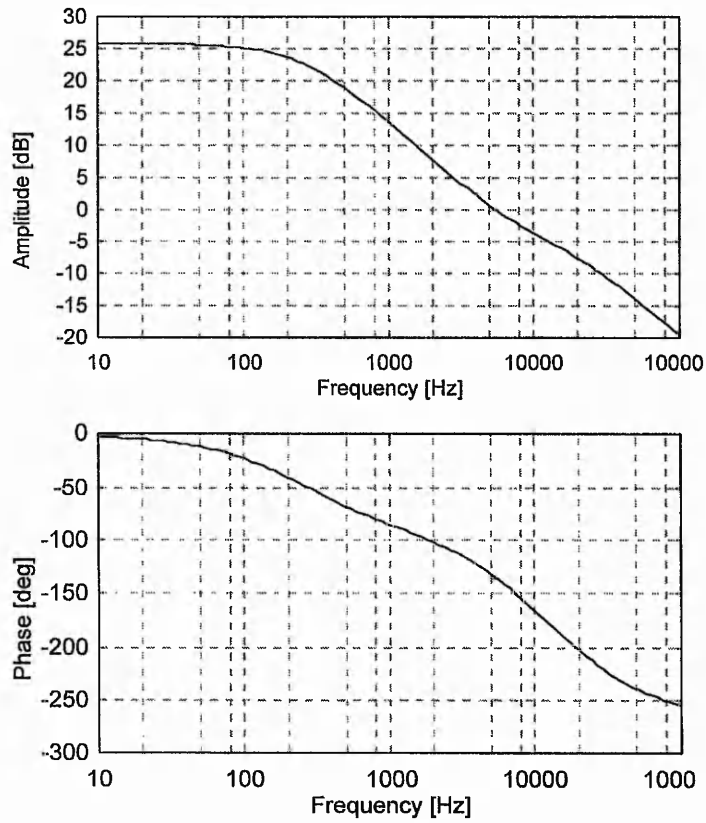

Figure 5-15: Control-to-output transfer function of boost ZVS-MRC.

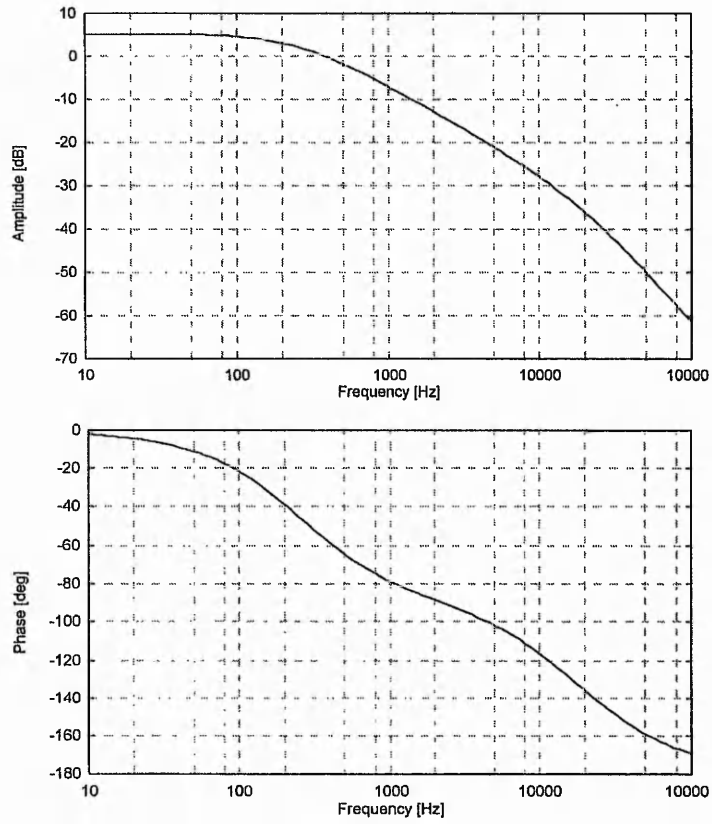

Figure 5-16: Line-to-output transfer function of boost ZVS-MRC.

The same Bode diagrams are obtained by simulating the equivalent small-signal circuit in PSPICE with the k-parameters as coefficients of the controlled voltage and current sources.

5.3. Hardware Implementation

Since 1986, when the quasi-resonant ZCS converter has been first developed, interest in resonant mode power conversion has been continuously increasing. Integrated circuit (IC) manufacturers have been quick to respond with offers of control ICs. The resonant mode power supply controllers can be split into two main categories, depending whether or not they incorporate or not a zero wave-crossing detector.

Resonant mode power supply controllers are optimised either for zero-current-switching applications, which require a constant on-time of the switch, or for zero-voltage-switching applications requiring constant off-time of the switch. Examples of resonant power supply controllers operating in constant on-time mode are UC3860 from Unitrode [105,106], MC33066 from Motorola [107] and CS-360 from Cherry Semiconductor [108]. For operation in constant off-time mode, controllers like MC33067 [109] or CS-161 [110] are available. None of the ICs mentioned above incorporate zero-detection.

The Unitrode UC3861-3868 family of ICs [111,112], optimised for the control of ZCS and ZVS quasi-resonant converters, includes a zero-wave detection comparator. By sensing the zero-crossing of the resonant waveform, the control circuit adapts to different resonant component values and varying line/load conditions.

A zero-voltage-switching quasi-resonant boost converter has been designed, built and tested. The resonant elements are L_r=47μH and C_r=13.3nF, giving rise to a resonant frequency of 200kHz and having a characteristic impedance of Z_r=60Ω. The load resistance R_0 is 30Ω and the normalised load resistance r=0.5.

A power MOSFET (IRF740) is used as the main switching device S. Resonant converters generally employ power MOSFETs as switching devices due to their capability of operating at high switching frequencies (over 100 kHz). In certain applications, especially for converters operating with high currents, insulated gate bipolar transistors (IGBTs) can be used.

The control system of the converter is designed around Unitrode's resonant-mode power supply controller UC3864. Figure 5-17 shows the schematic of the quasi-resonant boost converter and its control system.

For ZVS converters, a decrease in frequency corresponds to an increase in output voltage. For these applications the error amplifier's inverting input is connected to a reference voltage, while the output voltage is fed back to the non-inverting input. The output of the error amplifier is fed to the VCO. The frequency of the clock generated by the VCO depends on the error amplifier's output voltage. The zero detect comparator senses the instant when the zero pin goes below 0.5V. This offset is selected to accommodate propagation delays between the instant the threshold is sensed and the instant that the switch is actually turned on. Although brief, these delays can become significant in high frequency applications, and if left unaccounted, can cause nonzero switching transitions.

The Soft-Ref pin serves the functions of system reference and soft-start. It is used as the input reference for the error amplifier. By ramping the reference from zero during soft-start, the converter output will follow the ramp up under closed loop control. This technique allows controlled starts with no significant overshoot.

The paralleled outputs are connected to the MOSFET gate with a small-value resistor. A diode parallels the output pins to protect the chip from negative voltage spikes that might result from parasitic ringing in the gate circuit. A pnp is used to clamp the zero voltage to prevent damage to the chip.

The boost ZVS-QRC is operated at a switching frequency of 100 kHz and an input voltage of 15 V. The waveforms of the voltage across the power MOSFET and of the control signal are shown in figure 5-18 for three operating cycles and figure 5-19 for one single cycle, respectively.

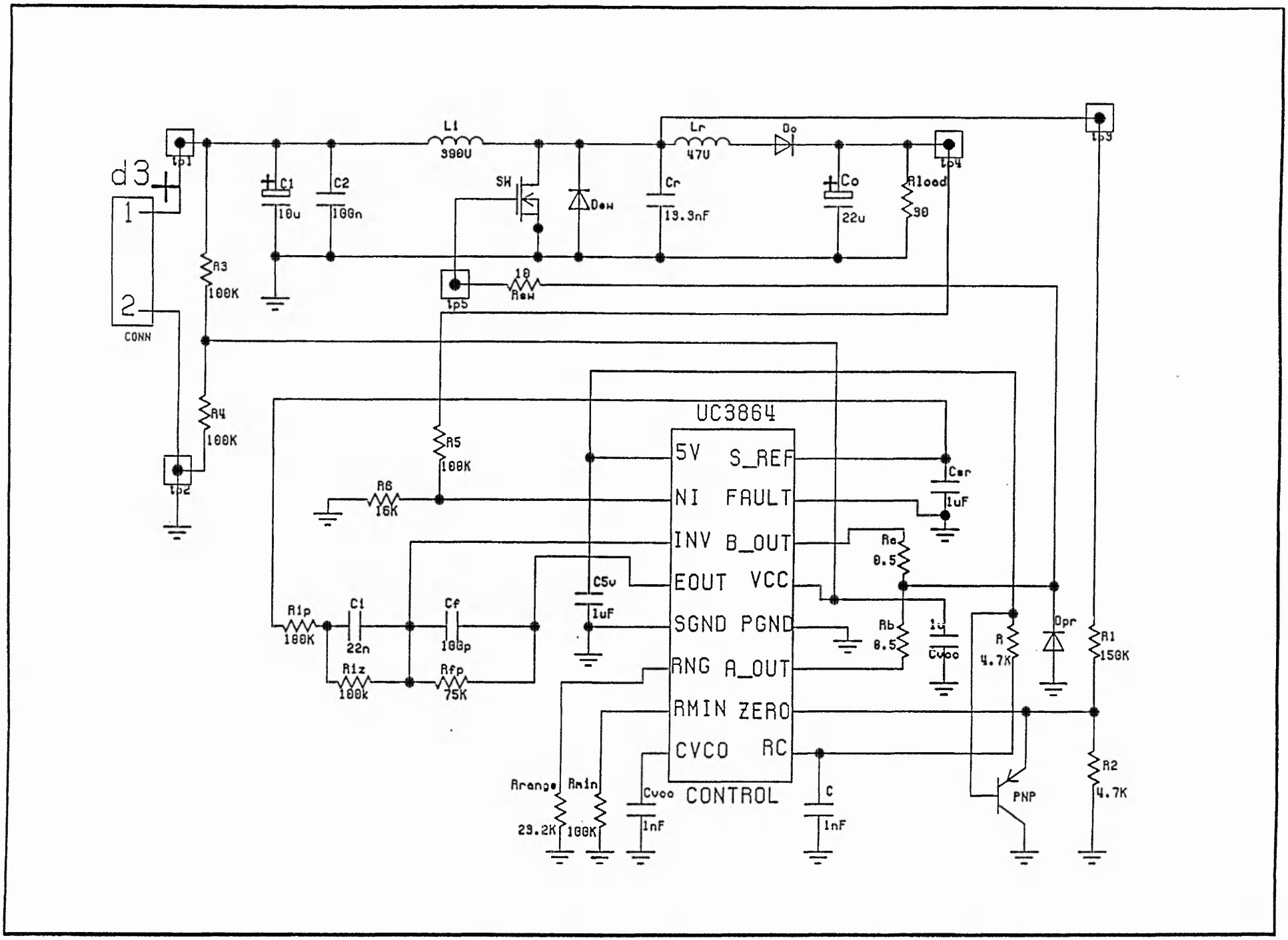

Figure 5-17: Boost ZVS-QRC and its control system.

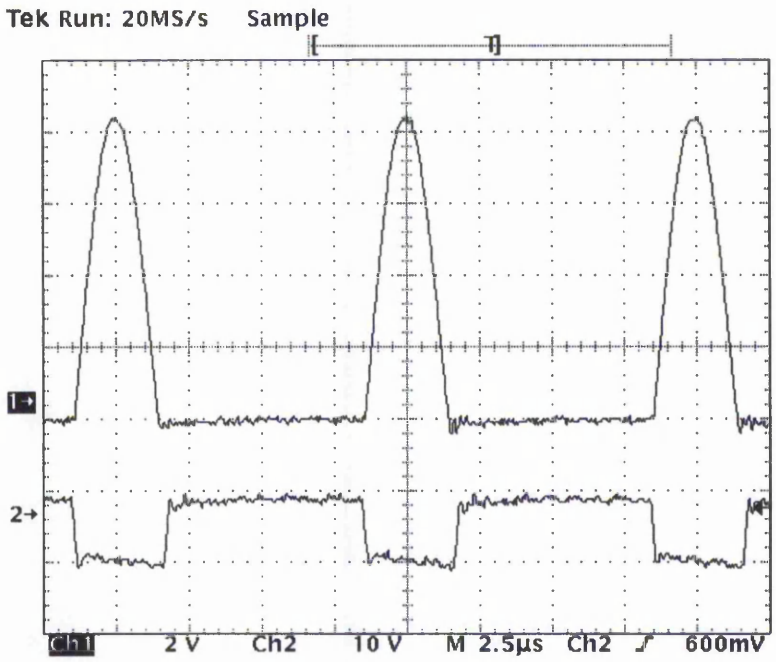

Figure 5-18: Waveforms of the drain-to-source (channel 1) and gate-to-source (channel 2) voltages of the power MOSFET of the boost ZVS-QRC for three cycles.

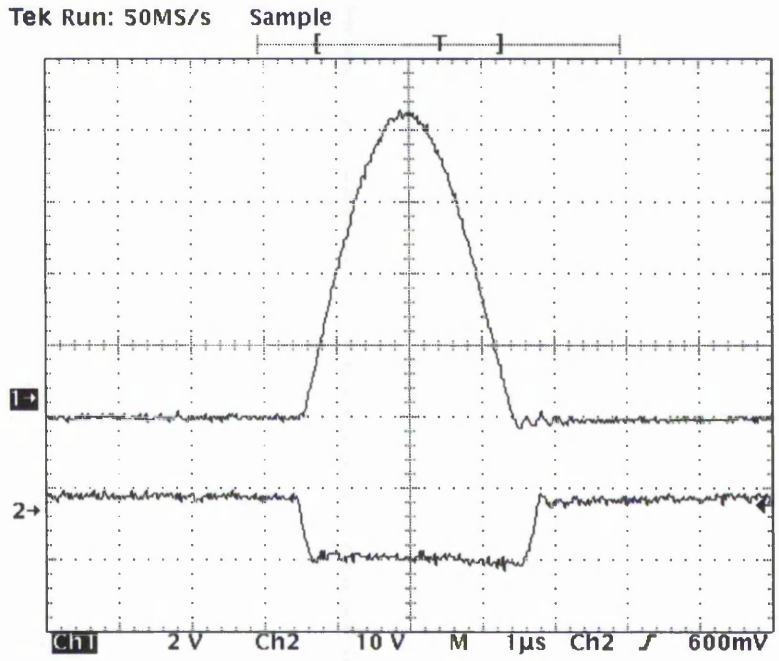

Figure 5-19: Waveforms of the drain-to-source (channel 1) and gate-to-source (channel 2) voltages of the power MOSFET of the boost ZVS-QRC for one cycle.

Figure 5-20 shows the voltages across the power MOSFET, which operates under zero-voltage-switching conditions, and across the output diode of the quasi-resonant converter.

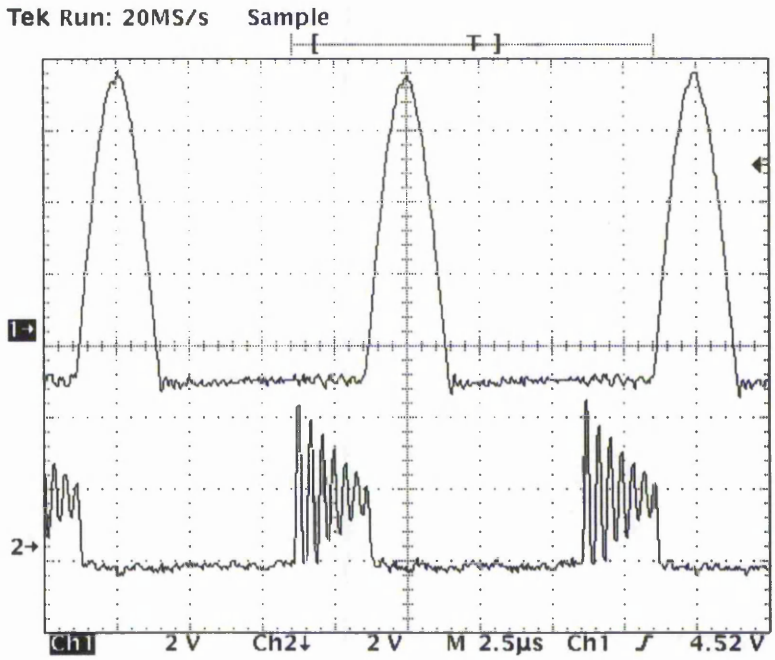

Figure 5-20: Voltage waveforms across the power MOSFET (channel 1) and output diode (channel 2) of the boost ZVS-QRC.

When the output diode D turns off, the voltage across the diode is oscillatory. The oscillations [48] are due to the parasitic junction capacitance of D, which forms a series resonant circuit with the resonant inductor L_r. This effect becomes more pronounced with the increase of the switching frequency. The oscillations are damped by the parasitic resistances of the components and cause power dissipation at high frequencies [40].

A zero-voltage-switching multi-resonant boost converter has been designed, built and tested. The resonant elements are L_r=47µH, C_S=13.3nF and C_D=39.8nF, giving rise to a resonant frequency of 200kHz and having a characteristic impedance of Z_r=60Ω. The load resistance R_0 is 30Ω and the normalised load resistance r=0.5.

The control system of the boost multi-resonant converter is designed in a similar way to the one of the quasi-resonant converter using Unitrode's power supply controller UC3864.

The boost ZVS-MRC is operated at a switching frequency of 100kHz and an input voltage of 15 V. The waveforms are shown in figures 5-21 and 5-22.

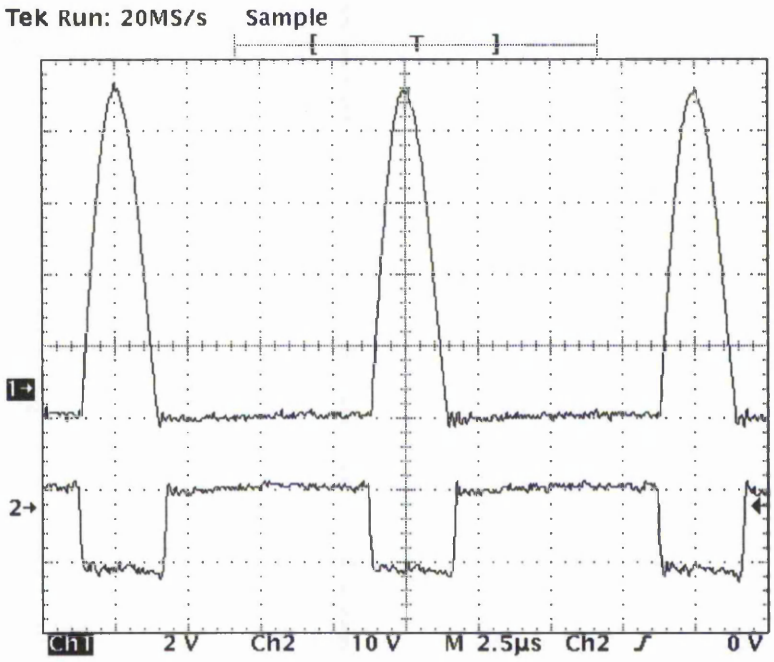

Figure 5-21: Waveforms of the drain-to-source (channel 1) and gate-to-source (channel 2) voltages of the power MOSFET of the boost ZVS-MRC.

Both power MOSFET and output diode operate under zero-voltage-switching conditions. There are no parasitic oscillations because the junction capacitance of the diode D is incorporated in the resonant capacitance C_D.

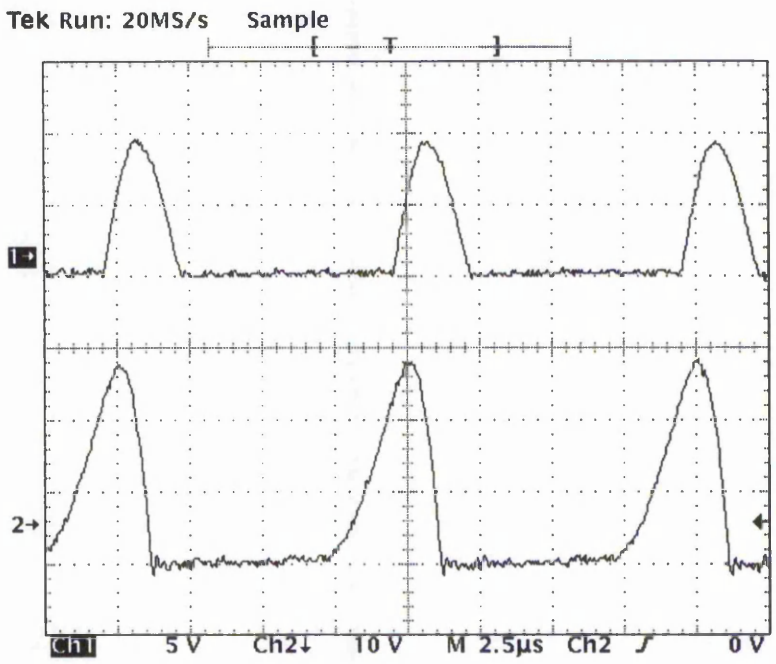

Figure 5-22: Voltage waveforms across the power MOSFET (channel 1) and output diode (channel 2) of the boost ZVS-MRC.

5.4. Comparison of Results

The theoretical steady-state modelling of the boost zero-voltage-switching quasi-resonant converters is presented in chapter 3. The voltage conversion ratio is determined from equation (3.41),

$$x = \frac{1}{1 - G_{ZVS}(f_n, \alpha)},$$

where G_{ZVS} is the characteristic function and its expression is given by equation (3.38). The parameter α is equal to the ratio of the voltage conversion ratio x and normalised load resistance r, $\alpha = x/r$.

To verify the theoretical steady-state modelling, the voltage conversion ratio is determined using experimental measurements and computer simulations and is compared to the mathematical calculations. With an input voltage V_{in}=15V, the switching frequency is varied between 48 kHz and 145 kHz, corresponding to a normalised switching frequency range of 0.24 to 0.72. The output voltage is measured

and the voltage conversion ratio V_{out}/V_{in} is determined. The experimental results are plotted in figure 5-23 together with the simulation results using PSPICE and the theoretical calculations.

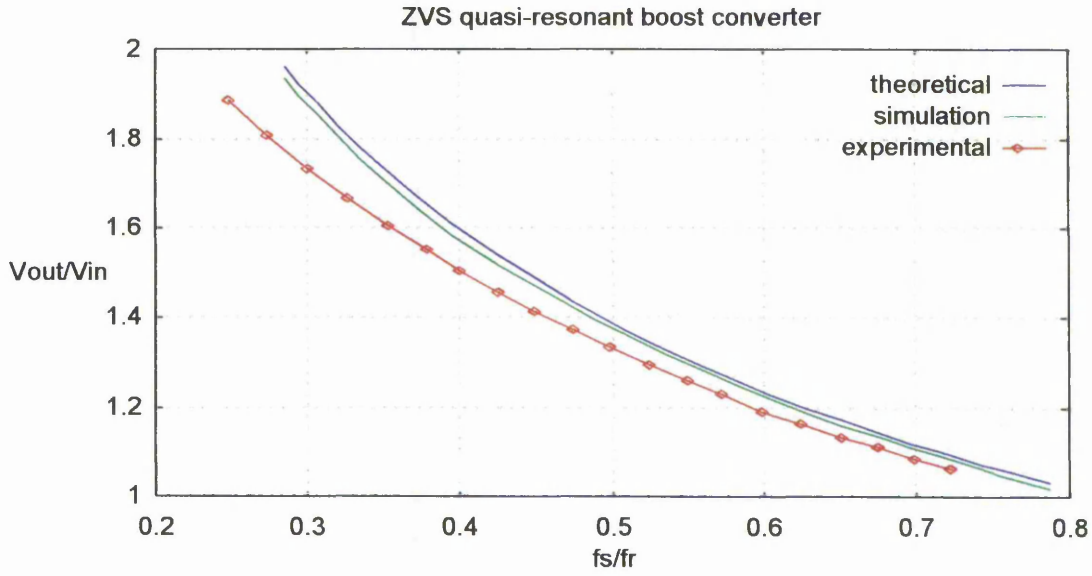

Figure 5-23: Comparison of experimental, simulation and theoretical results for a boost ZVS-QRC having r=0.5.

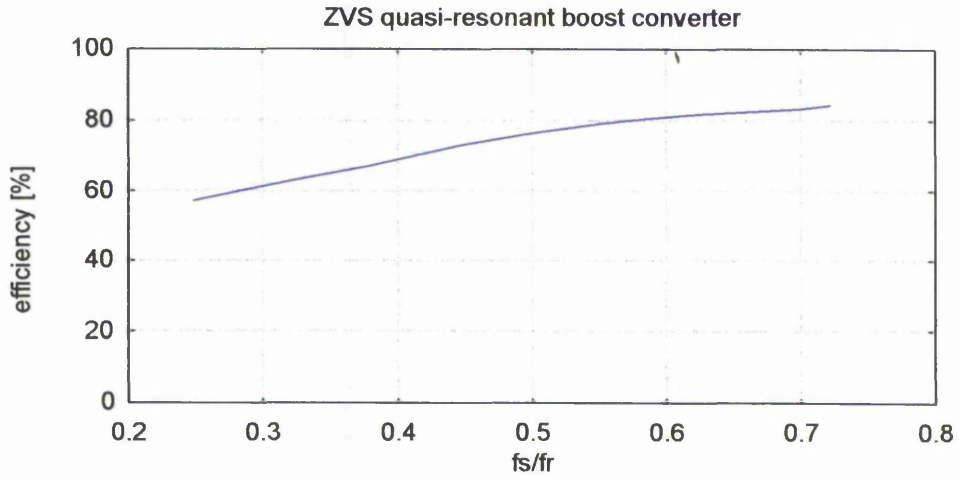

Figure 5-24: Measured efficiency of boost ZVS-QRC.

The simulation results are in close agreement with the theoretical calculations. The small deviation between simulation and theoretical results is due to the voltage drop

during the on-state of the output diode and to the on-resistance of the switch S, which has a value of 1 mΩ for the simulated converters.

The deviation between the experimental and theoretical results can be explained by the occurrence of power losses in the experimental converter. The main types of losses in a resonant dc-dc boost converter are the following:

(i) Losses of the power MOSFET:
- conduction losses due to the on-state drain-to-source resistance, which is R_{DS}=0.55Ω for the IRF 740 power MOSFET;
- drive power losses (power dissipated in the gate structure of the MOSFET);
- power losses due to drain-source leakage current when the device is off;
- MOSFET output capacitance losses.

(ii) Losses in the output diode:
- conduction losses of the diode during the on-state;
- reverse recovery (turn-off) losses of the diode.

(iii) Losses of passive elements due to the equivalent series resistance (ESR) of the input inductor, output capacitor, resonant inductor and resonant capacitors.

The efficiency of the boost ZVS-QRC is measured. Figure 5-24 shows the variation of efficiency with the normalised switching frequency.

A detailed analysis of losses in quasi-resonant converters is undertaken by Tatakis and Polyzos [35-38]. At a operating frequency of around 100kHz, the main losses are the conduction losses of the power MOSFET and the losses in the output diode. The other types of losses are small and can be neglected. It is shown [35-38] that the diode losses do not vary significantly with the switching frequency. But the conduction losses of the power MOSFET increase significantly with the decrease of the switching frequency. When the switching frequency decreases, since the off-time of the zero-voltage-switching converters is constant, the on-time increases and, therefore, conduction losses

increase. The fact that the deviation between the theoretical and experimental steady-state characteristics in figure 5-23 increases and the efficiency of the converter decreases at lower frequency is due to higher conduction losses.

To further verify the steady-state mathematical model of the boost ZVS-QRC, the voltage conversion ratio is determined using experimental measurements and simulations for two other different load values. The first set of results is obtained for a load resistance R=12Ω, corresponding to a normalised load resistance r=0.2. The second set of results is obtained for a load resistance R=42Ω, or a normalised load resistance r=0.7. The theoretical, simulation and experimental characteristics of the converter are plotted in figure 5-25.

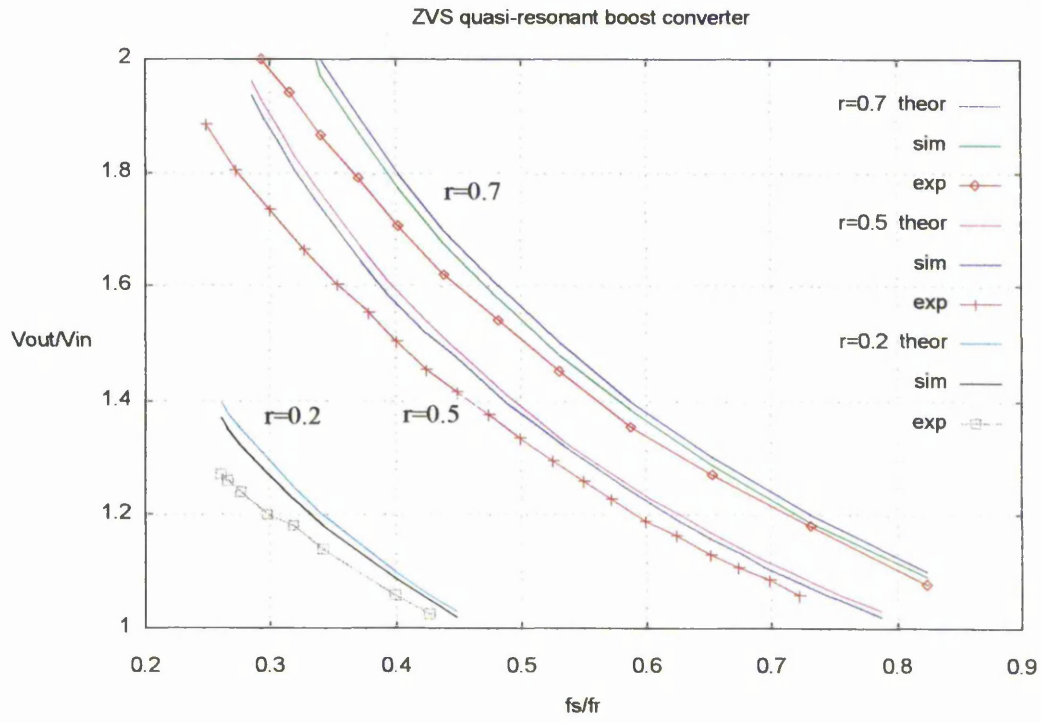

Figure 5-25: Steady-state characteristics of the boost ZVS-QRC for different loads.

The theoretical steady-state characteristics of the zero-voltage-switching multi-resonant boost converter are determined in chapter 3. The voltage conversion ratio is determined using equation (3.80),

$$x = \frac{1}{1 - G_v(\alpha, f_n)},$$

where the characteristic function G_v is determined using a numeric procedure. The theoretical results are verified by experimental measurements and simulations using PSPICE.

The experimental results obtained for the boost ZVS multi-resonant converter are plotted in figure 5-26 together with the simulation results and theoretical calculations. The experimental and simulated voltage conversion ratios are measured at an input voltage of 15 V and frequencies between 72 kHz and 148 kHz, corresponding to a normalised switching frequency range of 0.36 to 0.74.

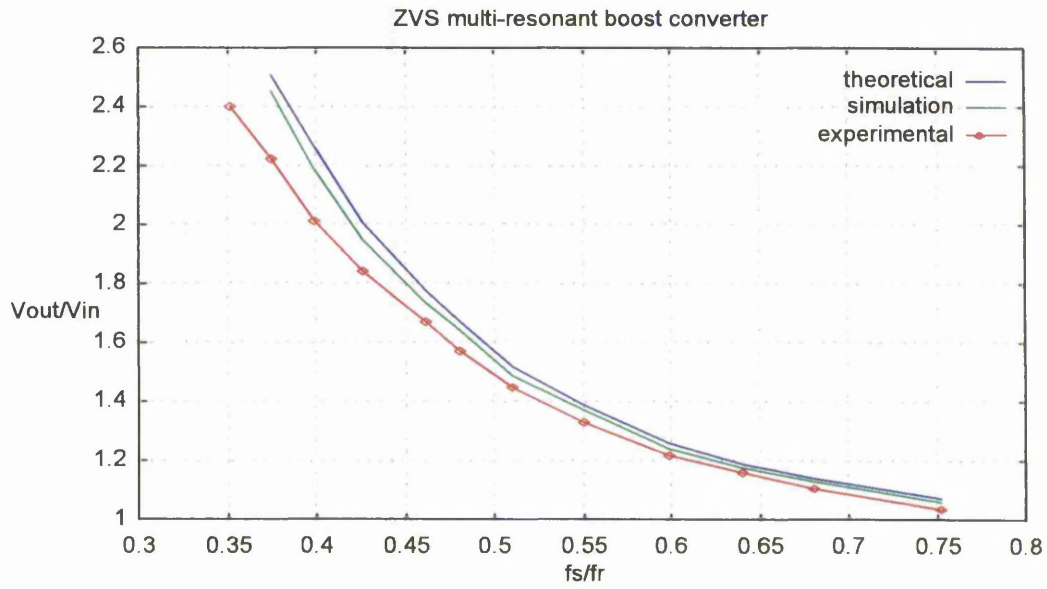

Figure 5-26: Comparison of experimental, simulation and theoretical results for a boost ZVS-MRC having r=0.5.

There is a deviation between the three sets of results, which can be explained by the power losses in the converter. As the switching frequency decreases, the conduction losses of the power MOSFET increase and the efficiency of the converter decreases. The experimentally measured efficiency is shown in figure 5-27.

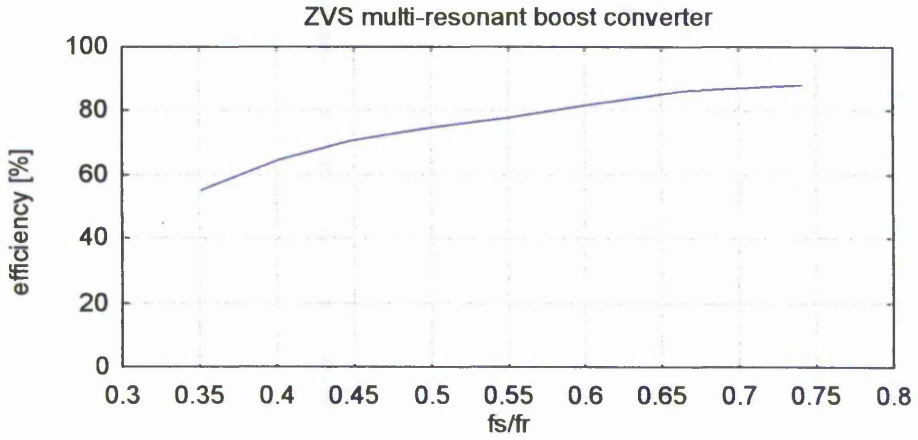

Figure 5-27: Measured efficiency of boost ZVS-MRC.

The characteristics of the multi-resonant converter are determined for other two load resistances, R=12Ω or r=0.2 and R=60Ω or r=1. The experimental, simulation and theoretical results are shown in figure 5-28. Figure 5-29 shows the steady-state characteristics for different values of the normalised ratio of resonant capacitances.

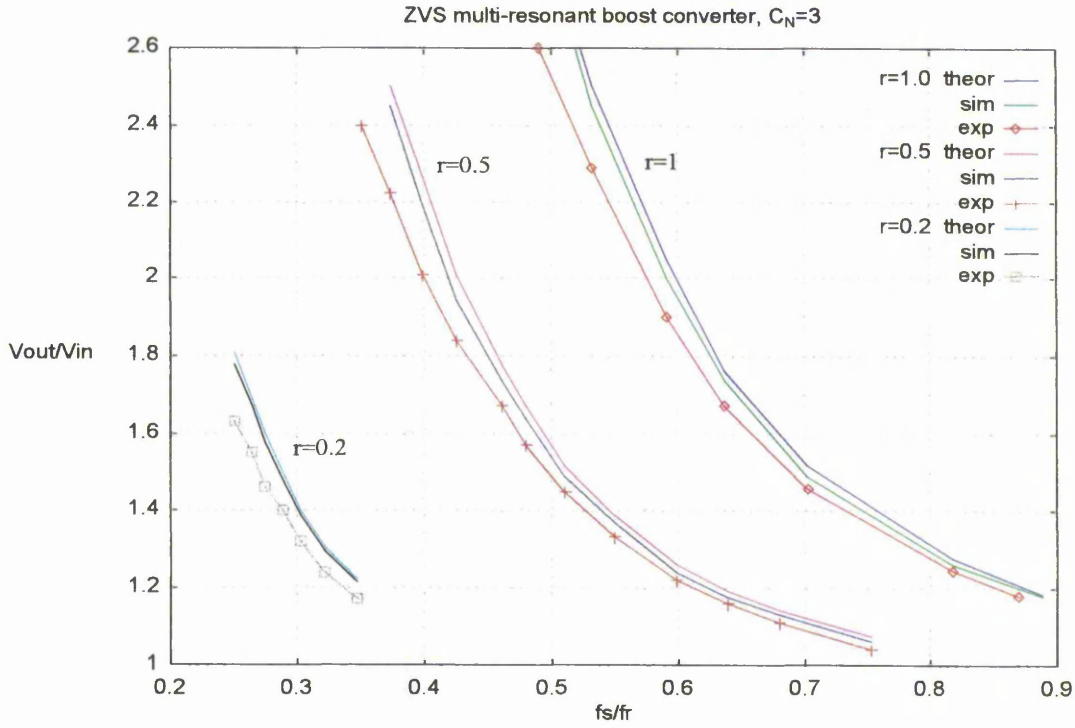

Figure 5-28: Steady-state characteristics of the boost ZVS-MRC for C_N=3 and different load values.

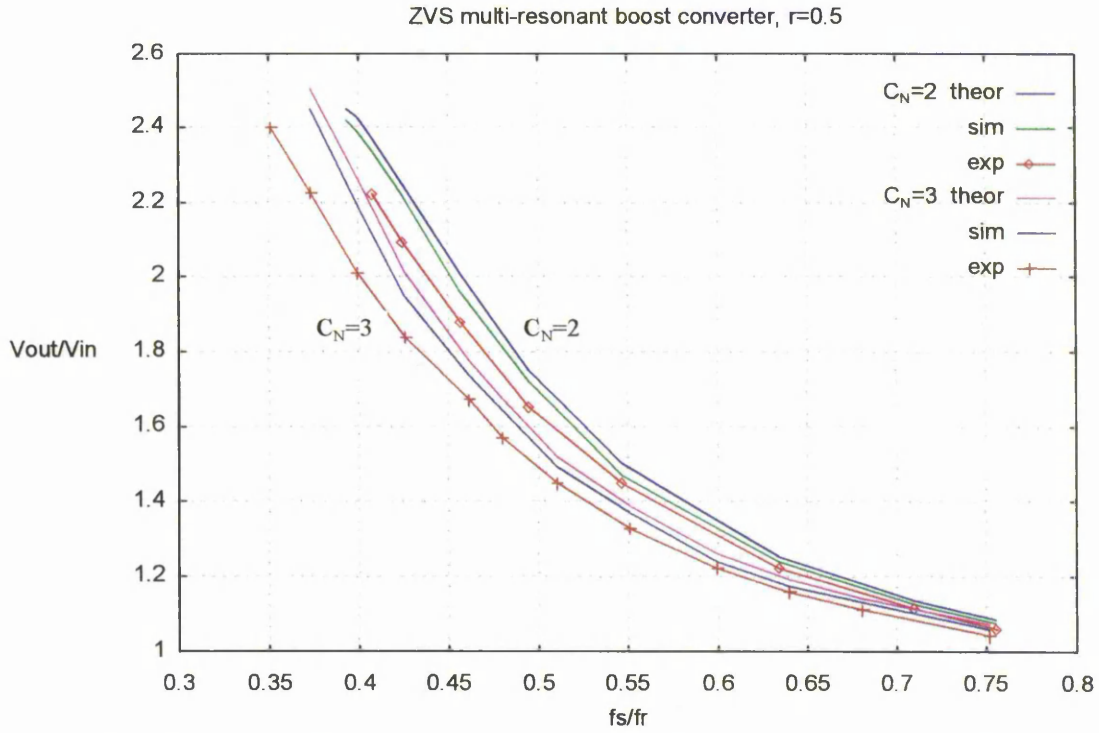

Figure 5-29: Steady-state characteristics of the boost ZVS-MRC for two different normalised ratios of resonant capacitances C_N.

5.5. Conclusions

The simulation and hardware implementation of boost quasi-resonant and multi-resonant converters are presented in this chapter.

Microsim's Design Center software package is used to undertake both time-domain and frequency-domain simulations. To verify the theoretical steady-state characteristics of the resonant boost converters, open-loop simulations are carried out. Two approaches can be used to simulate resonant converters. For the first approach, no zero detection is implemented. The simulation is fast but the off-time (for ZVS converters) or on-time (for ZCS converters) has to be accurately determined before the simulation is started. The second approach implements a true zero-detection, but since a mixed-mode analogue-digital simulation is carried out, the simulation time is long. The simulated waveforms and the voltage conversion ratio are in close agreement with the theoretical waveforms and calculations.

The Bode plots of the transfer functions of the boost converters are obtained by undertaking a frequency-domain simulation of the equivalent small-signal circuit of the converters. The same Bode plots are obtained by calculating the analytical expression of the transfer functions using the models derived in chapter 4.

The steady-state models of the zero-voltage-switching quasi-resonant and multi-resonant converters are verified by experimental measurements. Two converters operating at frequencies between 50 kHz and 150 kHz have been designed, built and tested. The experimental results are in agreement with the theoretical calculations. There is a deviation between the two sets of results which is due to the power losses in the experimental converters. The deviation increases with the decrease of the switching frequency because the on-time increases and the conduction losses of the power MOSFET become higher and the efficiency of the converter decreases.

6. A General Approach to the Modelling of Dc-Dc Converters

6.1. Introduction

Quasi-resonant and multi-resonant converters are recently introduced families of single-switch converters featuring zero-current or zero-voltage switching. The most striking feature of the new converters is the wide variety of topologies available. Different quasi-resonant converters [19] and multi-resonant converters [40] are illustrated in the literature.

Recognition of the topological structure uniting these converters and PWM converters on which they are based leads to the theorems and rules presented in chapter 2. This makes possible the derivation of general models of their dc and ac behaviour.

This chapter extends the modelling of the boost QRCs and MRCs to the other dc-dc resonant converters and presents a general method that can be applied to the modelling of the dc-dc converters. The concept of characteristic functions introduced in chapter 3 is generalised. An expression is derived that yields the dc conversion ratio of a QRC and MRC from the one of the underlying PWM converter. Small-signal dynamic models are also developed and the order of the model of resonant converters is compared to that of the corresponding PWM converters.

6.2. DC Modelling

The quantities V_{off} and I_{on} are defined in section 2.2 as the peak voltage across the diode D and the peak current through the main switch S, respectively. The peak values are determined for PWM converters. Figure 6-1 shows the diode voltage and switch current waveforms in any PWM converter.

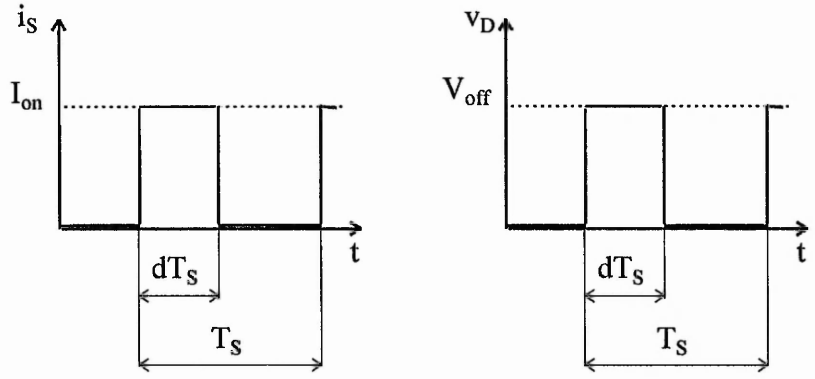

Figure 6-1: Diode voltage and switch current waveforms in any PWM converter.

The average values of v_D and i_S can be easily determined and are, respectively:

$$\bar{v}_D = dV_{off}; \tag{6.1}$$

$$\bar{i}_S = dI_{on}. \tag{6.2}$$

The function x_P which represents the voltage conversion ratio of a PWM converter is defined. It uniquely depends on the duty ratio d and its expression is given below for each basic dc-dc converter:

- buck converter: $x_P(d)=d;$ (6.3)

- boost converter: $x_P(d) = \frac{1}{1-d};$ (6.4)

- buck-boost converter: $x_P(d) = \frac{d}{1-d}.$ (6.5)

The definition of the characteristic functions $G_v(f_n,\alpha)$ and $G_i(f_n, \alpha)$ given for multi-resonant and quasi-resonant dc-dc boost converters is generalised. G_v and G_i are defined for a dc-dc QRC or MRC as follows:

$$\bar{v}_D = G_v(f_n,\alpha)V_{off}; \tag{6.6}$$

$$\bar{i}_S = G_i(f_n,\alpha)I_{on}. \tag{6.7}$$

For multi-resonant converters, $G_v(f_n,\alpha)$ and $G_i(f_n,\alpha)$ have different values. The characterisitc functions G_v and G_i are independent of the considered converter type and are determined numerically using the algorithm presented in section 3.

For quasi-resonant converters, the characteristic functions are equal,

$$G_v=G_i=G\ (f_n,\alpha) \tag{6.8}$$

and the expression of G is analytically determined from the steady-state analysis of quasi-resonant converters. Its expression is independent of the converter type and is given by equations (3.35) and (3.36) for ZCS and ZVS converters, respectively.

The voltage conversion ratio x of a multi-resonant or quasi-resonant converter is obtained by replacing d in equations (6.3) to (6.5) by the characteristic function G_v:

$$x = x_P\left(G_v(f_n,\alpha)\right) \tag{6.9}$$

As an example, figure 6-2 shows the voltage conversion ratio of a buck ZVS-QRC. The mathematical expression and graph are similar to those presented in [21].

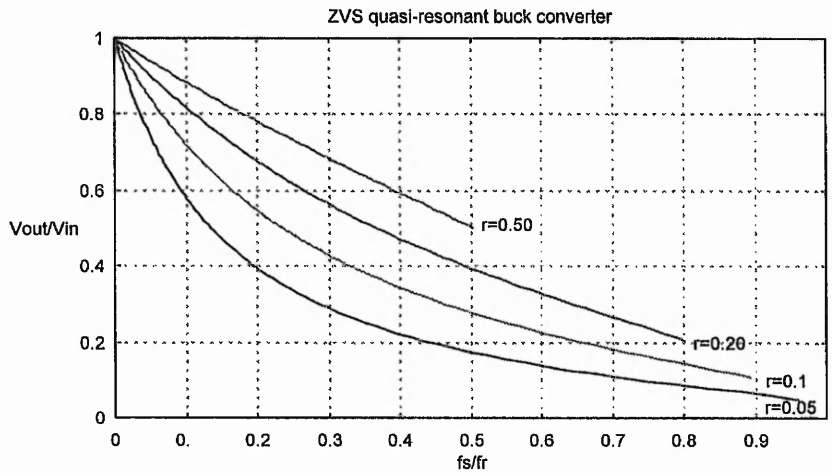

Figure 6-2: Voltage conversion ratio of buck ZVS-QRC.

6.3. Small-Signal Modelling

To obtain the small-signal model of a multi-resonant or quasi-resonant converter, equations (6.6) and (6.7) are perturbed and linearised around a static point. The small-signal variations of the average values of the voltage $\bar{v}_D$ across the diode and of the current $\bar{i}_S$ through the power switch, respectively, are expanded as a function of the small-signal variation of the quantities $\tilde{v}_{off}$, $\tilde{i}_{on}$ and $\tilde{f}_S$:

$$\tilde{v}_D = k_{vv}\tilde{v}_{off} + k_{vi}\tilde{i}_{on} + k_{vf}\tilde{f}_S; \tag{6.10}$$

$$\tilde{i}_S = k_{iv}\tilde{v}_{off} + k_{ii}\tilde{i}_{on} + k_{if}\tilde{f}_S. \tag{6.11}$$

The k-parameters are determined by calculating the partial derivatives of the average values and have the expressions given below:

$$k_{vv} = \frac{\partial \bar{v}_D}{\partial V_{off}} = G_v(f_n,\alpha) - \alpha\frac{\partial G_v(f_n,\alpha)}{\partial \alpha};$$

$$k_{vi} = \frac{\partial \bar{v}_D}{\partial I_{on}} = Z_r\frac{\partial G_v(f_n,\alpha)}{\partial \alpha};$$

$$k_{vf} = \frac{\partial \bar{v}_D}{\partial f_S} = \frac{V_{off}}{f_r}\frac{\partial G_v(f_n,\alpha)}{\partial f_n}; \tag{6.12}$$

$$k_{iv} = \frac{\partial \bar{i}_S}{\partial V_{off}} = -\frac{1}{Z_r}\alpha^2\frac{\partial G_i(f_n,\alpha)}{\partial \alpha};$$

$$k_{ii} = \frac{\partial \bar{i}_S}{\partial I_{on}} = G_i(f_n,\alpha) + \alpha\frac{\partial G_i(f_n,\alpha)}{\partial \alpha};$$

$$k_{if} = \frac{\partial \bar{i}_S}{\partial f_S} = \frac{I_{on}}{f_r}\frac{\partial G_i(f_n,\alpha)}{\partial f_n}.$$

The small-signal equivalent circuits of the converters are derived using a similar procedure to the one described in chapter 4 for the boost converter. Kirchhoff's laws for small-signal perturbations are written and are transformed into the s-domain by using the Laplace transformation. The quantities $\tilde{v}_D$ and $\tilde{i}_S$ are replaced by their expressions

in equations (6.10) and (6.11) and the transfer functions of the buck, boost and buck-boost converters are determined.

(i) Buck Converter.

The small-signal equivalent circuit of quasi-resonant and multi-resonant buck converters is shown in figure 6-3 .

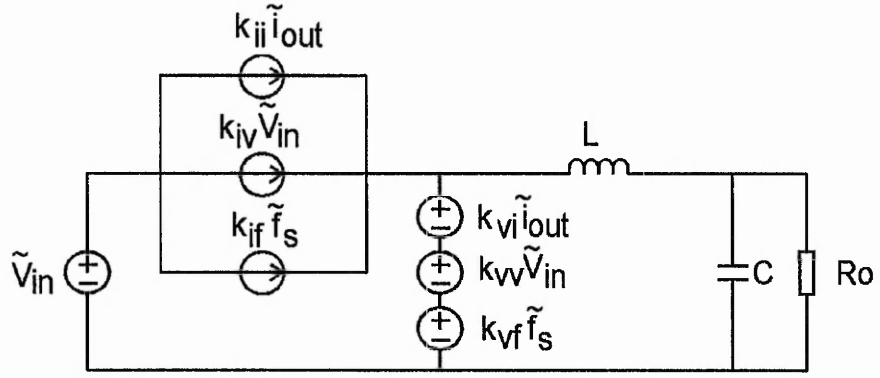

Figure 6-3: Small-signal equivalent circuit of resonant buck converters.

Kirchhoff's laws in the s-domain are:

$$\tilde{v}_D = sL\tilde{i}_L + \tilde{v}_{out};$$

$$\tilde{i}_L = sC\tilde{v}_{out} + \frac{\tilde{v}_{out}}{R}.$$

The control-to-output transfer function is:

$$\frac{\tilde{v}_{out}}{\tilde{f}_s} = \frac{k_{vf}}{LC} \frac{1}{s^2 + s\left(\frac{1}{R_0C} - \frac{k_{vi}}{L}\right) + \frac{1}{LC}\left(1 - \frac{k_{vi}}{R_0}\right)}. \tag{6.13}$$

The line-to-output transfer function is:

$$\frac{\tilde{v}_{out}}{\tilde{v}_{in}} = \frac{k_{vv}}{LC} \frac{1}{s^2 + s\left(\frac{1}{R_0C} - \frac{k_{vi}}{L}\right) + \frac{1}{LC}\left(1 - \frac{k_{vi}}{R_0}\right)}. \tag{6.14}$$

(ii) Boost Converter.

The small-signal equivalent circuit of quasi-resonant and multi-resonant boost converters is shown in figure 4-5.

Kirchhoff's laws in the s-domain are:

$$\tilde{v}_{in} = sL\tilde{i}_L - \tilde{v}_D + \tilde{v}_{out};$$

$$\tilde{i}_L = \tilde{i}_S + sC\tilde{v}_{out} + \frac{\tilde{v}_{out}}{R}.$$

The control-to-output transfer function is:

$$\frac{\tilde{v}_{out}}{\tilde{f}_s} = -\frac{k_{if}}{C}\frac{s - \frac{1}{Lk_{if}}[k_{vf}(1-k_{ii}) + k_{vi}k_{if}]}{s^2 + s\left(\frac{1}{R_0C} + \frac{k_{iv}}{C} - \frac{k_{vi}}{L}\right) + \frac{1}{LC}\left[(1-k_{ii})(1-k_{vv}) - k_{iv}k_{vi} - \frac{k_{vi}}{R_0}\right]}. \quad (6.15)$$

The line-to-output transfer function is:

$$\frac{\tilde{v}_{out}}{\tilde{v}_{in}} = \frac{1-k_{ii}}{LC}\frac{1}{s^2 + s\left(\frac{1}{R_0C} + \frac{k_{iv}}{C} - \frac{k_{vi}}{L}\right) + \frac{1}{LC}\left[(1-k_{ii})(1-k_{vv}) - k_{iv}k_{vi} - \frac{k_{vi}}{R_0}\right]}. \quad (6.16)$$

(iii) Buck-Boost Converter.

The small-signal equivalent circuit of quasi-resonant and multi-resonant buck-boost converters is shown in figure 6-4.

Kirchhoff's laws in the s-domain are:

$$\tilde{v}_D = sL\tilde{i}_L + \tilde{v}_{out};$$

$$\tilde{i}_L = \tilde{i}_S + sC\tilde{v}_{out} + \frac{\tilde{v}_{out}}{R}.$$

The control-to-output transfer function is:

$$\frac{\tilde{v}_{out}}{\tilde{f}_s} = -\frac{k_{if}}{C}\frac{s-\frac{1}{Lk_{if}}[k_{vf}(1-k_{ii})+k_{vi}k_{if}]}{s^2+s\left(\frac{1}{R_0C}+\frac{k_{iv}}{C}-\frac{k_{vi}}{L}\right)+\frac{1}{LC}\left[(1-k_{ii})(1-k_{vv})-k_{iv}k_{vi}-\frac{k_{vi}}{R_0}\right]}. \quad (6.17)$$

The line-to-output transfer function is:

$$\frac{\tilde{v}_{out}}{\tilde{v}_{in}} = -\frac{k_{iv}}{C}\frac{s-\frac{1}{Lk_{iv}}[k_{vv}(1-k_{ii})+k_{vi}k_{iv}]}{s^2+s\left(\frac{1}{R_0C}+\frac{k_{iv}}{C}-\frac{k_{vi}}{L}\right)+\frac{1}{LC}\left[(1-k_{ii})(1-k_{vv})-k_{iv}k_{vi}-\frac{k_{vi}}{R_0}\right]}. \quad (6.18)$$

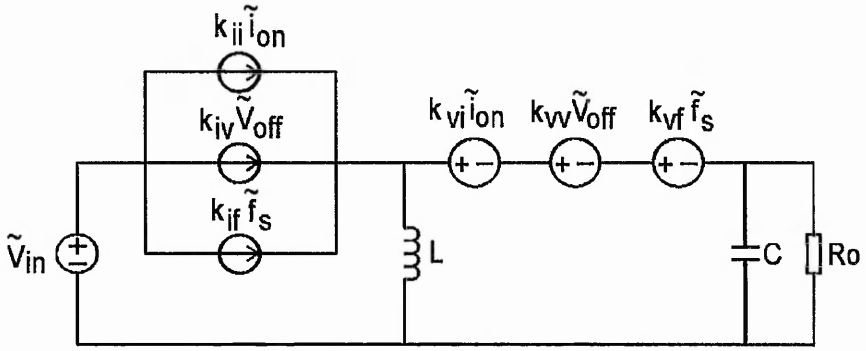

Figure 6-4: Small-signal equivalent circuit of resonant buck-boost converters.

The same technique can be applied for PWM converters. The characteristic functions are equal and uniquely depend on the duty ratio d, G_v=G_i=d.

Since PWM operate with constant frequency and variable duty ratio, f_S in the equations (6.12) must be replaced with the duty ratio d. The values of the k-parameters of PWM converters are given below:

$$k_{vv} = \frac{\partial \overline{v}_D}{\partial V_{off}} = d;$$

$$k_{vi} = \frac{\partial \overline{v}_D}{\partial I_{on}} = 0;$$

$$k_{vf} = \frac{\partial \overline{v}_D}{\partial d} = V_{off}; \quad (6.19)$$

$$k_{iv} = \frac{\partial \bar{i}_S}{\partial V_{off}} = 0;$$

$$k_{ii} = \frac{\partial \bar{i}_S}{\partial I_{on}} = d;$$

$$k_{if} = \frac{\partial \bar{i}_S}{\partial d} = I_{on}.$$

The control-to-output and line-to-output transfer functions of the PWM buck, boost and buck-boost converters are given below.

(i) Buck Converter:

$$\frac{\tilde{v}_{out}(s)}{\tilde{d}(s)} = \frac{V_{in}}{LC} \frac{1}{s^2 + \frac{1}{R_0 C} s + \frac{1}{LC}}; \tag{6.20}$$

$$\frac{\tilde{v}_{out}(s)}{\tilde{v}_{in}(s)} = \frac{d}{LC} \frac{1}{s^2 + \frac{1}{R_0 C} s + \frac{1}{LC}}. \tag{6.21}$$

(ii) Boost Converter:

$$\frac{\tilde{v}_{out}(s)}{\tilde{d}(s)} = -\left(\frac{I_{in}}{C}\right) \frac{s - \frac{(1-d)V_{out}}{LI_{in}}}{s^2 + \frac{1}{R_0 C} s + \frac{(1-d)^2}{LC}}; \tag{6.22}$$

$$\frac{\tilde{v}_{out}(s)}{\tilde{v}_{in}(s)} = \frac{\frac{1-d}{LC}}{s^2 + \frac{1}{R_0 C} s + \frac{(1-d)^2}{LC}}. \tag{6.23}$$

(iii) Buck-Boost Converter:

$$\frac{\tilde{v}_{out}(s)}{\tilde{d}(s)} = -\left(\frac{I_L}{C}\right)\frac{s-\frac{V_{in}}{LI_L}}{s^2+\frac{1}{R_0C}s+\frac{(1-d)^2}{LC}}; \tag{6.24}$$

$$\frac{\tilde{v}_{out}(s)}{\tilde{v}_{in}(s)} = \frac{d(1-d)}{LC}\frac{1}{s^2+\frac{1}{R_0C}s+\frac{(1-d)^2}{LC}}. \tag{6.25}$$

The general expressions for the control-to-output and line-to-output transfer functions are, respectively:

$$\frac{\tilde{v}_{out}}{\tilde{f}_S} = k_C\frac{1-\frac{s}{\omega_{ZC}}}{1+\frac{1}{Q}\frac{s}{\omega_0}+\left(\frac{s}{\omega_0}\right)^2}; \tag{6.26}$$

$$\frac{\tilde{v}_{out}}{\tilde{v}_{in}} = k_L\frac{1-\frac{s}{\omega_{ZL}}}{1+\frac{1}{Q}\frac{s}{\omega_0}+\left(\frac{s}{\omega_0}\right)^2}. \tag{6.27}$$

The coefficients are given below for each topology.

(i) Buck converter:

$$k_C = \frac{k_{vf}}{1-\frac{k_{vi}}{R_0}};$$

$$k_L = \frac{k_{vv}}{1-\frac{k_{vi}}{R_0}};$$

$$\omega_{ZC} = \infty;$$

$$\omega_{ZL} = \infty;$$

$$\omega_0 = \sqrt{\frac{1}{LC}(1-\frac{k_{vi}}{R_0})}\ ;$$

$$Q = \frac{\omega_0}{\frac{1}{R_0 C} - \frac{k_{vi}}{L}}.$$

(ii) Boost converter:

$$k_C = \frac{k_{vf}(1-k_{ii}) + k_{vi}k_{if}}{(1-k_{ii})(1-k_{vv}) - k_{iv}k_{vi} - \frac{k_{vi}}{R_0}};$$

$$k_L = \frac{1-k_{ii}}{(1-k_{ii})(1-k_{vv}) - k_{iv}k_{vi} - \frac{k_{vi}}{R_0}};$$

$$\omega_{ZC} = \frac{k_{vf}(1-k_{ii}) + k_{vi}k_{if}}{Lk_{if}};$$

$$\omega_{ZL} = \infty;$$

$$\omega_0 = \sqrt{\frac{1}{LC}\left[(1-k_{ii})(1-k_{vv}) - k_{iv}k_{vi} - \frac{k_{vi}}{R_0}\right]};$$

$$Q = \frac{\omega_0}{\frac{1}{R_0 C} + \frac{k_{iv}}{C} - \frac{k_{vi}}{L}}.$$

(iii) Buck-boost converter:

k_C, ω_{ZL}, ω_0 and Q are the same as for the boost converter;

$$k_L = \frac{k_{vv}(1-k_{ii}) + k_{vi}k_{iv}}{(1-k_{ii})(1-k_{vv}) - k_{iv}k_{vi} - \frac{k_{vi}}{R_0}};$$

$$\omega_{ZL} = \frac{k_{vv}(1-k_{ii}) + k_{vi}k_{iv}}{Lk_{iv}}.$$

6.4. Conclusions

This chapter presents a general method for the dc and small-signal modelling of quasi-resonant and multi-resonant converters. The voltage conversion ratio of a QRC and MRC is related to its PWM counterpart. The small-signal control-to-output and line-to-output transfer functions are determined for each of the buck, boost and buck-boost converters. It is shown that the small-signal dynamic behaviour of the converters is characterised by a second-order system. Both families of boost and buck-boost converters possess a finite zero in the right half of the s-plane.

The small-signal models of resonant converters are compared to the ones of PWM converters.The resonant elements do not increase the order of small-signal model. Since the small-signal control-to-output transfer functions of QRCs and MRCs are similar to PWM converters, all classes of converters can be analysed using a unified method. Therefore, the large body of existing knowledge concerning PWM converters can be extended to QRCs and MRCs.

The line-to-output transfer functions of the resonant buck and boost converters are similar to the ones of PWM converters. However, the buck-boost QRCs and MRCs have a finite right-half plane zero in their line-to-output transfer function. This property does not appear in the conventional PWM buck-boost converters. This zero brings the reverse response of the output voltage when the input voltage has a steep variation, like a step input.

7. Conclusions and Further Work

7.1. Overall Conclusions

In recent years, quasi-resonant and multi-resonant converter topologies have been introduced aiming at more compact and more efficient power conversion. The technological innovation brings a strong desire to develop a generalised mathematical method for the modelling of switched-mode converters.

This thesis presents the steady-state and small-signal modelling of quasi-resonant and multi-resonant boost converters and extends the proposed method to buck and buck-boost converters. The modelling presented provides a considerable body of knowledge which is applied to the analysis and design of QRCs and MRCs.

To obtain a unified model of resonant boost converters, the concept of characteristic functions is introduced. The characteristic functions of a boost converter are defined by the following equations:

$$\bar{v}_D = G_v(f_n, \alpha) V_{out};$$

$$\bar{i}_S = G_i(f_n, \alpha) I_{in}.$$

The characteristic functions G_v and G_i describe the average behaviour of the switching devices and their expressions depend on the normalised switching frequency f_n and the normalised inductor current α.

Quasi-resonant converters operate with variable switching frequency and an operating cycle is divided into four stages. The steady-state analysis of both zero-current-switching and zero-voltage-switching quasi-resonant boost converters is undertaken. The duration of each stage is calculated and the dependence of the voltage conversion ratio on the switching frequency and load is determined. It is shown that QRCs have a limited load range for which zero-current or zero-voltage operation is achieved. The

voltage conversion ratio is load dependent for the half-wave mode of operation. The analytic expressions of the characteristic functions are determined and it is shown that these are equal, $G_v=G_i=G$. Quasi-resonant converters are described by a single characteristic function, which can be seen as the equivalent duty ratio of the QRCs.

Multi-resonant converters, similarly to quasi-resonant converters, operate with variable switching frequency and the operating cycle is divided into four stages. However, due to the increased complexity of the resonant network, two modes of operation are possible, depending on the operating conditions. The duration of one of the resonant stages in an operating cycle is obtained from a transcendental equation and, therefore, a numeric method has to be used to calculate the duration. A numeric algorithm for the analysis and modelling of multi-resonant converters is developed and implemented in the C-programming language. The characteristic functions are calculated using this algorithm and it is found that they have different values. Unlike quasi-resonant converters, multi-resonant converters are described by two characteristic functions, which are calculated numerically. The voltage conversion ratio of the multi-resonant boost converter is determined. It is shown that the load range of MRCs is improved compared to QRCs.

A unified dc model for quasi-resonant and multi-resonant boost converters is derived using the characteristic functions. The voltage conversion ratio of a resonant boost converter is obtained by replacing the duty ratio with the characteristic function G_v in the mathematical expression for the voltage conversion ratio of the boost PWM converter. The following equation represents the mathematical dc (steady-state) model for quasi-resonant and multi-resonant boost converters:

$$x = \frac{1}{1 - G_v(\alpha, f_n)}.$$

The mathematical model is verified by computer simulations and hardware implementation for the zero-voltage-switching quasi-resonant and multi-resonant boost converters. The measured and simulated voltage conversion ratio is compared to the theoretical ratio for different load values and over a wide operating frequency range.

The experimental and simulation results are in agreement with the theoretical calculations. There is a small deviation between the experimental and theoretical results, which is explained by the power losses in the experimental converter.

To derive the small-signal models for the converters, the averaging technique is applied. The averaged model of the boost converter is derived. The switching devices are replaced by voltage and current sources whose values depend on the characteristic functions of the boost converter. This approach allows the undertaking of a unified small-signal analysis and modelling for both quasi-resonant and multi-resonant boost converters.

The average model of a resonant boost converter is nonlinear because the characteristic functions are nonlinear. To obtain a linear circuit model, a small-signal perturbation is applied to the averaged circuit of the boost converter. By neglecting the higher order terms and separating the steady-state and perturbed components, the equivalent small-signal model of the converter in circuit form is obtained. In this model, which is valid for both quasi-resonant and multi-resonant boost converters, the switching devices are represented by controlled voltage and current sources, whose coefficients depend on the characteristic functions. By using this linear circuit model, the small-signal control-to-output and line-to-output transfer functions are obtained. Although the small-signal equivalent circuit of resonant boost converters is different from the one of the PWM boost converter, the small-signal transfer functions are similar. The control-to-output transfer functions are of second order and have a zero in the right-half of the s-plane. The resonant elements do not increase the order of the transfer functions. Therefore, the conventional methods that are used to design the feedback loop of the PWM boost converter can be applied to the quasi-resonant and multi-resonant boost converters.

The transfer function below represents the mathematical small-signal model of a quasi-resonant and multi-resonant converter:

$$\frac{\tilde{v}_{out}}{\tilde{f}_s} = -\frac{k_{if}}{C}\frac{s - \frac{1}{Lk_{if}}[k_{vf}(1-k_{ii}) + k_{vi}k_{if}]}{s^2 + s\left(\frac{1}{R_0C} + \frac{k_{iv}}{C} - \frac{k_{vi}}{L}\right) + \frac{1}{LC}\left[(1-k_{ii})(1-k_{vv}) - k_{iv}k_{vi} - \frac{k_{vi}}{R_0}\right]}.$$

All k-parameters depend on the characteristic functions and on the steady-state operating point. The control-to-output transfer function of the power converter is used for the design of the feedback loop of the converter in order to achieve the desired dynamic performance and stability. The line-to-output transfer function of resonant boost converters, which is also determined, is used to establish the effect on the output voltage of a perturbation in the input.

The above model can be applied to PWM converters as well, noting that the switching frequency has to be replaced by the duty ratio. For QRCs and MRCs, the control quantity is the switching frequency since these converters operate with variable frequency, and for PWM converters the control quantity is the duty ratio, since these operate with constant switching frequency. The characteristic functions of PWM converters are equal and uniquely depend on the duty ratio.

The proposed method for the steady-state and small-signal modelling of boost converters is extended to the other main types of dc-dc converters, buck and buck-boost. The expressions of the characteristic functions of buck and buck-boost converters are the same as for the boost converter.

By defining the quantities V_{off} and I_{on} as the peak voltage and current of the switching devices of a PWM converter and by using the concept of characteristic functions, a general dc model applicable to all types (buck, boost, buck-boost) and all families (quasi-resonant and multi-resonant) of converters is given. The definition of the characteristic functions is extended as follows:

$\bar{v}_D = G_v(f_n, \alpha)V_{off}$;

$\bar{i}_S = G_i(f_n, \alpha)I_{on}$.

The voltage conversion ratio of a resonant converter is related to the one of the corresponding PWM converter. The duty ratio is replaced with the characteristic function G_v in the mathematical expression $x_P(d)$ for the conversion ratio of the PWM converter. The mathematical dc (steady-state) model for a resonant dc-dc converter is given by the expression:

$$x = x_P(G_v(\alpha, f_n)).$$

The expressions for the small-signal control-to-output and line-to-output transfer functions of each converter type are derived. The transfer functions of resonant converters are compared to the transfer functions of PWM converters. The small-signal control-to-output transfer functions of resonant converters have the same order as the conventional PWM converters and, therefore, the well-known methods for the design of the control system of PWM converters can be applied to resonant converters. The control-to-output transfer function of a resonant dc-dc converter is:

$$\frac{\tilde{v}_{out}}{\tilde{f}_S} = k_C \frac{1 - \frac{s}{\omega_{ZC}}}{1 + \frac{1}{Q}\frac{s}{\omega_0} + \left(\frac{s}{\omega_0}\right)^2}.$$

Its coefficients are determined for each converter type. The line-to-output transfer functions of the buck and boost QRCs and MRCs have the same order as the PWM converters. The only difference in the line-to-output transfer functions occurs for the buck-boost converter, for which a right-half-plane zero appears in the resonant topologies, which is not present in the PWM converter.

The author considers that the present thesis significantly contributes to knowledge in the area of dc-dc multi-resonant and quasi-resonant converters. The novel concept of characteristic functions is used to derive unified models for dc-dc converters, which, to the knowledge of the author, were not previously available. The derivation of the small-

signal transfer functions for multi-resonant converters has not been reported in the literature. It is hoped that the time and effort for the design of multi-resonant and quasi-resonant converters will be reduced by applying the models presented in this thesis.

7.2. Further Work

The further work relating to this project can be split into three categories:

(i) the analysis and modelling of ZCS-MRCs;
(ii) the analysis of multi-loop control of quasi-resonant and multi-resonant converters.

(i) The analysis and modelling of ZCS-MRCs.

Although the zero-current-switching multi-resonant technique is not used for high-frequency applications, it could be applied in high-power high-current converters. The analysis and modelling of ZCS-MRCs has not been undertaken, but similar principles as for the analysis and modelling of ZVS-MRCs can be applied. A numerical method for the calculation of the characteristic function has to be developed. It is expected that the mathematical dc model of a ZCS-MRC will be $x = x_P(G_i(\alpha, f_n))$ and the small-signal model will be the same as for the ZVS-MRC.

(ii) The analysis of multi-loop control of quasi-resonant and multi-resonant converters.

This thesis presents the small-signal modelling of QRCs and MRCs for single-loop control or voltage-mode control. Closed-loop regulation is achieved by feedback of the output voltage through an error-amplifier circuit and a voltage-controlled-oscillator. Sometimes it can be quite difficult to achieve a good closed-loop response with single-loop control, especially for boost and buck-boost derived circuits with right-half-plane zeros in their control-to-output transfer function.

Multi-loop control or current-mode control offers improvements in closed-loop response of PWM converters [113-116]. A similar scheme for the control of quasi-resonant converters has also been implemented [117-119] and is referred to as current-sense frequency modulation (CSFM). A signal proportional to the inductor current is compared with an error voltage signal to modulate the switching frequency. This control scheme offers all of the small-signal benefits expected from current-mode control. The control-to-output and line-to-output transfer functions have first-order characteristics and the voltage compensation is therefore simpler to design and optimise. The VCO, which can be difficult to implement at higher frequencies, is replaced with a comparator. The dynamic performance and stability of quasi-resonant converters is improved by using current-mode control [120].

A unified modelling technique for current-mode controlled dc-dc PWM converters is presented in [115]. There is no unified method for the analysis of quasi-resonant multi-loop converters and, to the knowledge of the author, the study of multi-resonant multi-loop control has not been reported in the literature. The study of both topics could be the object of a future research project.

Appendix 1: Half-Wave and Full-Wave Operation of Resonant Converters

The resonant switches operate in two modes, half-wave and full-wave, depending on the structure of the switch, as described in section 2.3.1. This appendix presents in more detail the difference between the two operating modes for both ZCS and ZVS boost quasi-resonant converters.

A1.1. Boost Zero-Current-Switching Quasi-Resonant Converters

For a ZCS-QRC, the implementation of the zero-current resonant switch is shown in figures 2-6 and 2-7. The difference between half-wave and full-wave mode consists in the moment in time when the resonant stage (stage 3 of operation of the converter) ends. The current through the resonant inductor is given by equation (3.12),

$$i_{Lr}(t) = I_{in} + \frac{V_{out}}{Z_r}\sin\omega_r t.$$

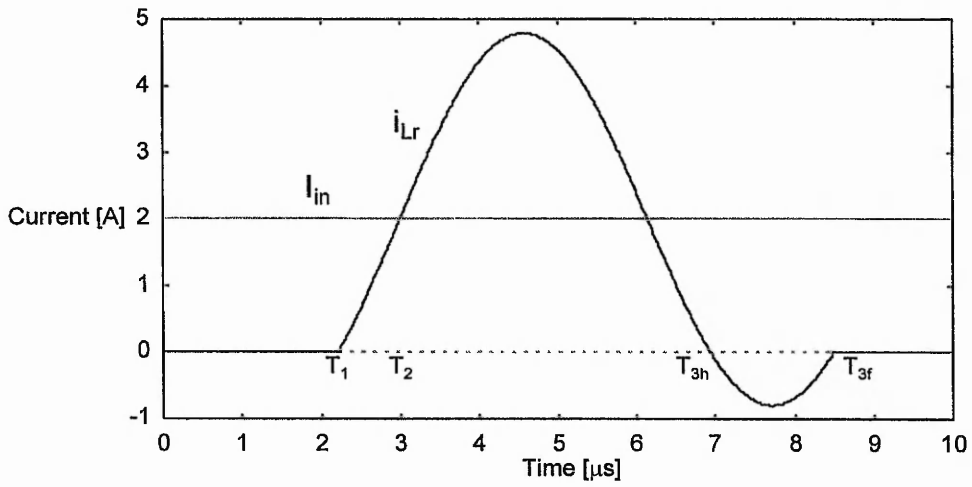

Figure A1-1: Current waveform of a ZCS-QRC during the resonant stage.

Notice that the waveform of the current i_{Lr} contains a dc component I_{in} and an ac component with the amplitude V_{out}/Z_r. In order to achieve zero-current-switching, the ac component needs to be larger than the dc component,

$$\frac{V_{out}}{Z_r} > I_{in} \text{ or}$$

$r > x$.

The waveform of i_{Lr} during the resonant stage is shown in figure A1-1. In half-wave mode of operation, when i_{Lr} drops to zero at T_{3h}, it is prevented by the series diode D_S to become negative. In full-wave mode of operation, i_{Lr} continues to oscillate to a negative value and returns to zero at time T_{3f}. For the half-wave mode, the end of this stage is T_{3h}; for full-wave mode, it is T_{3f}.

The duration T_{23} of the resonant stage is determined by setting $i_{Lr}(T_{23})=0$ and is

$$T_{23} = \frac{1}{\omega_r}\arcsin(-\frac{x}{r}) \text{ or}$$

$$T_{23} = \frac{a_{zcs}}{\omega_r},$$

where $a_{zcs} = \arcsin(-\frac{x}{r})$.

The equation $i_{Lr}(T_{23})=0$ has two solutions, one corresponding to the half-wave mode for which

$$\pi < \omega_r T_{23} < \frac{3\pi}{2}$$

and the other one corresponding to the full-wave mode,

$$\frac{3\pi}{2} < \omega_r T_{23} < 2\pi.$$

Therefore, for half-wave converters

$$\pi < a_{zcs} < \frac{3\pi}{2} \text{ and}$$

$$a_{zcs} = \pi + \arcsin(\frac{x}{r});$$

for full-wave converters

$$\frac{3\pi}{2} < a_{zcs} < 2\pi \text{ and}$$

$$a_{zcs} = 2\pi - \arcsin(\frac{x}{r}).$$

A1.2. Boost Zero-Voltage-Switching Quasi-Resonant Converters

For a ZVS-QRC, the implementation of the zero-voltage resonant switch is shown in figures 2-8 and 2-9. The difference between half-wave and full-wave mode consists in the moment in time when the resonant stage (stage 3 of operation of the converter) ends. The voltage across the resonant capacitor is given by equation (3.26),

$v_{Cr}(t) = V_{out} + Z_r I_{in} \sin \omega_r t$.

Notice that the voltage waveform of v_{Cr} contains a dc component V_{out} and an ac component with the amplitude $Z_r I_{in}$. In order to achieve zero-voltage-switching, the ac component needs to be larger than the dc component,

$Z_r I_{in} > V_{out}$ or

$r < x$.

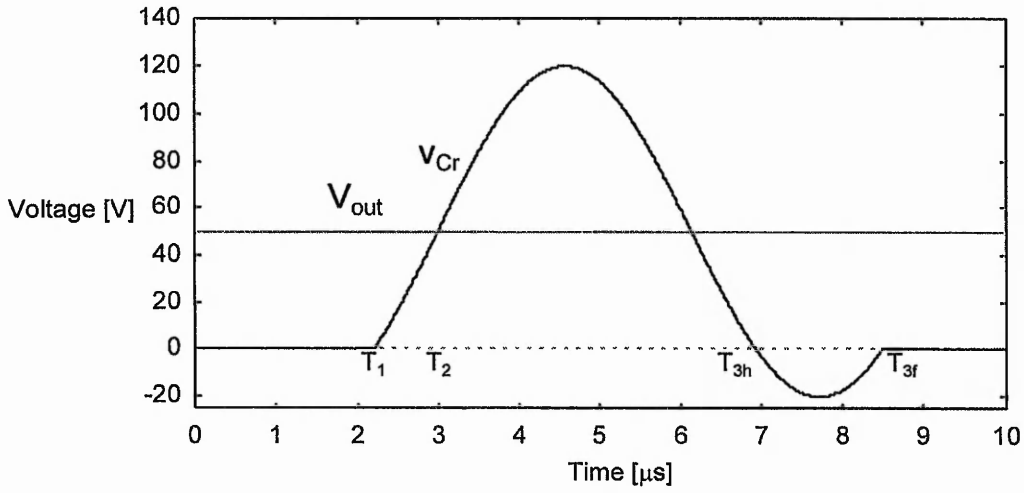

Figure A1-2: Voltage waveform of a ZVS-QRC during the resonant stage.

The waveform of v_{Cr} during the resonant stage is shown in figure A1-2. In half-wave mode of operation, when v_{Cr} drops to zero at T_{3h}, it is clamped at zero by the anti-parallel diode D_S, which carries the reverse current. In full-wave mode of operation, v_{Cr} continues to oscillate to a negative value and returns to zero at time T_{3f}. For the half-wave mode, the end of this stage is T_{3h}; for full-wave mode, it is T_{3f}.

The duration T_{23} of the resonant stage is determined by setting $v_{Cr}(T_{23})=0$ and is

$$T_{23} = \frac{1}{\omega_r}\arcsin(-\frac{r}{x}) \text{ or}$$

$$T_{23} = \frac{a_{zvs}}{\omega_r},$$

where $a_{zvs} = \arcsin(-\frac{r}{x})$.

The equation $v_{Cr}(T_{23})=0$ has two solutions, one corresponding to the half-wave mode for which

$$\pi < \omega_r T_{23} < \frac{3\pi}{2}$$

and the other one corresponding to the full-wave mode,

$$\frac{3\pi}{2} < \omega_r T_{23} < 2\pi .$$

Therefore, for half-wave converters

$$\pi < a_{zvs} < \frac{3\pi}{2} \text{ and}$$

$$a_{zvs} = \pi + \arcsin(\frac{r}{x});$$

for full-wave converters

$$\frac{3\pi}{2} < a_{zvs} < 2\pi \text{ and}$$

$$a_{zvs} = 2\pi - \arcsin(\frac{r}{x}).$$

Appendix 2: Voltage-Conversion Ratio of Boost Quasi-Resonant Converters

A2.1. Zero-Current-Switching Boost Converters

The dc voltage conversion ratio $x=V_{out}/V_{in}$ as a function of normalised load resistance and switching frequency can be derived by equating the input energy per cycle E_{in} and the output energy per cycle E_{out}.

The input energy per cycle is:

$E_{in} = V_{in} I_{in} T_s$.

The output energy per cycle is:

$$E_{out} = V_{out} \int_0^{T_s} i_{out} dt ;$$

$$E_{out} = V_{out} \int_{T_0}^{T_1} i_{out} dt + V_{out} \int_{T_1}^{T_2} i_{out} dt ;$$

$$E_{out} = V_{out} \int_0^{T_{01}} I_{in} dt + V_{out} \int_0^{T_{12}} (I_{in} - \frac{V_{out}}{L_r} t) dt ;$$

$$E_{out} = V_{out} I_{in} \left(T_{01} + \frac{T_{12}}{2} \right) .$$

From equations (3.11), (3.14) and (3.17),

$T_{01} = T_S - T_{12} - T_{23} - T_{34}$;

$$T_{12} = \frac{1}{\omega_r} \frac{x}{r} ;$$

$$T_{23} = \frac{a_{zcs}}{\omega_r} ;$$

$$T_{34} = \frac{1}{\omega_r} \frac{r}{x} (1 - \cos a_{zcs}) ;$$

$$a_{zcs} = \arcsin\left(-\frac{x}{r}\right).$$

For half-wave ZCS converters:

$$a_{zcs} = \pi + \arcsin\left(\frac{x}{r}\right);$$

$$\cos a_{zcs} = -\sqrt{1-\frac{x^2}{r^2}}.$$

For full-wave ZCS converters:

$$a_{zcs} = 2\pi - \arcsin\left(\frac{x}{r}\right);$$

$$\cos a_{zcs} = \sqrt{1-\frac{x^2}{r^2}}.$$

By equating E_{in} and E_{out}:

$$\frac{V_{out}}{V_{in}} = \frac{T_S}{T_{01} + \frac{T_{12}}{2}};$$

$$x = \frac{T_S}{T_S - \frac{T_{12}}{2} - T_{23} - T_{34}};$$

$$\frac{1}{x} = 1 - \frac{1}{T_S}\left(\frac{T_{12}}{2} + T_{23} + T_{34}\right);$$

$$\frac{(x-1)}{x} = \frac{f_S}{2\pi f_r}\left(\frac{x}{2r} + \arcsin\left(-\frac{x}{r}\right) + \frac{r}{x}(1-\cos a_{zcs})\right).$$

By rearranging the above equations it is found:

- for the half-wave ZCS boost converter

$$\frac{f_S}{f_r} = 2\pi\frac{(x-1)}{x}\frac{1}{\frac{x}{2r} + \pi + \arcsin\left(\frac{x}{r}\right) + \frac{r}{x}\left(1+\sqrt{1-\frac{x^2}{r^2}}\right)};$$

- for the full-wave ZCS boost converter

$$\frac{f_S}{f_r} = 2\pi \frac{(x-1)}{x} \frac{1}{\frac{x}{2r} + 2\pi - \arcsin\left(\frac{x}{r}\right) + \frac{r}{x}\left(1 - \sqrt{1 - \frac{x^2}{r^2}}\right)}.$$

A2.2. Zero-Voltage-Switching Boost Converters

The dc voltage conversion ratio $x=V_{out}/V_{in}$ as a function of normalised load resistance and switching frequency can be derived by equating the input energy per cycle E_{in} and the output energy per cycle E_{out}.

The input energy per cycle is:

$$E_{in} = V_{in} I_{in} T_S .$$

The output energy per cycle is:

$$E_{out} = V_{out} \int_{T_2}^{T_3} i_{Lr} dt + V_{out} \int_{T_3}^{T_4} i_{Lr} dt ;$$

$$E_{out} = V_{out} \int_{0}^{T_{23}} I_{in}(1 - \cos\omega_r t) dt + V_{out} \int_{0}^{T_{34}} (I_{in} - I_{in}\cos a_{zvs} - \frac{V_{out}}{L_r} t) dt ;$$

$$E_{out} = V_{out} I_{in} \left(T_{23} + \frac{1}{\omega_r} \sin a_{zvs} + \frac{1}{2} T_{34}(1 - \cos a_{zvs}) \right).$$

From equations (3.24), (3.27) and (3.30),

$T_{01} = T_S - T_{12} - T_{23} - T_{34}$;

$$T_{12} = \frac{1}{\omega_r} \frac{r}{x};$$

$$T_{23} = \frac{a_{zvs}}{\omega_r};$$

$$T_{34} = \frac{1}{\omega_r} \frac{x}{r} (1 - \cos a_{zvs});$$

$$a_{zvs} = \arcsin\left(-\frac{r}{x}\right).$$

For half-wave ZVS converters:

$$a_{zvs} = \pi + \arcsin\left(\frac{r}{x}\right);$$

$$\cos a_{zvs} = -\sqrt{1-\frac{r^2}{x^2}}.$$

For full-wave ZVS converters:

$$a_{zvs} = 2\pi - \arcsin\left(\frac{r}{x}\right);$$

$$\cos a_{zvs} = \sqrt{1-\frac{r^2}{x^2}}.$$

It is found that for the half-wave implementation of the ZVS boost converter:

$$\frac{f_S}{f_r} = \left(\frac{2\pi}{x}\right)\frac{1}{\left[\frac{r}{2x} + \pi + \arcsin\frac{r}{x} + \frac{x}{r}\left(1+\sqrt{1-\frac{r^2}{x^2}}\right)\right]}.$$

For converters having a full-wave switch:

$$\frac{f_S}{f_r} = \left(\frac{2\pi}{x}\right)\frac{1}{\left[\frac{r}{2x} + 2\pi - \arcsin\frac{r}{x} + \frac{x}{r}\left(1-\sqrt{1-\frac{r^2}{x^2}}\right)\right]}.$$

Appendix 3: Characteristic Functions

A3.1. Boost Zero-Current-Switching Quasi-Resonant Converters

The average value of the switch current is:

$$\bar{i}_S = \frac{1}{T_S}\int_0^{T_s} i_S(t)dt;$$

$$\bar{i}_S = \frac{1}{T_S}\int_{T_1}^{T_2} i_S(t)dt + \frac{1}{T_S}\int_{T_2}^{T_3} i_S(t)dt;$$

$$\bar{i}_S = \frac{1}{T_S}\int_0^{T_{12}} \frac{V_{out}t}{L_r}dt + \frac{1}{T_S}\int_0^{T_{23}} (I_{in} + \frac{V_{out}}{Z_r}\sin\omega_r t)dt;$$

$$\bar{i}_S = I_{in}\frac{1}{2\pi}\frac{f_S}{f_r}\left[\frac{x}{2r} + \pi + \arcsin\left(\frac{x}{r}\right) + \frac{r}{x}\left(1+\sqrt{1-\frac{x^2}{r^2}}\right)\right].$$

The average value of the voltage across the diode is:

$$\bar{v}_D = \frac{1}{T_S}\int_0^{T_s} v_D(t)dt;$$

$$\bar{v}_D = \frac{1}{T_S}\int_{T_2}^{T_3} v_D(t)dt + \frac{1}{T_S}\int_{T_3}^{T_4} v_D(t)dt;$$

$$\bar{v}_D = \frac{1}{T_S}\int_0^{T_{23}} (V_{out} - V_{out}\cos\omega_r t)dt + \frac{1}{T_S}\int_0^{T_{34}} (V_{out} - V_{out}\cos a_{zcs} - \frac{I_{in}}{C_r}t)dt;$$

$$\bar{v}_D = V_{out}\frac{1}{2\pi}\frac{f_S}{f_r}\left[\frac{x}{2r} + \pi + \arcsin\left(\frac{x}{r}\right) + \frac{r}{x}\left(1+\sqrt{1-\frac{x^2}{r^2}}\right)\right].$$

A3.2. Boost Zero-Voltage-Switching Quasi-Resonant Converters

The average value of the switch current is:

$$\bar{i}_S = \frac{1}{T_S}\int_0^{T_s} i_S(t)dt;$$

$$\bar{i}_S = \frac{1}{T_S}\int_{T_0}^{T_1} i_S(t)dt + \frac{1}{T_S}\int_{T_3}^{T_4} i_S(t)dt;$$

$$\bar{i}_S = \frac{1}{T_S}\int_{0}^{T_{01}} I_{in}dt + \frac{1}{T_S}\int_{0}^{T_{34}} \left(I_{in} + \frac{V_{out}}{L_r}t - I_{in}(1-\cos a) \right) dt;$$

$$\bar{i}_S = I_{in}\left[1 - \frac{1}{2\pi}\frac{f_S}{f_r}\left(\frac{r}{2x} + \pi + \arcsin\frac{r}{x} + \frac{x}{r}\left(1 + \sqrt{1 - \frac{r^2}{x^2}} \right) \right) \right].$$

The average value of the voltage across the diode is:

$$\bar{v}_D = \frac{1}{T_S}\int_{0}^{T_S} v_D(t)dt;$$

$$\bar{v}_D = \frac{1}{T_S}\int_{T_0}^{T_1} v_D(t)dt + \frac{1}{T_S}\int_{T_1}^{T_2} v_D(t)dt;$$

$$\bar{v}_D = \frac{1}{T_S}\int_{0}^{T_{01}} V_{out}dt + \frac{1}{T_S}\int_{0}^{T_{12}} (V_{out} - \frac{I_{in}}{C_r}t)dt;$$

$$\bar{v}_D = V_{out}\left[1 - \frac{1}{2\pi}\frac{f_S}{f_r}\left(\frac{r}{2x} + \pi + \arcsin\frac{r}{x} + \frac{x}{r}\left(1 + \sqrt{1 - \frac{r^2}{x^2}} \right) \right) \right].$$

A3.3. Boost Zero-Voltage-Switching Multi-Resonant Converters

The average values of the normalised voltages across the switching devices for a boost ZVS-MRC are given below for both operating modes.

(i) Operation Mode 1:

$$\bar{v}_D^* = \frac{1}{T_S}\left[T_{01} - \frac{1}{\omega_D}\sin\omega_D T_{01} + cV_{DT1}^* T_{12} + (1-c)T_{12} + \frac{1}{2}\alpha\sqrt{c}(1-c)\omega_{SD}T_{12}^2 - \right.$$

$$\left. - \frac{1}{\omega_{SD}}\sqrt{c}(c\alpha - I_{LT1}^*)\frac{1}{C_N}(\cos\omega_{SD}T_{12} - 1) + \frac{1}{\omega_{SD}}(1-c)(V_{DT1}^* - 1)\sin\omega_{SD}T_{12} \right];$$

$$\bar{v}_S^* = \frac{1}{T_S}\left[-cV_{DT1}^* T_{12} + cT_{12} + \frac{1}{2}\alpha\sqrt{c}(1-c)\omega_{SD}T_{12}^2 - \frac{\sqrt{c}(c\alpha - I_{LT1}^*)}{\omega_{SD}}(\cos\omega_{SD}T_{12} - 1) + \right.$$

$$\left. + \frac{c(V_{DT1}^* - 1)}{\omega_{SD}}\sin\omega_{SD}T_{12} + T_{23} + \frac{I_{LT2}^* - \alpha}{\omega_S}(\cos\omega_S T_{23} - 1) + \frac{V_{ST2}^* - 1}{\omega_S}\sin\omega_S T_{23}\right].$$

(ii) Operation Mode 2:

$$\bar{v}_D^* = \frac{1}{T_S}\left[T_{01} - \frac{1}{\omega_D}\sin\omega_D T_{01} + cV_{DT1}^* T_{12} + (1-c)T_{12} + \frac{1}{2}\alpha\sqrt{c}(1-c)\omega_{SD}T_{12}^2 - \right.$$

$$- \frac{1}{\omega_{SD}}\sqrt{c}(c\alpha - I_{LT1}^*)\frac{1}{C_N}(\cos\omega_{SD}T_{12} - 1) + \frac{1}{\omega_{SD}}(1-c)(V_{DT1}^* - 1)\sin\omega_{SD}T_{12} + T_{23} +$$

$$\left. + \frac{I_{LT2}^*}{\omega_D\sqrt{C_N}}(\cos\omega_D T_{23} - 1) + \frac{V_{DT2} - 1}{\omega_D}\sin\omega_D T_{23}\right];$$

$$\bar{v}_S^* = \frac{1}{T_S}\left[-cV_{DT1}^* T_{12} + cT_{12} + \frac{1}{2}\alpha\sqrt{c}(1-c)\omega_{SD}T_{12}^2 - \frac{\sqrt{c}(c\alpha - I_{LT1}^*)}{\omega_{SD}}(\cos\omega_{SD}T_{12} - 1) + \right.$$

$$\left. + \frac{c(V_{DT1}^* - 1)}{\omega_{SD}}\sin\omega_{SD}T_{12}\right].$$

The average values of the normalised currents are given below.

(i) Operation mode 1:

$$\bar{i}_D^* = \frac{1}{T_S}\frac{1}{\alpha}\left[\frac{1}{\omega_S}(I_{LT2}^* - \alpha)\sin\omega_S T_{23} + \alpha T_{23} - \frac{1}{\omega_S}(V_{ST2}^* - 1)(\cos\omega_S T_{23} - 1) + \right.$$

$$\left. + I_{LT3}^* T_{34} - \frac{1}{2}\omega_S T_{34}^2\right];$$

$$\bar{i}_S^* = \frac{1}{T_S}\frac{1}{\alpha}\left[-\frac{1}{\omega_D}\sqrt{C_N}(\cos\omega_D T_{01} - 1) + \alpha(T_{01} + T_{34}) - I_{LT3}^* T_{34} + \frac{1}{2}\omega_S T_{34}^2\right];$$

$$\bar{i}_{Lr}^{*} = \frac{1}{T_S}\frac{1}{\alpha}\left[\frac{1}{\omega_D}\sqrt{C_N}(\cos\omega_D T_{01} - 1) + c\alpha T_{12} + \frac{1}{\omega_{SD}}(I_{LT1}^{*} - c\alpha)\sin\omega_{SD} T_{12} - \right.$$
$$-\frac{1}{\omega_{SD}}\sqrt{c}(V_{DT1}^{*} - 1)(\cos\omega_{SD} T_{12} - 1) + \alpha T_{23} + \frac{1}{\omega_S}(I_{LT2}^{*} - \alpha)\sin\omega_S T_{23} -$$
$$\left.-\frac{1}{\omega_S}(V_{ST2}^{*} - 1)(\cos\omega_S T_{23} - 1) + I_{LT3}^{*} T_{34} - \frac{1}{2}\omega_S T_{34}^{2}\right].$$

(ii) Operation mode 2:

$$\bar{i}_S^{*} = \frac{1}{T_S}\frac{1}{\alpha}\left[I_{LT3}^{*} T_{34} - \frac{1}{2}\omega_S T_{34}^{2}\right];$$
$$\bar{i}_D^{*} = \frac{1}{T_S}\frac{1}{\alpha}\left[-\frac{1}{\omega_D}\sqrt{C_N}(\cos\omega_D T_{01} - 1) + \alpha(T_{01} + T_{23} + T_{34}) - \frac{1}{\omega_D} I_{LT2}^{*}\sin\omega_D T_{23} + \right.$$
$$\left.+\frac{1}{\omega_D}(V_{DT2}^{*} - 1)\sqrt{C_N}(\cos\omega_D T_{23} - 1) - I_{LT3}^{*} T_{34} + \frac{1}{2}\omega_S T_{34}^{2}\right];$$

$$\bar{i}_{Lr}^{*} = \frac{1}{T_S}\frac{1}{\alpha}\left[\frac{1}{\omega_D}\sqrt{C_N}(\cos\omega_D T_{01} - 1) + c\alpha T_{12} + \frac{1}{\omega_{SD}}(I_{LT1}^{*} - c\alpha)\sin\omega_{SD} T_{12} - \right.$$
$$-\frac{1}{\omega_{SD}}\sqrt{c}(V_{DT1}^{*} - 1)(\cos\omega_{SD} T_{12} - 1) + \frac{1}{\omega_D} I_{LT2}^{*}\sin\omega_D T_{23} -$$
$$\left.-\frac{1}{\omega_D}(V_{DT2}^{*} - 1)\sqrt{C_N}(\cos\omega_D T_{23} - 1) + I_{LT3}^{*} T_{34} - \frac{1}{2}\omega_S T_{34}^{2}\right].$$

Appendix 4: Design of Resonant Boost Converters

The design procedure [121,122] for a dc-dc boost converter assumes the following input data:

- $V_{in,min}$ is the minimum input voltage;
- $V_{in,max}$ is the maximum input voltage;
- V_{out} is the output voltage;
- $I_{out,max}$ is the maximum output current;
- $I_{out,min}$ is the minimum output current;
- ΔV_{out} is the output voltage ripple;
- ΔI_{in} is the input current ripple.

As the output load and input voltage vary, the control circuit adjusts the switching frequency to maintain a constant output voltage V_{out}.

For a boost ZCS-QRC operating with a fixed on-time, the maximum switching frequency $f_{S,max}$ will occur at low line $V_{in,min}$ and full load $I_{out,max}$. The constraint that zero-current-switching is maintained for the whole operating range is

$$Z_r < \frac{V_{in,min}}{I_{out,max}}. \qquad \text{(A4-1)}$$

For a boost ZVS-QRC operating with a fixed off-time, the maximum switching frequency $f_{S,max}$ will occur at high line $V_{in,max}$ and light load $I_{out,min}$. The constraint that zero-voltage-switching is maintained for the whole operating range is

$$Z_r > \frac{V_{in,max}}{I_{out,min}}. \qquad \text{(A4-2)}$$

The topology coefficients [123] k_1 and k_2 are defined. The first coefficient k_1 equals the maximum switching frequency divided by the resonant tank frequency f_r,

$$f_{S,max}=k_1 f_r. \quad \text{(A4-3)}$$

In practice, the topology coefficient k_1 is determined from the steady-state characteristics of the converter, shown in figures 3-12 and 3-19.

The second coefficient k_2 is defined from the following equations:

- for ZCS converters $Z_r = k_{2,ZCS} \frac{V_{in,min}}{I_{out,max}}$; (A4-4)

- for ZVS converters $Z_r = k_{2,ZVS} \frac{V_{in,max}}{I_{out,min}}$. (A4-5)

In ZCS-QRCs, it is desirable to select maximum Z_r to minimise the peak resonant current and, consequently, minimise the current stress on the switching device. In practice [39] it is sufficient to make Z_r slightly lower (e.g. 10-20%) than the maximum possible value given by equation (A4-1) and a value of $k_{2,ZCS} = 0.8...0.9$ is used.

In ZVS-QRCs, a minimum value of Z_r is selected to minimise the peak resonant voltage and, consequently, minimise the voltage stress on the switching device. In practice it is sufficient to make Z_r slightly higher (e.g. 10-20%) than the minimum value calculated from equation (A4-2) and a value of $k_{2,ZVS} = 1.1...1.2$ is used.

The design procedure for a quasi-resonant boost converter is the following [23,34,123]:

- Selection of the maximum switching frequency $f_{S,max}$.
- Determination of the resonant frequency and of the characteristic impedance Z_r using the topology coefficients k_1 and k_2 and equations (A4-3) to (A4-5).
- Calculation of the resonant tank component values L_r and C_r considering equations (3.6) and (3.7).
- Selection of switches and rectifier diodes. [123]
- Calculation of input inductance and output capacitor based on the current and voltage ripples, respectively.

A detailed description of the design procedure of a ZVS-MRC is given by Tabisz [41,43]. The three resonant elements are calculated from equations (3.45) to (3.47) after C_N, Z_r and f_r are determined. The maximum switching frequency is selected and the values of the resonant frequency, characteristic impedance and normalised capacitance are chosen from the graphs presented in figures 3-37 to 3-40.

Appendix 5: Design of the Feedback Loop of a Dc-Dc Converter

A5.1. Stability of the Feedback System

Most control systems are feedback systems and a feature of dynamic feedback systems is that they can sometimes sustain self-excited oscillations and therefore become unstable. At a certain frequency, the additional phase shift from reactive components and time delays comes back in phase with the original signal. If the total of all amplitude gains and losses around the loop is one or greater than one at this frequency, then the error signal is self-perpetuating and the circuit becomes an oscillator. The object of the stability analysis is to find a way to keep the system from reaching the critical state which causes instability.

In the following paragraphs the Bode plots are used. The critical point on the Bode diagrams are 0 dB gain and -180° phase. The difference between the actual phase shift when the gain is unity (0 dB) and 180 degrees is called *phase margin*. The amount of gain below unity when the phase shift reaches 180 degrees is called *gain margin*. Bode plots are an excellent vehicle for designing closed loop systems. They provide good visibility into the gain/phase characteristics of the various loop elements. Calculation of the overall loop is made simple by adding gain in dB and phase in degrees.

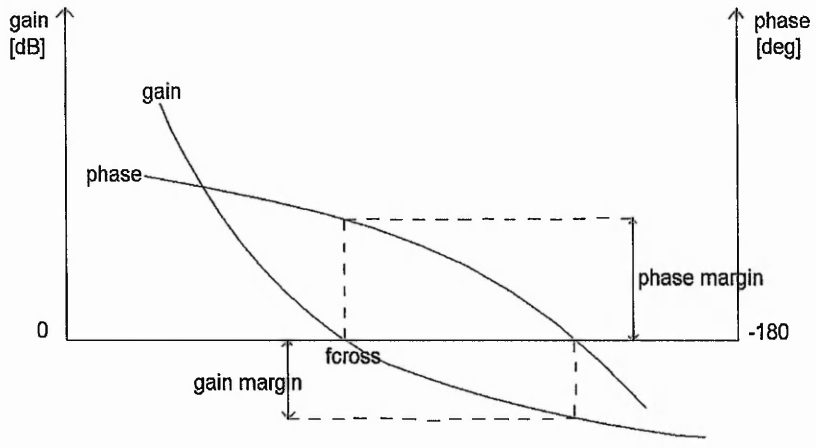

Figure A5-1: Gain and phase margins.

It is possible to stabilise a loop just by reducing the gain of the amplifier until loop cross-over occurs at a frequency f_{cross} well below that where phase shifts from reactive components start to become significant. The problem with this approach is that the response time of the loop to a transient disturbance is slowed down to the point where it is usually unacceptable. In any high-performance loop, the object is to cross over at as high a frequency as possible, while maintaining a good phase margin. This is accomplished by tailoring the frequency response of the error amplifier to compensate for some of the modulator (power circuit) phase shift in the region of cross-over.

A5.2. Compensation of the Feedback Loop

The task of designing the compensation network in the feedback loop is to define the characteristics of the compensator to achieve good dynamic response, line and load regulations and stability [14,124-129]. In the closed-loop feedback system shown in figure A5-2, the overall open-loop transfer function is:

$T_{OL}(s)=T_1(s)\bullet T_C(s)$,

where $T_1(s)$ is the transfer function of the boost converter and switching controller and $T_C(s)$ is the transfer function of the compensated error amplifier.

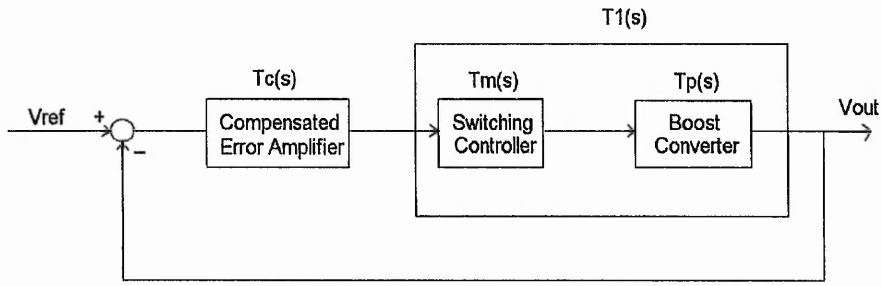

Figure A5-2: Linearised feedback control system.

For a given $T_1(s)$, the transfer function of the compensated error amplifier $T_C(s)$ must be properly tailored so that $T_{OL}(s)$ meets the performance requirements expected of the power circuit. The desired characteristics of the open loop transfer function $T_{OL}(s)$ are as follows:

(i) High gain at low frequencies and small gain at high frequencies.

If the dc gain is increased, the transient response improves (the system becomes more responsive) and the steady-state error in the converter output decreases. However, the overshoot increases (the response becomes more oscillatory). If the gain is made too high, the system may be either unstable or it may become very difficult to control. If the gain is reduced to a very low value, the system may become too sluggish.
High gain at high frequencies is undesirable as thin, high-frequency noise spikes would be transmitted at large amplitudes to the output. Thus gain should be permitted to fall off at high frequencies.

(ii) The crossover frequency should be as high as possible.

Crossover frequency is a measure of bandwidth, so of speed of response. The higher the crossover frequency, the better the dynamic response.
The crossover frequency is limited by two factors: switching frequency and RHP zero. Sampling theory shows that the crossover frequency must be less than half the switching frequency. But, to avoid large-amplitude switching frequency ripple at the output, f_{cross} should be less than one-fifth the switching frequency.
The RHP zero has the same positive gain slope as the conventional (left-half plane) zero, but the phase slope is negative, like a single pole. Above RHP zero corner frequency, loop gain is held up, yet more phase lag is added. This makes it virtually impossible to achieve an open loop crossover frequency above the RHP zero frequency

(iii) The phase margin should be as high as possible.

The higher the phase margin, the better the stability of the closed-loop system. A low phase margin is unacceptable, as a small deviation in system parameters or small unmodelled lags or delays in the system could readily cause instability.

To meet the requirements stated above simultaneously, a general error amplifier is shown in figure A5-3, where the amplifier can be assumed to be ideal.

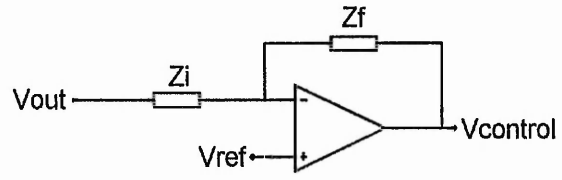

Figure A5-3: A general compensated error amplifier.

One of the inputs to the amplifier is the output voltage V_{out} of the converter, the other input is the desired (reference) value V_{ref} of V_{out}. The output of the error amplifier is the control voltage v_c. In terms of Z_i and Z_f, the transfer function between the input and the output perturbations can be obtained as:

$$\frac{\tilde{v}_c(s)}{\tilde{v}_{out}(s)} = -\frac{Z_f(s)}{Z_i(s)} = -T_c(s).$$

The error amplifier compensation circuit to be used is shown in figure A5-4. This amplifier, together with a mathematical concept called the k factor, allows the circuit designer to choose the desired result, i.e., a particular loop crossover frequency and phase margin, and then determine the necessary component values to achieve these results from a few straight-forward algebraic equations [127].

This amplifier, also known as type 3 amplifier, has a pole at the origin and two zero-pole pairs. The two zeros are coincident and the two poles are coincident. Type 3 amplifiers have the most phase boost of any practical amplifier configuration.

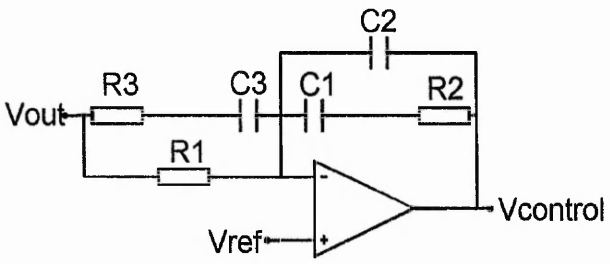

Figure A5-4: Error amplifier compensation circuit.

The transfer function is:

$$T(s) = \frac{R_1 + R_3}{R_1 R_3 C_2} \frac{(s + \frac{1}{R_2 C_1})\ (s + \frac{1}{(R_1 + R_3) C_3})}{s\ (s + \frac{1}{R_3 C_3})\ (s + \frac{1}{R_2 \frac{C_1 C_2}{C_1 + C_2}})}$$

or

$$T(s) = kG\omega_{cross} \frac{(s + \omega_z)\ (s + \omega_z)}{s\ (s + \omega_p)\ (s + \omega_p)},$$

where:

$\omega_{cross} = 2\pi f_{cross}$,

ω_{cross} = crossover frequency in rad/s,

f_{cross} = crossover frequency in Hz,

G = required amplifier gain at crossover (expressed as a ratio, not as dB),

k = factor which describes the required separation of double poles and zeros to accomplish the desired phase boost,

$\omega_z = \frac{\omega_{cross}}{\sqrt{k}}$ (double zero),

$\omega_p = \omega_{cross}\sqrt{k}$ (double pole).

When using the k-factor-method to design the compensation network, the following steps are necessary:

1. Determination of the Bode Plots of the power circuit.

2. Choice of the crossover frequency f_{cross}.

3. Choice of the desired phase margin.

4. Determination of the required amplifier gain G at cross-over (G is dimensionless):
   amplifier gain G = 1/power circuit gain.

If the gain is expressed in dB, then the amplifier gain is simply the negative of the modulator gain.

5. Calculation of the amount of phase boost required

boost = M - P - 90,

where M = desired phase margin (degrees)

P = power circuit phase shift (degrees)

6. Choice of the value of R_1, the input resisstor to the amplifier.

7. The following equations apply:

$$k = \left(\tan\left(\frac{\text{boost}}{4} + 45\right)\right)^2;$$

$$C_2 = \frac{1}{2\pi f_{cross} G R_1};$$

$$C_1 = C_2(k-1);$$

$$R_2 = \frac{\sqrt{k}}{2\pi f_{cross} C_1};$$

$$R_3 = \frac{R_1}{k-1};$$

$$C_3 = \frac{1}{2\pi f_{cross} \sqrt{k} R_3}.$$

Appendix 6: Listing of the C-Program for Analysis of Multi-Resonant Boost Converter

```
/* Steady-State Analysis of Boost Multi-Resonant Converters */

/* Normalised equations are used.
   Automatic selection of operation modes 1 and 2.
   The peak voltages across the switch and diodes are calculated.
   The characteristic functions Gv and Gi are determined.    */

# include <stdio.h>
# include <math.h>
# include <conio.h>

float newraph1 (float, float, float, float);
float newraph2 (float, float, float);
void stage_1(void);
void stage_4(void);
void opmod_1(void);
void opmod_2(void);
void det_Gv1(void);
void det_Gv2(void);
void det_Gi1(void);
void det_Gi2(void);

float In, Vout, Vin, Lr, Cs, Cd, Cn, c;
float wd, ws, wsd, Zr, f, Gvs, Gvd, Gil, Gid, Gis, x, r;

float T01, T12, T23, T34, Ts, fs, fr;
float Vdt1, Ilt1, Vst2, Vdt2, Ilt2, Ilt3;
float vd, vs, vsmax, vdmax, il, time, timet, tstep, tvdmax, tvsmax;
float anr, bnr, cnr, dnr, sol;

FILE *fvd, *fvs, *fil;

void main(void)
{

   float T12mod1, T12mod2;

   /* Input parameters */

   Lr=47;                    /* resonant inductor in uH */
   Cs=13;                          /* resonant capacitors in nF */
   Cd=39;
   In=3;                           /* normalised input current */
   T01=1.693;                      /* duration of stage 1 in us */

   fvs=fopen("c:\\programc\\vswitch.dat","wb");
   fvd=fopen("c:\\programc\\vdiode.dat","wb");
   fil=fopen("c:\\programc\\il.dat","wb");

   clrscr();
```

```
/* Resonant frequencies in MHz */

wd=100/sqrt(10*Lr*Cd);
ws=100/sqrt(10*Lr*Cs);
wsd=100/sqrt(10*Lr*Cs*Cd/(Cd+Cs));

fr=ws/2/M_PI;
printf("fr=%5.4f  ",fr);  getch();

/* Characteristic impedance */

Zr=sqrt(1000*Lr/Cs);
printf("Zr=%5.4f\n",Zr);

printf("In=%5.4f     T01=%5.4f\n",In,T01);

/* Normalised ratio of the resonant capacitances */

Cn=Cd/Cs;

c=Cd/(Cs+Cd);

/* Stage 1 */

stage_1();

/* Stage 2 - opmod 1 */

anr = c*Vdt1 + (1-c);
bnr = -In*sqrt(c)*(1-c);
cnr = (c*In-Ilt1)*sqrt(c)/Cn;
dnr = (1-c)*(Vdt1-1);

printf("a=%4.2f  b=%4.2f  c=%4.2f  d=%4.2f\n",anr,bnr,cnr,dnr);   getch();

sol=newraph1(anr,bnr,cnr,dnr);
T12mod1=sol/wsd;

 /* Stage 2  - opmod 2 */

anr = - c*Vdt1 + c;
bnr = In*sqrt(c)*(1-c);
cnr = (c*In-Ilt1)*sqrt(c);
dnr = c*(Vdt1-1);

printf("a=%4.2f  b=%4.2f  c=%4.2f  d=%4.2f\n",anr,bnr,cnr,dnr);   getch();

sol=newraph1(anr,bnr,cnr,dnr);
T12mod2=sol/wsd;

printf("\nT12mod1=%5.4f   T12mod2=%5.4f\n",T12mod1, T12mod2);

if (T12mod1 < T12mod2) {
                        printf("Operation mode 1\n");
                        T12=T12mod1;
                        opmod_1();
                       }
                else
```

```
                                {
                                 printf("Operation mode 2\n");
                                 T12=T12mod2;
                                 opmod_2();
                                }

 stage_4();

 /* Determination of the switching frequency */

 Ts=T01+T12+T23+T34;
 fs=1/Ts;

 printf("Ts=%5.4f   fs=%5.4f   ",Ts,fs);
 getch();

 /* Normalised switching frequency */

 f=fs/fr;

 printf("f=%5.4f\n",f);   getch();

 fclose(fvd);
 fclose(fvs);
 fclose(fil);

 /* Determination of function G */

 if (T12mod1 < T12mod2) {
                                 printf("Operation mode 1\n");
                                 det_Gv1();
                                 det_Gi1();
                                }
                    else
                                {
                                 printf("Operation mode 2\n");
                                 det_Gv2();
                                 det_Gi2();
                                }

 /* Voltage conversion ratio */

 x=1/(1-Gvd);
 printf("Voltage conversion ratio x=%5.4f\n",x);  getch();

 /* Normalised load resistance */

 r=x/In;
 printf("Normalised load resistance r=%5.4f\n",r);   getch();

 return;

}

/* Stage 1 */

void stage_1(void)
{
```

```
  tstep=T01/50;
  vs=0;

  for (time=0; time<T01; time=time+tstep)  {

  vd = 1-cos(wd*time);
  il = -sqrt(Cn)*sin(wd*time);

  fprintf(fvs,"%f\t %f\n",time,vs);
  fprintf(fvd,"%f\t %f\n",time,vd);
  fprintf(fil,"%f\t %f\n",time,il);

  }

  Vdt1 = 1-cos(wd*T01);
  Ilt1 = -sqrt(Cn)*sin(wd*T01);

  return;

}

/* Stages 2 and 3 - operation mode 1 */

void opmod_1 (void)
{

  Vst2 = - c*Vdt1 + c + In*sqrt(c)*(1-c)*wsd*T12;
  Vst2 = Vst2 + (c*In-Ilt1)*sqrt(c)*sin(wsd*T12);
  Vst2 = Vst2 + c*(Vdt1-1)*cos(wsd*T12);

  Ilt2 = c*In + (Ilt1-c*In)*cos(wsd*T12);
  Ilt2 = Ilt2 + sqrt(c)*(Vdt1-1)*sin(wsd*T12);

  printf("\nStage 2:  T12=%5.4f\n",T12);
  getch();

  tstep=T12/100;

  for (time=0; time<T12; time=time+tstep)  {

  vs = - c*Vdt1 + c + In*sqrt(c)*(1-c)*wsd*time;
  vs = vs + (c*In-Ilt1)*sqrt(c)*sin(wsd*time);
  vs = vs + c*(Vdt1-1)*cos(wsd*time);

  vd = c*Vdt1 + (1-c) - In*sqrt(c)*(1-c)*wsd*time;
  vd = vd + (c*In-Ilt1)*sqrt(c)/Cn*sin(wsd*time);
  vd = vd + (1-c)*(Vdt1-1)*cos(wsd*time);

  il = c*In + (Ilt1-c*In)*cos(wsd*time);
  il = il + sqrt(c)*(Vdt1-1)*sin(wsd*time);

  timet=time+T01;

  fprintf(fvs,"%f\t %f\n",timet,vs);
  fprintf(fvd,"%f\t %f\n",timet,vd);
  fprintf(fil,"%f\t %f\n",timet,il);
```

```
}

/* Determination of the peak switch voltage during stage 2 - opmod 1 */

anr = In*sqrt(c)*(1-c);
bnr = -wsd*c*(Vdt1-1);
cnr = (c*In-Ilt1)*sqrt(c)*wsd;

tvsmax=newraph2(anr,bnr,cnr);
tvsmax=tvsmax/wsd;

vsmax = - c*Vdt1 + c + In*sqrt(c)*(1-c)*wsd*tvsmax;
vsmax = vsmax + (c*In-Ilt1)*sqrt(c)*sin(wsd*tvsmax);
vsmax = vsmax + c*(Vdt1-1)*cos(wsd*tvsmax);

printf("a=%4.2f  b=%4.2f  c=%4.2f\n",anr,bnr,cnr);
printf("Vsmax=%5.4f  tsmax=%5.4f\n",vsmax,tvsmax);

/* Determination of the peak diode voltage during stage 2  -opmod 1 */

anr = -In*sqrt(c)*(1-c);
bnr = -wsd*(1-c)*(Vdt1-1);
cnr = (c*In-Ilt1)*sqrt(c)/Cn*wsd;

tvdmax=newraph2(anr,bnr,cnr);
tvdmax=tvdmax/wsd;

vdmax = c*Vdt1 + (1-c) - In*sqrt(c)*(1-c)*wsd*tvdmax;
vdmax = vdmax + (c*In-Ilt1)*sqrt(c)/Cn*sin(wsd*tvdmax);
vdmax = vdmax + (1-c)*(Vdt1-1)*cos(wsd*tvdmax);

printf("a=%4.2f  b=%4.2f  c=%4.2f\n",anr,bnr,cnr);
printf("Vdmax=%5.4f  tdmax=%5.4f\n",vdmax,tvdmax);


/* Stage 3 - opmod 1 */

anr = 1;
bnr = -(Ilt2-In);
cnr = Vst2-1;

printf("a=%4.2f  b=%4.2f   c=%4.2f\n",anr,bnr,cnr);  getch();

sol=newraph2(anr,bnr,cnr);
T23=sol/ws;

Ilt3 = In + (Ilt2-In)*cos(ws*T23) + (Vst2-1)*sin(ws*T23);

printf("Stage 3:  T23=%5.4f\n",T23);   getch();

tstep=T23/100;
vd=0;

for (time=0; time<T23; time=time+tstep)  {

il = In + (Ilt2-In)*cos(ws*time) + (Vst2-1)*sin(ws*time);
vs = 1 -(Ilt2-In)*sin(ws*time) + (Vst2-1)*cos(ws*time);
```

```
  timet=time+T01+T12;

  fprintf(fvs,"%f\t %f\n",timet,vs);
  fprintf(fvd,"%f\t %f\n",timet,vd);
  fprintf(fil,"%f\t %f\n",timet,il);

  }

return;

}

/* Stages 2 and 3 - operation mode 2 */

void opmod_2 (void)
{

  Vdt2 = c*Vdt1 + 1-c - In*sqrt(c)*(1-c)*wsd*T12;
  Vdt2 = Vdt2 + (c*In-Ilt1)*sqrt(c)/Cn*sin(wsd*T12);
  Vdt2 = Vdt2 + (1-c)*(Vdt1-1)*cos(wsd*T12);

  Ilt2 = c*In + (Ilt1-c*In)*cos(wsd*T12);
  Ilt2 = Ilt2 + (Vdt1-1)*sqrt(c)*sin(wsd*T12);

  printf("\nStage 2:  T12=%5.4f\n",T12);
  getch();

  tstep=T12/100;

  for (time=0; time<T12; time=time+tstep)  {

  vs = - c*Vdt1 + c + In*sqrt(c)*(1-c)*wsd*time;
  vs = vs + (c*In-Ilt1)*sqrt(c)*sin(wsd*time);
  vs = vs + c*(Vdt1-1)*cos(wsd*time);

  vd = c*Vdt1 + (1-c) - In*sqrt(c)*(1-c)*wsd*time;
  vd = vd + (c*In-Ilt1)*sqrt(c)/Cn*sin(wsd*time);
  vd = vd + (1-c)*(Vdt1-1)*cos(wsd*time);

  il = c*In + (Ilt1-c*In)*cos(wsd*time);
  il = il + sqrt(c)*(Vdt1-1)*sin(wsd*time);

  timet=time+T01;

  fprintf(fvs,"%f\t %f\n",timet,vs);
  fprintf(fvd,"%f\t %f\n",timet,vd);
  fprintf(fil,"%f\t %f\n",timet,il);

                              }

  /* Determination of the peak switch voltage during stage 2 - opmode 2*/

  anr = In*sqrt(c)*(1-c);
  bnr = -wsd*c*(Vdt1-1);
  cnr = (c*In-Ilt1)*sqrt(c)*wsd;

  tvsmax=newraph2(anr,bnr,cnr);
```

```
tvsmax=tvsmax/wsd;

vsmax = - c*Vdt1 + c + In*sqrt(c)*(1-c)*wsd*tvsmax;
vsmax = vsmax + (c*In-Ilt1)*sqrt(c)*sin(wsd*tvsmax);
vsmax = vsmax + c*(Vdt1-1)*cos(wsd*tvsmax);

printf("a=%4.2f  b=%4.2f  c=%4.2f\n",anr,bnr,cnr);
printf("Vsmax=%5.4f  tsmax=%5.4f\n",vsmax,tvsmax);

/* Determination of the peak diode voltage during stage 2 - opmode 2 */

anr = -In*sqrt(c)*(1-c);
bnr = -wsd*(1-c)*(Vdt1-1);
cnr = (c*In-Ilt1)*sqrt(c)/Cn*wsd;

tvdmax=newraph2(anr,bnr,cnr);
tvdmax=tvdmax/wsd;

vdmax = c*Vdt1 + (1-c) - In*sqrt(c)*(1-c)*wsd*tvdmax;
vdmax = vdmax + (c*In-Ilt1)*sqrt(c)/Cn*sin(wsd*tvdmax);
vdmax = vdmax + (1-c)*(Vdt1-1)*cos(wsd*tvdmax);

printf("a=%4.2f  b=%4.2f  c=%4.2f\n",anr,bnr,cnr);
printf("Vdmax=%5.4f  tdmax=%5.4f\n",vdmax,tvdmax);


/* Stage 3 - opmode 2 */

anr = 1;
bnr = -Ilt2/sqrt(Cn);
cnr = Vdt2-1;

printf("a=%4.2f  b=%4.2f   c=%4.2f\n",anr,bnr,cnr);  getch();
sol=newraph2(anr,bnr,cnr);
T23=sol/wd;

Ilt3 = Ilt2*cos(wd*T23) + (Vdt2-1)*sqrt(Cn)*sin(wd*T23);

printf("Stage 3:  T23=%5.4f\n",T23);   getch();

tstep=T23/100;
vs=0;

for (time=0; time<T23; time=time+tstep)  {

il = Ilt2*cos(wd*time) + (Vdt2-1)*sqrt(Cn)*sin(wd*time);
vd = 1 - Ilt2/sqrt(Cn)*sin(wd*time) + (Vdt2-1)*cos(wd*time);

timet=time+T01+T12;

fprintf(fvs,"%f\t %f\n",timet,vs);
fprintf(fvd,"%f\t %f\n",timet,vd);
fprintf(fil,"%f\t %f\n",timet,il);

}

return;
```

```
}

/* Stage 4 */

void stage_4(void)
{

  T34 = Ilt3/ws;

  printf("Stage 4:  T34=%5.4f\n", T34);   getch();

  tstep=T34/50;
  vs=0;  vd=0;

  for (time=0; time<T34; time=time+tstep)  {

  il = Ilt3 - ws*time;

  timet=time+T01+T12+T23;

  fprintf(fvs,"%f\t %f\n",timet,vs);
  fprintf(fvd,"%f\t %f\n",timet,vd);
  fprintf(fil,"%f\t %f\n",timet,il);


  }

  return;

}

/* Determination of function Gv for operation mode 1 */

void det_Gv1(void)

{
 /* Average value of vd - mode 1 */

  Gvd = T01 - 1/wd*sin(wd*T01) + c*Vdt1*T12 + (1-c)*T12;
  Gvd = Gvd + 1/2*In*sqrt(c)*(1-c)*wsd*T12*T12          ;
  Gvd = Gvd - sqrt(c)/wsd/Cn*(c*In-Ilt1)*(cos(wsd*T12)-1) ;
  Gvd = Gvd + 1/wsd*(1-c)*(Vdt1-1)*sin(wsd*T12);
  Gvd = Gvd/Ts;

  /* Average value of vs - mode 1 */

  Gvs = -c*Vdt1*T12 + c*T12 + 1/2*In*sqrt(c)*(1-c)*wsd*T12*T12;
  Gvs = Gvs - sqrt(c)*(c*In-Ilt1)/wsd*(cos(wsd*T12)-1);
  Gvs = Gvs + c*(Vdt1-1)/wsd*sin(wsd*T12) + (Vst2-1)/ws*sin(ws*T23);
  Gvs = Gvs + T23 + (Ilt2-In)/ws*(cos(ws*T23)-1);
  Gvs = Gvs/Ts;

  printf(" Gvd=%5.4f  Gvs=%5.4f\n",Gvd,Gvs);
  return;

 }
```

```
/* Determination of Gi for operation mode 1 */

void det_Gi1(void)
{

  /* Average value of il for operation mode 1 */

  Gil = sqrt(Cn)*(cos(wd*T01)-1)/wd + c*In*T12 - ws*T34*T34/2;
  Gil = Gil + (Ilt1-c*In)*sin(wsd*T12)/wsd +In*T23 ;
  Gil = Gil - sqrt(c)*(Vdt1-1)*(cos(wsd*T12)-1)/wsd + Ilt3*T34;
  Gil = Gil + (Ilt2-In)*sin(ws*T23)/ws -(Vst2-1)*(cos(ws*T23)-1)/ws;
  Gil = Gil/Ts/In;

  /* Average value of id for operation mode 1 */

  Gid = - ws*T34*T34/2 + In*T23 + Ilt3*T34;
  Gid = Gid + (Ilt2-In)*sin(ws*T23)/ws -(Vst2-1)*(cos(ws*T23)-1)/ws;
  Gid = Gid/Ts/In;

  /* Average value of is for operation mode 1 */

  Gis = sqrt(Cn)*(cos(wd*T01)-1)/wd + Ilt3*T34 - ws*T34*T34/2;
  Gis = In*(T01+T34) - Gis;
  Gis = Gis/Ts/In;

  printf(" Gis=%5.4f  Gid=%5.4f  Gil=%5.4f\n",Gis,Gid,Gil);
  return;

}

/* Determination of Gi for operation mode 2 */

void det_Gi2(void)
{

  /* Average value of il for operation mode 2 */

  Gil = sqrt(Cn)*(cos(wd*T01)-1)/wd + c*In*T12 - ws*T34*T34/2;
  Gil = Gil + (Ilt1-c*In)*sin(wsd*T12)/wsd;
  Gil = Gil - sqrt(c)*(Vdt1-1)*(cos(wsd*T12)-1)/wsd + Ilt3*T34;
  Gil = Gil + Ilt2*sin(wd*T23)/wd - sqrt(Cn)*(Vdt2-1)*(cos(wd*T23)-1)/wd;
  Gil = Gil/Ts/In;

  /* Average value of id for operation mode 2 */

  Gid = Ilt3*T34 - ws*T34*T34/2;
  Gid = Gid/Ts;
  Gid = Gid/In;

  /* Average value of is for operation mode 2 */

  Gis = sqrt(Cn)*(cos(wd*T01)-1)/wd - ws*T34*T34/2;
  Gis = Gis + Ilt3*T34;
  Gis = Gis + Ilt2*sin(wd*T23)/wd - sqrt(Cn)*(Vdt2-1)*(cos(wd*T23)-1)/wd;
  Gis = In*(T01+T23+T34) - Gis;
  Gis = Gis/Ts/In;
```

```
  printf(" Gis=%5.4f  Gid=%5.4f  Gil=%5.4f\n",Gis,Gid,Gil);
  return;

}

/* Determination of function Gv for operation mode 2 */

void det_Gv2(void)
{
 /* Average value of vd - mode 2 */

  Gvd = T01 - 1/wd*sin(wd*T01) + c*Vdt1*T12 + (1-c)*T12;
  Gvd = Gvd + 1/2*In*sqrt(c)*(1-c)*wsd*T12*T12          ;
  Gvd = Gvd - sqrt(c)/wsd/Cn*(c*In-Ilt1)*(cos(wsd*T12)-1) ;
  Gvd = Gvd + 1/wsd*(1-c)*(Vdt1-1)*sin(wsd*T12) + T23;
  Gvd = Gvd + Ilt2/wd/sqrt(Cn)*(cos(wd*T23)-1) + (Vdt2-1)/wd*sin(wd*T23);
  Gvd = Gvd/Ts;

  /* Average value of vs - mode 2 */

  Gvs = -c*Vdt1*T12 + c*T12 + 1/2*In*sqrt(c)*(1-c)*wsd*T12*T12;
  Gvs = Gvs - sqrt(c)*(c*In-Ilt1)/wsd*(cos(wsd*T12)-1);
  Gvs = Gvs + c*(Vdt1-1)/wsd*sin(wsd*T12);
  Gvs = Gvs/Ts;

  printf(" Gvd=%5.4f   Gvs=%5.4f\n",Gvd,Gvs);
  return;

}


/* solve a+b*x+c*sin(x)+d*cos(x)=0   */

float newraph1 (float a, float b, float c, float d)
{
 float soli=1,solf=3,func,funcder,err=0.0001;
 while ( fabs(solf-soli) > err)
 {
  soli=solf;
  func=a+b*soli+c*sin(soli)+d*cos(soli);
  funcder=b+c*cos(soli)-d*sin(soli);
  solf=soli-func/funcder;
  printf("soli=%5.4f solf=%5.4f\n",soli,solf);
  getch();
 }
 return solf;
}

/* solve a+b*sin(x)+c*cos(x)=0  */

float newraph2 (float a, float b, float c)
{
 float soli=0,solf=0.5,func,funcder,err=0.0001;
 while ( fabs(solf-soli) > err)
 {
  soli=solf;
  func=a+b*sin(soli)+c*cos(soli);
  funcder=b*cos(soli)-c*sin(soli);
```

```
    solf=soli-func/funcder;
    printf("soli=%5.4f solf=%5.4f\n",soli,solf);
    getch();
   }
  return solf;
}
```

Appendix 7: Publications

1. A Szabo, M Kansara, P G Holmes and E S Ward, "Mathematical Modelling of Quasi-Resonant Converters", IEE Electronics Letters, vol.31, no.24, 1995, pp.2057-2058.
2. A Szabo, M Kansara and E S Ward, "Analysis of Boost Power Factor Correction Topologies", Proceedings of the Third European Power Quality Conference, Bremen, Germany, 1995, pp.451-460.
3. M Kansara, A Szabo and E S Ward, "The Evaluation of Modern Single-Phase Boost Converter Topologies", Proceedings of the 30th Universities Power Engineering Conference, London, UK, 1995, vol.2, pp.698-701.
4. A Szabo, M Kansara and E S Ward, "Analysis of Zero-Current-Switching Boost Converters", Proceedings of the 31st Universities Power Engineering Conference, Iraklio, Greece, 1996, vol.2, pp.429-433.
5. A Szabo, M Kansara and E S Ward, "Small-Signal Modelling of Quasi-Resonant Step-Up Converters", Proceedings of the 5th International Conference on Optimisation of Electric and Electronic Equipment, Brasov, Romania, 1996, vol.5, pp.1305-1314.
6. A Szabo and E S Ward, "High-Frequency Zero-Voltage-Switching Boost Converters", Proceedings of the 5th International Conference on Optimisation of Electric and Electronic Equipment, Brasov, Romania, 1996, vol.5, pp.1315-1324.
7. A Szabo, M Kansara and E S Ward, "Analysis of High-Frequency Quasi-Resonant Boost Converters", Proceedings of the International Symposium of Electronics and Telecommunications, Timisoara, Romania, 1996, vol.3, pp.75-80.
8. A Szabo, M Kansara and E S Ward, "A Unified Analysis of Zero-Voltage-Switching Multi-Resonant and Quasi-Resonant Converters", 32nd Universities Power Engineering Conference, Manchester , UK, 1997, vol.2, pp.818-821.
9. A Szabo, M Kansara and E S Ward, "Static Characteristics and Dynamic Modelling of Multi-Resonant Converters", International Symposium on Signals, Circuits and Systems, Iasi, Romania, 1997, vol.2, pp.342-345.

10.M Kansara, A Szabo and J Redgate, "The Impact of the Use of High-Efficiency Power Supplies for Electronic Equipment on the Environment", 'Researching the Environment' Conference, Nottingham, UK, 1997.

11.A Szabo, M Kansara and E S Ward, "A General Approach for the Study of DC-DC Converters", 6th International Conference on Optimisation of Electric and Electronic Equipment, Brasov, Romania, May 1998.

12.A Szabo, M Kansara and E S Ward, "A Unified Method for the Small-Signal Modelling of Multi-Resonant and Quasi-Resonant Converters", IEEE International Symposium on Circuits and Systems, ISCAS'98, Monterey, USA, June 1998.

13.A Szabo, M Kansara and E S Ward, "The Averaging Technique Applied to the Modelling of Multi-Resonant and Quasi-Resonant Converters", IEE International Conference on Power Electronics and Variable Speed Drives, London, UK, September 1998.

References

[1] Bose, B.K., "Power Electronics - A Technology Review", Proceedings of the IEEE, vol.80, no.8, 1992, pp.303-1334.

[2] Bose, B.K., "Evaluation of Modern Power Semiconductor Devices and Future Trends of Converters", IEEE Transactions on Industry Applications, vol.28, no.2, 1992, pp.403-413.

[3] Bose, B.K., "Recent Advances in Power Electronics", IEEE Transactions on Power Electronics, vol.7, no.1, 1992, pp.2-16.

[4] Van Wyk, J.D., "Present and Future Trends in Power Electronic Converters", 6th European Conference on Power Electronics and Applications, 1995, vol.0, pp.0.001-0.0016.

[5] Hua, G. and Lee, F.C., "Evaluation of Switched-Mode Power Conversion Technologies", IPEMC'94, 1994, pp.1-15.

[6] Harashima, F., "Power Electronics and Motion Control - A Future Perspective", Proceedings of the IEEE, vol.82, no.8, 1994, pp.1107-1111.

[7] Pedder, D.A.G., "Power Conditioning for the Millennium", Keynote Address II, Sixth International Conference on Power Electronics and Variable Speed Drives, 1996, pp.1-6.

[8] Grant, D., "Power Semiconductor Devices - After Revolution in the 70's and 80's, Evolution in the 90's", Keynote Address III, Sixth International Conference on Power Electronics and Variable Speed Drives, 1996, pp.1-6.

[9] Burns, W.W. and Kociecki, J., "Power Electronics in the Minicomputer Industry", Proceedings of the IEEE, vol.76, no.4, 1988, pp.311-324.

[10] Kassakian, J.G. and Schlecht, M.F., "High-Frequency High-Density Converters for Distributed Power Supply Systems", Proceedings of the IEEE, vol.76, no.4, 1988, pp.362-376.

[11] Greenland, P., Ueki, M., and Lee, M.J., "Power Multi-Chip Modules for Quasi-Resonant Converters", Colloquium on 'Resonant Systems', January 1995, pp.8/1-8/22.

[12] Brakus, B., "Power Supply Hybrids", INTELTEC, 1994, pp.581-587.

[13] Lee, F.C., "High-Frequency Resonant, Quasi-Resonant and Multi-Resonant Converters", Virginia Power Electronics Centre, 1989.

[14] Mohan, N., Undeland, T.M. and Robbins, W.P., "Power Electronics - Converters, Applications and Design", Second Edition, John Wiley & Sons, Inc., 1995.

[15] Liu, K.H. and Lee,F.C., "Resonant Switches - A Unified Approach to Improve Performances of Switching Converters", IEEE International Telecommunications Energy Conference, 1984, pp.334-351.

[16] Liu, K.H., Oruganti, R. and Lee, F.C., "Resonant Switches - Topologies and Characteristics", PESC'85 Record, 1985, pp.106-116.

[17] Liu, K.H., "High-Frequency Quasi-Resonant Converter Techniques", Phd Thesis, Virginia Polytechnic Institute and State University, 1986.

[18] Liu, K.H. and Lee, F.C., "Zero-voltage Switching Technique in DC/DC Converters", PESC'86 Record, 1986, pp. 58-70. (*also* IEEE Transactions on Power Electronics, vol.5, no.3, 1990, pp. 293-304)

[19] Zeng, T., Chen, D.Y. and Lee, F.C., "Variations of Quasi-Resonant DC-DC Converter Topologies", PECS'86 Record, 1986, pp.381-392.

[20] Jovanovic, M.M., Liu, K.H., Oruganti, R. and Lee, F.C., "State-Plane Analysis of Quasi-Resonant Converters", IEEE Transactions on Power Electronics, vol.2, no.1, January 1987, pp.36-44.

[21] Tabisz, W.A., Gradzki, P. and Lee, F.C., "Zero-Voltage-Switched Quasi-Resonant Buck and Flyback Converters - Experimental Results at 10 MHz", PESC'87 Record, 1987, pp.404-413.

[22] Freeland, S. and Middlebrook, R.D., "A Unified Analysis of Converters with Resonant Switches", IEEE Power Electronics Specialists Conference Record, 1987, pp.20-30.

[23] Jovanovic, M.M., Tabisz, W.A. and Lee, F.C., "Zero-Voltage-Switching Technique in High-Frequency Off-Line Converters", Proceedings of APEC, 1988, pp.23-32.

[24] Lee, F.C., "High-Frequency Quasi-Resonant Converter Technologies", Proceedings of the IEEE, vol.76, no.4, 1988, pp. 377-390.

[25] Kazimierczuk, M.K., "Design-Oriented Analysis of Boost Zero-Voltage-Switching Resonant DC/DC Converter", IEEE Transactions on Power Electronics, vol.3, no.2, 1988, pp.126-136.

[26] Schlecht, M.F. and Casey, L.F., "Comparison of the Square-Wave and Quasi-Resonant Topologies", IEEE Transactions on Power Electronics, vol.3, no.1, 1988, pp.83-92.

[27] Lotfi, A.W., Vorperian, V. and Lee,F.C., "Comparison of Stresses in Quasi-Resonant and Pulse-Width-Modulated Converters", PESC'88 Record, 1988, vol.2, pp.591-598.

[28] Kazimierczuk, M.K. and Morse, W.D., "State-Plane Analysis of Zero-Voltage-Switching Resonant DC/DC Converters", IEEE Transactions on Aerospace and Electronic Systems, vol.25, no.2, 1989, pp.232-240.

[29] Kazimierczuk, M.K. and Morse, W.D., "State-Plane Analysis of Zero-Current-Switching Resonant DC/DC Converters", IEEE Transactions on Power Electronics, vol.4, no.2, 1989, pp.265-271.

[30] Kazimierczuk, M.K. and Jozwik, J., "Optimal Topologies of Resonant DC/DC Converters", IEEE Transactions on Aerospace and Electronic Systems, vol.25, no.3, 1989, pp. 363-372.

[31] Carrasco, J.M., Ridao, F.P., Quero, Q.C., Janer, C. and Franquelo, L.G., "Industrial Application, 1 MHz, Quasi-Resonant Converter", Fifth European Conference on Power Electronics and Applications, 1993, vol.3, pp.178-183.

[32] Mucko, J. and Greczko, E., "Quasi-Resonant Buck Converter - Possible Topologies, Similarities and Differences", Proceedings of ISIE'96, 1996, pp.719-723.

[33] Forsyth, A.J., "Review of Resonant Techniques in Power Electronic Systems", IEE Power Engineering Journal, June 1996, pp.110-120.

[34] Andreycak, B., "Zero Voltage Switching Resonant Power Conversion", Application Note U-138, Unitrode - Product & Applications Handbook 1993-1994.

[35] Tatakis, E., Polyzos, N. and Safacas, A., "Predicting real characteristics of boost zero-voltage-switching quasi-resonant converters", ISIE'95 - Proceedings of the IEEE International Symposium on Industrial Electronics, 1995, vol.2, pp.759-765.

[36] Polyzos, N., Tatakis, E. and Safacas, A., "Comparison Between Theoretical and Real Characteristics of Zero-Voltage-Switching Quasi-Resonant Converters", EPE'95, 1995, vol.2, pp.2.731-2.736.

[37] Tatakis, E. and Polyzos, N., "A Novel Approach to Evaluate the Behavioral Characteristics of Zero-Voltage-Switching Quasi-Resonant Converters", PESC'96 Record, 1996, pp.1388-1393.

[38] Tatakis, E. and Polyzos, N., "Power Losses Simulation in Practical Zero-Voltage-Switching Quasi-Resonant Converters", Proceedings of ISIE'96, 1996, pp.724-729.

[39] Jovanovic, M. M., "High-Frequency Off-Line Power Conversion Using Quasi-Resonant and Multi-Resonant Techniques", Phd Thesis, Virginia Polytechnic Institute and State University, 1988.

[40] Tabisz, W.A. and Lee, F.C., "Zero-Voltage-Switching Multi-Resonant Technique - A Novel Approach to Improve Performance of High-Frequency Quasi-Resonant Converters", PESC'88 Record, 1988, pp.9-17.

[41] Tabisz, W.A. and Lee, F.C., "DC Analysis and Design of Zero-Voltage-Switched Multi-Resonant Converters", PESC'89 Record, 1989, vol.1, pp.243-251.

[42] Lee, F.C., Tabisz, W.A., Jovanovic, M.M., "Recent Developments in High-Frequency Quasi-Resonant and Multi-Resonant Converter Technologies", Proceedings of the 1989 European Power Electronics Conference, 1989, pp.401-410.

[43] Tabisz, W.A., "High-Frequency Multi-Resonant Power Conversion Techniques", Phd Thesis, Virginia Polytechnic Institute and State University, 1990.

[44] Tabisz, W.A., Jovanic, M.M. and Lee,F.C., "High-Frequency Multi-Resonant Converter Technology and Its Applications", Fourth International Conference on Power Electronics and Variable-Speed Drives, 1990, pp.1-8.

[45] Lee, F.C., Tabisz, W.A. and Jovanic, M.M., "High-Frequency Quasi-Resonant and Multi-Resonant Converter Technologies", Archiv fur Elektrotechnik, vol 74, no.2, 1990, pp.107-116.

[46] Tabisz, W.A. and Lee, F.C., "Design of High-Density On-Board Single- and Multiple-Output Multi-Resonant Converters", Proceedings of High Frequency Power Conversion Conference, 1990, pp.45-57.

[47] Franck, F. and Schroder, D., "A Contribution to the Design Specifications of Single-Cell Multi-Resonant Converters", PESC'90 Record, 1990, pp.552-559.

[48] Tabisz, W.A. and Lee, F.C., "Principles of Quasi- and Multi-Resonant Power Conversion Techniques", IEEE International Symposium on Circuits and Systems, 1991, pp.1053-1056.

[49] Cai, X.S. and Zhang, S.H., "Nonlinear Design Optimisation for the Resonant Tank of Zero-Voltage-Switching Multi-Resonant Converters", 13th International Telecommunications Energy Conference - INTELTEC'91, 1991, pp.509-514.

[50] Lee, I.H., Oh, S.H., Kim, H.J. and Ahn, T.Y., "A 2MHz Resonant DC/DC Converter Module for Telecommunication Application", 13th International Telecommunications Energy Conference - INTELTEC'91, 1991, pp.502-508.

[51] Lee, I.H., Oh, S.H., Kim, H.J. and Ahn, T.Y., "A 2MHz Resonant DC/DC Converter Module for Telecommunication Application", INTELTEC'91, 1991, pp.502-508.

[52] Nuno, F., Diaz, J., Sebastian, J. and Lopera, J., "A Unified Analysis of Multi-Resonant Converters", PESC'92 Record, 1992, vol.2, pp.822-829.

[53] De la Cruz, E., Ollero, S., Cobos, J.A., Uceda, J., Lopera, J.M. and Nuno, F., "Performances Comparison of Four Practical Implementations Based on PWM, Quasi and Multiresonant Topologies for On Board DC/DC Converters in Distributed Power

Archtectures", PESC'92 Record, 23rd Annual IEEE Power Electronics Specialists Conference, 1992, vol.2, pp.917-925.

[54] De la Cruz, E., Ollero, S., Rodriguez, J., Uceda, J. and Cobos, J.A., "Review of Suitable Topologies for On Board DC/DC Converters in Distributed Power Architectures for Telecom Applications", 14th International Telecommunications Energy Conference - INTELTEC'92 , 1992, pp.59-65.

[55] Jovanovic, M.M., "Resonant, quasi-resonant, multi-resonant and soft-switching techniques - merits and limitations", International Journal of Electronics, vol.77, no.5, 1994, pp.537-554.

[56] Yang, E.X., Li, Q. and Lee, F.C., "Analysis and Design of Single-Ended-Parallel Multi-Resonant Converter", PESC'94 Record, 1994, vol.2, pp.1405-1412.

[57] Cobos, J.A., Garcia, O., Uceda, J., Sebastian, J. and de la Cruz, E., "Comparison of High Efficiency Low Output Voltage Forward Topologies", PESC'94, 1994, vol.2, pp.887-894.

[58] Liu, R., Caldeira, P. and Kustera, D., "A Low Noise, Multi-Output and Multi-Resonant Flyback Power Supply for Television Application", Proceedings of SOUTHCON'94, 1994, pp.546-551.

[59] Liu, R., Caldeira, P. and Kustera, D., "Analysis and Design of a Low EMI, Multi-Output and Multi-Resonant Forward Power Supply for TV Applications", Proceedings of IPEMC'94, First International Power Electronics and Motion Control Conference, 1994, vol.1, pp.289-264.

[60] Moo, C.S. and Mok, P.P., "Multi-Resonant Boost Converter as Active Filter for Power Factor Correction", APEC'96, vol.1, pp.166-171.

[61] Tang, W., Leu, C.S. and Lee, F.C., "Charge Control for Zero-Voltage-Switching Multi-Resonant Converter", IEEE Transactions on Power Electronics, vol.11, no.2, 1996, pp.270-274.

[62] Turner, M.D., "Multi-Resonant Power Conversion", Electrotechnology, vol.7, no.3, June/July 1996, pp.30-34.

[63] Bowman, W.C., Balicki, J.F., Dickens, F.T., Honeycutt, R.M., Nitz, W.A., Strauss, W., Suiter, W.B. and Ziesse, "A Resonant DC-to-DC Converter Operating at 22 Megahertz", Proceedings of APEC, 1988, pp.3-11.

[64] Hosotani, T., Harada, K., Ishihara, Y., and Todaka, T., "A Novel ZVS Multi-Resonant Converter with Rectfiers' Deadtime Control Operated in 20MHz Range", 16th International Telecommunications Energy Conference INTELTEC, 1994, pp.115-122.

[65] Tan, L.S. and McMahon, R.A., "A Study of the Operation of a Class E Amplifier at 13.56 MHz", Sixth International Conference on Power Electronics and Variable Speed Drives, 1996, pp.168-172.

[66] Dixon, L.H., "Switching Power Supply Topology Review", Unitrode Power Supply Design Seminar, 1996, pp. P1-1/12.

[67] Bayoumi, M.A. and Jenkins, W.K., "Spectral Analysis and EMI Comparison of PWM, Quasi-Resonant and Resonant Converters", Proceedings of the 37th Midwest Symposium on Circuits and Systems, 1994, vol.2, pp.1285-1288.

[68] Chung, H., Hui, S.Y.R. and Tse, K.K., "Reduction of EMI Emission from Power Converters using Soft-Switching Technique", Sixth International Conference on Power Electronics and Variable Speed Drives, 1996, pp.156-161.

[69] Kassakian, J.G., Schlecht, M.F. and Verghese, G.C., "Principles of Power Electronics", Addison-Wesley Publishing Company, Reading, Massachusetts, 1991.

[70] Middlebrook, R.D. and Cuk, S., "A General Unified Approach to Modelling Switching-Converter Power Stages", PESC'76 Record, 1976, pp.18-34.

[71] Middlebrook, R.D., "Small-Signal Modeling of Pulse-Width-Modulated Switched-Mode Converters", Proceedings of the IEEE, vol.76, no.4, 1988, pp.343-353.

[72] Yu, J. and Xu, J., "Time Averaging Equivalent Circuit Analysis for a Class of Periodically Switching Linear Linear Network", IEEE International Symposium on Circuits and Systems, 1988, vol.2, pp.1139-1142.

[73] Vorperian, V., Tymerski, R. and Lee, F.C.Y., "Equivalent Circuit Models for Resonant and PWM Switches", IEEE Transactions on Power Electronics, vol.4, no.2, April 1989, pp.205-214.

[74] Maksimovici, D. and Cuk, S., "A General Approach to Synthesis and Analysis of Quasi-Resonant Converters", IEEE 1989 Power Electronics Specialists Conference Records, pp.713-727.

[75] Nakahara, M., Higashi, T., Ninomiya, T. and Harada, K., "Dynamic Characteristics and Stability Analysis of Resonant Converter", PESC'89 Record, 1989, pp.752-759.

[76] Witulski, A.F. and Erickson, R.W., "Extension of State-Space Averaging to Resonant Switches and Beyond", IEEE Transactions on Power Electronics, vol.5, no.1, 1990, pp.98-109.

[77] Chau, K.T. and Ioinovici, A., "Small-Signal Model of Quasi-Resonant Converters in the Presence of Conduction Losses", 1991 IEEE International Symposium on Circuits and Systems, vol.2, pp.1081-1084.

[78] Chau, K.T., Lee, Y.S. and Ioinovici, A., "Computer-Aided Modeling of Quasi-Resonant Converters in the Presence of Parasitic Losses by Using the MISSCO Concept", IEEE Transactions on Industrial Electronics, vol.38, no.6, 1991, pp.454-461.

[79] Witulski, A.F., "Buck Converter Small-Signal Models and Dynamics: Comparison of Quasi-Resonant and Pulse-Width-Modulated Switches", IEEE Transactions on Power Electronics, vol.6, no.4, 1991, pp.727-738.

[80] Krein, P.T., Bentsman, J., Bass, R.M. and Lesieutre, B.L., "On the Use of Averaging for the Analysis of Power Electronic Systems", IEEE Transactions on Power Electronics, vol.5, no.2, 1990, pp.182-190.

[81] Sanders, S.R. and Verghese, G.C., "Synthesis of Averaged Circuit Models for Switched Power Converters", IEEE Transactions on Circuits and Systems, vol.38, no.8, 1991, pp.905-915.

[82] Sanders, S.R., Noworolski, J.M., Liu, X.Z. and Verghese, G.C., "Generalized Averaging Method for Power Conversion Circuits", IEEE Transactions on Power Electronics, vol.6, no.2, 1991, pp.251-259.

[83] Nakahara, M. and Ninomiya, T., "A General Computer Algorithm for Analysis of Switching Converter", PESC'92 Record, 1992, pp.1181-1188.

[84] Ben-Yaakov, S. and Adar, D., "Average Models as Tools for Studying the Dynamics of Switch Mode DC-DC Converters", PESC'94 Record, 1994, vol.2, pp.1369-1376.

[85] Lehman, B. and Bass, R.M., "Extensions of Averaging Theory for Power Electronic Systems", IEEE Transactions on Power Electronics, vol.11, no.4, July 1996, pp.542-553. (*also* PESC'94 Record, 1994, vol.2, pp.1053-1057)

[86] Sun, J. and Grotstollen, H., "A Symbolic Computation Package for Averaged Analysis of Power Electronic Systems", APEC'96, 1996, vol.1, pp.96-102. (*also* PESC'96, 1996, vol.1, pp.543-549.)

[87] Eng, S.C., Orungati, R. and Liang, Y.C., "An Automated Algorithm for Small-Signal Analysis of DC-DC Power Converters", IEEE Transactions on Power Electronics, vol.11, no.1, 1996, pp.132-141.

[88] Verghese, G.C., Elbuluk, M.E. and Kassakian, J.G., "A General Approach to Sampled-Data Modeling for Power Electronic Circuits", IEEE Transactions on Power Electronics, vol.1, no.2, 1986, pp.76-89.

[89] Lau, B.Y. and Middlebrook, R.D., "Small-Signal Frequency Response Theory for Piecewise-Constant Two-Switched-Network DC-to-DC Converter Systems", PESC'86 Record, 1986, pp.186-200.

[90] Groves, J., "Small-Signal Analysis Using Harmonic Balance Methods", PESC'91 Record, 1991, pp.74-79.

[91] Tymerski, R., "Frequency Analysis of Time-Interval-Modulated Switched Networks", IEEE Transactions on Power Electronics, vol.6, no.2, 1991, pp.287-295.

[92] Tymerski, R., "Application of the Time Varying Transfer Function for Exact Small-Signal Analysis", PESC'91 Record, 1991, pp.80-87.

[93] Yang, E.X., Lee, F.C. and Jovanovic, M.M., "Small-Signal Modelling of Power Electronic Circuits Using Extended Describing Function Technique", Proceedings of VPEC Seminar, 1991, pp.167-178.

[94] Yang, E.X., Lee, F.C. and Jovanovic, M.M., "Extended Describing Function Technique Applied to the Modeling of Resonant Converters", Proceedings of VPEC Seminar, 1991, pp.179-191.

[95] Yang, E.X., Guo, L. and Lee, F.C., "Describing Function Method in Modeling of Switching Converters", Proceedings of VPEC Seminar, 1993, pp.27-43.

[96] Yang, E.X.Q., "Extended Describing Function Method for Small-Signal Modelling of Resonant and Multi-Resonant Converters", Phd Thesis, Virginia Polytechnic Institute and State University, 1994.

[97] Yang, E.X., Lee, F.C. and Jovanovic, M.M., "Small-Signal Modeling of LCC Resonant Converter", PESC'92 Record, 1992, pp.941-948.

[98] Yang, E.X., Lee, F.C. and Jovanovic, M.M., "Small-Signal Modeling of Series and Parallel Resonant Converters", APEC'92, 1992, pp.785-792.

[99] Tymerski, R., "Volterra Series Modeling of Power Conversion Systems", IEEE Transactions on Power Electronics, vol.4, no.4, 1991, pp.712-718.

[100] Vilathgamuva, M. and Junghong, D., "Nonlinear Modelling of Quasi-Resonant Converters in Frequency Domain", PESC'96, 1996, vol.1, pp.563-569.

[101] Huynh, P. and Cho, B.H., "Empirical Small-Signal Modelling of Switching Converters Using Pspice", PESC'95, vol.2, pp.809-815.

[102] Lee, Y.S., "Computer-Aided Analysis and Design of Switch-Mode Power Supplies", Marcel Dekker Inc., 1993.

[103] Rashid, M.H., "SPICE for Power Electronics and Electric Power", Prentice Hall, 1993.

[104] Mohan, N., Robbins, W.P., Undeland, T.M., Nilssen, R. and Mo, O., "Simulation of Power Electronic and Motion Control Systems - An Overview", Proceedings of the IEEE, vol.82, no.8, 1994, pp.1287-1302.

[105] ***, "UC3860, Resonant Mode Power Supply Controller", Unitrode Integrated Circuits.

[106] Wofford, L., "UC1860 - New IC Controls Resonant Mode Power Supplies", Application Note U-117A, Unitrode - Product & Applications Handbook 1993-1994

[107] ***, "MC34066, High Performance Resonant Mode Controller", Motorola Analog IC Device Data.

[108] ***, "CS-360, One Megahertz Resonant-Mode Control", Cherry Semiconductor.

[109] ***, "MC34067, High Performance Resonant Mode Controller", Motorola Analog IC Device Data.

[110] ***, "CS-361, 2 MHz Resonant-Mode Control", Cherry Semiconductor.

[111] ***, "UC3861-3868, Resonant Mode Power Supply Controller", Unitrode Integrated Circuits.

[112] Wofford, L., "A New Family of Integrated Circuits Controls Resonant Mode Power Converters", Application Note U-122, Unitrode - Product & Applications Handbook 1993-1994

[113] Middlebrook, R.D., "Topics in Multi-Loop Regulators and Current-Mode Programming", PESC'85 Record, 1985, pp.716-732.

[114] Tang, W., Ridley, R.B. and Lee, F.C., "Small Signal Modeling of Average Current-Mode Control", Proceedings of VPEC Seminar, 1991, pp.193-201.

[115] Tan, F.D. and Middlebrook, R.D., "A Unified Model for Current-Programmed Converters", IEEE Transactions on Power Electronics, vol.10, no.4, 1995, pp.397-408.

[116] Redl, R. and Sokal, N.O., "Current-Mode Control, Five Different Types, Used with the Three Basic Classes of Power Converters: Small-Signal AC and Large-Signal DC Characterization, Stability Requirements, and Implementation of Practical Circuits", PESC'85, 1985, pp.771-785.

[117] Ridley, R.B., Lee, F.C. and Vorperian, V., "Multi-Loop Control for Quasi-Resonant Converters", High Frequency Power Conversion Conference, 1987, pp.116-125.

[118] Ridley, R.B., Tabisz, W.A., Lee, F.C.Y. and Vorperian, V., "Multi-Loop Control for Quasi-Resonant Converters", IEEE Transactions on Power Electronics, vol.6, no.1, January 1991, pp.28-38.

[119] Ridley, R.B., Tabisz, W.A. and Lee, F., "Multi-Loop Control Circuit for HF quasi-resonant converter pushes loop-gain crossover frequency beyond 1 MHz", Powerconversion and Intelligent Motion, vol.14, no.9, 1988, pp.105-112.

[120] Costa, J.M.F. and Silva, M.M., "Small-Signal Models and Dynamic Performance of Quasi-Resonant Converters with Current-Mode Control", PESC'94 Record, 1994, vol.2, pp.821-829.

[121] Pressman, A.I., "Switching Power Supply Design", McGraw-Hill, 1991.

[122] Brown, M., "Power Supply Cookbook", Butterworth-Heinemann, 1994.

[123] Andreycak, B., "1 MHz 150W Resonant Converter Design Review", Application Note U-121, Unitrode - Product & Applications Handbook 1993-1994.

[124] Shahian, B. and Hassul, M., "Control System Design Using Matlab", Prentice Hall, 1993.

[125] Golten, J. and Verwer, A., "Control System Design and Simulation", McGraw-Hill, 1991.

[126] Venable, H.D. and Foster, S.R., "Practical Techniques for Analysing, Measuring and Stabilising Feedback Control Loops in Switching Regulators and Converters", Proceedings of the 7th National Power Conversion Conference, Powercon7, 1980, pp.I2.1-17.

[127] Venable, H. D., "The K Factor: A New Mathematical Tool for Stability Analysis and Synthesis", Proceedings of Powercon 10, 1983, pp. H/1-12.

[128] Baha, B., "The Control of Quasi-Resonant Converters", Proceedings of the 5th European Conference on Power Electronics and Applications, 1993, vol.3, pp.304-309.

[129] Tam, W.K., Siu, K.W. and Lee, Y.S., "Computer-Aided Design of Feedback Compensation Networks for Switching Regulators", APEC'94, 1994, pp.1066-1071.